DOI: 10.002/anie.201105813

Strong Bonds: International Collaboration in Chemistry

Special Insert in *Angewandte Chemie* from the Deutsche Forschungsgemeinschaft

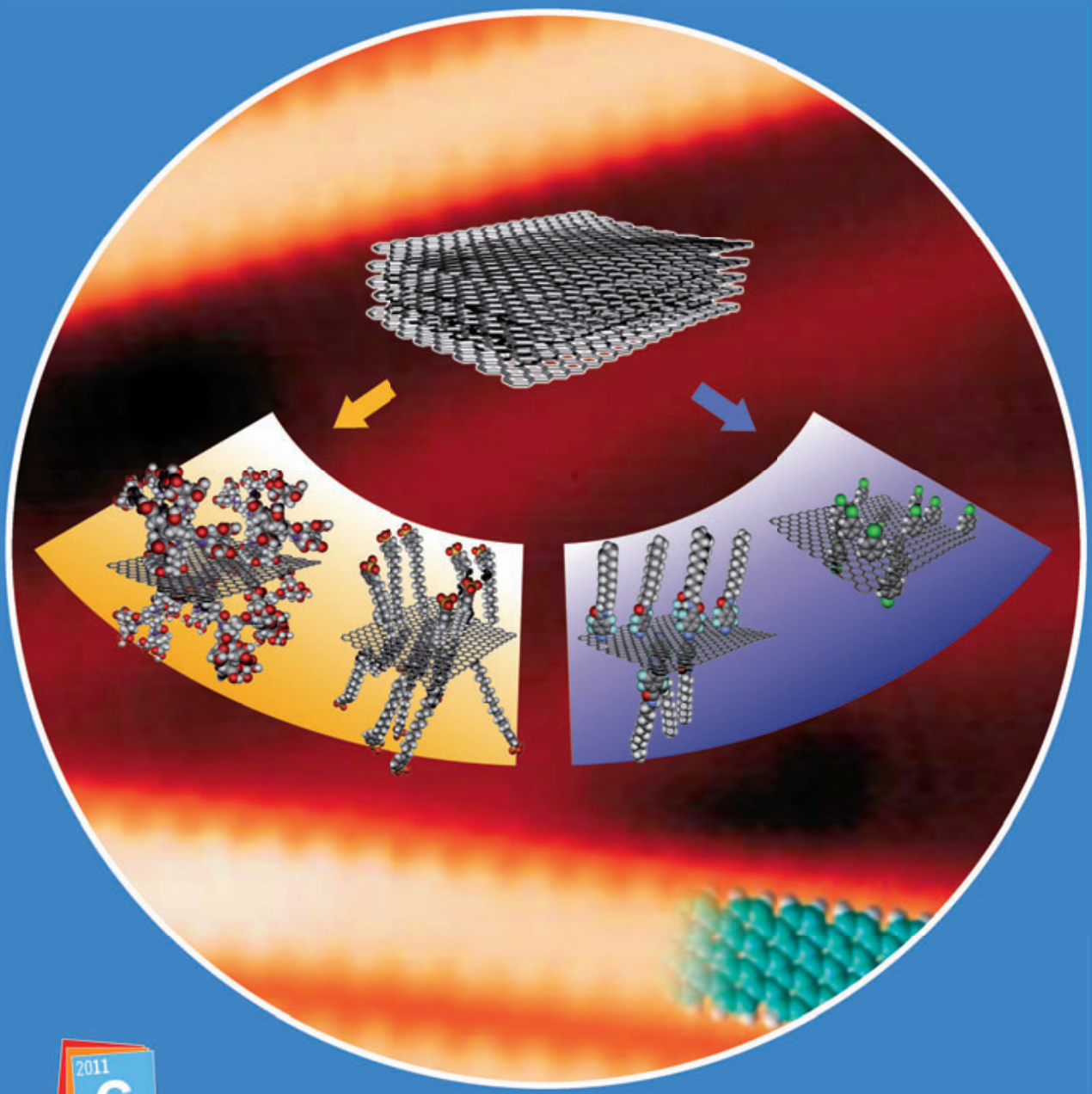

IYC 2011
International Year of CHEMISTRY

DFG

Foreword

Dear reader,

2011 has been announced as the International Year of Chemistry to celebrate the achievements of chemistry and its contributions to the well-being of humankind. The versatile and creative world of chemistry is presented in worldwide events. In Germany, various activities have been organised by national chemical organisations, funding institutions and companies in which both science and the public are invited to participate and encouraged to discover the fascinating world of chemistry.
With this special edition, "The German Research Foundation (Deutsche Forschungsgemeinschaft, DFG)" provides you an insight in the work of selected international chemical research projects and its funding programmes. You can imagine the diversity and interdisciplinarity of chemical research just by looking at the table of contents – I wish you a fascinating read!

Prof. Dr. Matthias Kleiner
President of the Deutsche Forschungsgemeinschaft

Table of Contents

Editorial

Ferdi Schüth

In 2011 we celebrate the International Year of Chemistry, IYC 2011, a joint initiative between IUPAC and the UNESCO. The unifying theme of IYC 2011 is "Chemistry – our life, our future", and this theme transports perfectly the role chemistry has today and which it will have in the future: chemistry is a science which affects everyday life in many different ways, and we use literally thousands of products made possible by the efforts of chemists and chemical engineers. If you read this editorial in a paper version of the journal, basically everything you have in hand is a product of chemical processing: the paper and the fillers, the pigments and dyes in the paper and the printing ink, and the glue to bind it all together. If you are looking at it on a computer screen, the same will hold: the phosphors, LEDs or liquid crystals in the display are chemical products, the frame of the screen is probably a polymer, and the silicon on which the whole electronic circuitry is based, is only possible by highly advanced chemical processing.

In the future, chemistry may have a more important role. Many of the great societal problems can and will only be solved by advances in chemistry: The energy supply of our societies requires novel solutions for energy harvesting, storage and more efficient use – solutions to which chemistry will, for instance, contribute by novel materials for photovoltaics, advanced battery electrodes and electrolytes, or novel organic LEDs. Health is of the highest concern to all of us, and the long average life expectancies reached in many societies today are a direct consequence of advances in drug development and the insight in the biochemical processes associated with many diseases. Feeding today's world population is only possible because the Haber-Bosch invention of producing ammonia as a fertilizer in the early 20th century allows food production at the current level. In order to feed another 3 billion people on the planet, advances in crop protection and fertilizers will be mandatory, as could be newly engineered plants, the development of which relies on chemistry as the underlying science of molecular biology. Food production for the world will also require clean and affordable water which is already lacking now in many places of the world. Cleaning water needs chemical processes, desalination using advanced membrane processes could help to compensate for the decreasing availability of ground and surface water.

However, the science of chemistry is not only addressing the great societal challenges – as important as they are. There are also many fundamental questions which are of a truly chemical nature: What is the origin of life? How was it possible that inanimate objects, such as molecules, assembled and produced bigger systems which can be considered as "living"? How do the molecules in complex systems, such as organisms, interact to produce the functions which organs or the whole organism fulfils? While the latter question may be considered to be one of molecular biology, molecular biology is, after all, "molecular", and molecules are the realm of the chemist, so that these questions have at least important chemical components. In the field of solid state materials, chemists mostly deal with equilibrium structures. However, there are probably many more possible meta-stable structures. What structures can exist, and are there pathways to synthesize them? What kind of materials can be assembled not from atoms, but from assemblies of atoms? Progress in these directions could open up completely new fields of research. We are just beginning to see the opportunities ahead.

The importance of these questions of both a fundamental and an applied nature has placed chemistry as one of the core fields of scientific research in the past. The dynamical nature of chemistry research today and the many young scientists active in the field allow drawing an optimistic picture also for the future: chemistry will accept the challenges ahead, and even if we do not know how solutions will look like, we should be reasonably confident that in concert with other disciplines we will find solutions.

An active research community needs flexible and dependable funding. DFG was and is a major source of research funds for the entire field of chemistry and chemical engineering in Germany, covering the whole range from fundamental work to studies of a more applied nature, provided that projects meet the criterion of scientific excellence. While chemistry traditionally has focused more strongly than many other disciplines on individual grants – due to the nature of many of the questions studied – there are also activities in collaborative programs, such as the priority programs and the collaborative research centers. In addition, many researchers in chemistry have strong international links, with numerous collaborations in Europe and all over the world. DFG, in cooperation with other European funding agencies, was able to provide an umbrella for joint projects on the European level with the establishment of the ERA-NET Chemistry. This provides a forum for research on a European level by funding bi- and trilateral projects involving partners from more than one country. With the importance of curiosity-driven research in mind, DFG has strongly supported the "Open Initiative" calls of ERA-Chemistry, where there is no thematic focus, and scientific excellence is the only criterion for funding.

The contributions in this special issue give an overview over the different kinds of questions studied in DFG-funded research projects. As the readers will realize, they do address key societal questions, but they also deal with important fundamental chemical problems. They were funded by different funding schemes of DFG, especially those allowing international

collaboration. The projects thus highlight the broad portfolio of DFG. It provides options for any type of scientific approach, which researchers deem to be suitable, and which are surveyed in the article of Sibylle Grandel in this issue.

The contributions in this issue are special, because they combine both aspects of chemical research discussed above: they relate to the great societal questions, such as energy, health, or global warming, but they also approach the problems from a fundamental point of view.

Organic electronics is one of the most promising fields of chemistry with relevance in the energy sector. Organic electronics is required in organic electronic devices, OLEDs or in organic photovoltaic cells. Understanding electron transfer in such systems is crucial, if one wants to build up such devices not based on purely empirical knowledge, but based on an in-depth understanding of the systems at hand. Cattani-Scholz and colleagues describe a new architecture of an organic thin film transistor based on organo-phosphonates. As a first step they prepared self-assembled monolayers from the organo-phosphonates, and studied charge transport through such layers.

A highly interesting class of materials for different applications in molecular electronics are graphene-related systems. Chemical functionalization and nanostructuring could allow tuning of electronic and optical properties of graphene-type materials. For some of these modifications, top-down approaches, i.e. exfoliation, are more suitable, while for others bottom-up strategies, i.e. chemical synthesis, are preferred. The article from the groups of Andreas Hirsch and Klaus Müllen covers these approaches and highlights recent novel developments in this field.

One of the most interesting challenges in chemistry is the development of practically useful light harvesting systems with subsequent conversion of the energy to fuels on the one hand, and the fundamental understanding of the processes relevant in such energy transformation chains on the other. The latter question is the topic of two contributions in this issue: Wang et al. have investigated the interfacial electron transfer at doped TiO_2 surfaces with confocal and tip-enhanced near-field Raman spectroscopy, amongst other techniques. They were able to detect single surface states using these techniques, in addition, also strong electronic coupling could be proven at the alizarin/TiO_2. Such interfaces could be interesting for photochemical water splitting. Surfaces are often more difficult to investigate than molecules, and Llobet and Meyer have thus studied bimetallic molecular model systems for water oxidation, in order to reach a better understanding of the relevant electron transfer processes for this key reaction in the conversion of light to chemical energy.

Energy supply without consumption of fossil fuels is a crucial requirement if global warming shall be reduced. This can be supplemented by capturing carbon dioxide and storing it, or by using it for the production of chemicals. While it is clear that chemical production can not be a major sink of carbon dioxide, it could improve the overall efficiency of the chemical industry and reduce the CO_2-footprint. ERA-Chemistry in 2008 had launched a call on "Chemical Activation of CO_2 and Methane", and two reports in this issue are related to this topic. An interesting biochemical approach for CO_2 removal from the atmosphere is described by Liebner et al. Lignin as a byproduct of the pulp and paper industry is ammonoxidized and used as a humus substitute. It binds CO_2, and can thus reinsert it into the mineralization cycle while at the same time improving soil quality. The work of this group aims at better understanding the mode of nitrogen-binding to the lignin. Di Dio and colleagues have theoretically studied the formation of carbamates from CO_2 and methane over palladium catalysts. The detailed understanding of one key step in this reaction may help in developing better catalysts for CO_2 fixation in carbamates.

Two contributions, from the Seeberger and from the Karst groups, highlight how advanced analytics leads to a better understanding of problems in medicine. The Seeberger team has developed a novel, very efficient cantilever-based assay for the analysis of carbohydrate-protein interactions, which are very important, for instance, in protecting organisms against infections. The combination of purely instrumental methods described by Faber et al. allows the investigation of drug candidates in an early stage by simulating their oxidative metabolism. This could give important information on the suitability of molecules as drugs, without the need for extensive testing involving cell tissue.

Materials chemistry can also lead to materials with interesting applications in the medical field, such as the luminescent magnetic nanoparticles introduced by Wolfbeis and coworkers. Such nanoparticles are useful, for instance, in medical diagnostics via magnetic resonance imaging. Particles, not necessarily in the nanosize domain, are also important as fillers in polymers. The interaction between nanoparticle surface and polymer matrix is crucial for the performance of the composites, and thus needs to be understood for optimization of materials on which often our lives rely, such as tyre rubber. The final article in this issue by Lequeux et al. addresses this technologically important question from a fundamental point of view.

These contributions highlight exemplarily the diverse range of topics covered by chemistry research and funded by the DFG. We hope that readers will benefit from the insight provided by the authors, and be stimulated for their own research.

Ferdi Schüth is Director and Scientific Member at the Max-Planck Institute of Coal Research in Mülheim since 1998.

Email: schueth@mpi-muelheim.mpg.de

Address:
Department of Heterogeneous Catalysis, Max-Planck Institute of Coal Research, Kaiser-Wilhelm Platz 1, 45470 Mülheim a. d. Ruhr

Research Funding

International Research Supported by the German Research Foundation (DFG) – Examples of Activities in the Field of Chemistry

Sibylle Grandel

Chemical sciences play an important role in addressing global challenges such as energy supply and storage, health, or environment. Research in these complex areas requires more and more international collaborative work. In fact collaborative research has been common practice for many years in the field of chemistry. This situation is also reflected by the increasing number of German funding programs, which promote international and joint research collaborations, in order to achieve a more effective use of both national and international resources in the field of chemistry.

1. Introduction

Topics like energy, health and environment – key areas of chemical research – have always been characterized by comprehensive and cross-border questions and challenges. The need for international collaborative approaches has increased even more due to the growing social, economic and ecological challenges in the course of globalization. Scientists, representatives of national research councils and funding agencies thus aim - both in bottom-up and top-down approaches - to intensify the already on-going international and interdisciplinary dialogue, in order to achieve a more efficient use of national resources and knowledge. In addition, such international collaborations are regarded as fruitful scientific and personal experiences and stimulating precursors for the careers of both young and more advanced researchers.

Germany provides a wide variety of funding opportunities for national and foreign researchers: The main "players" among the funding institutions are the Federal Ministry of Research and Education (BMBF), the German Research Foundation (DFG), the German Academic Exchange Service (DAAD), and the Alexander von Humboldt Foundation. In addition non-university research institutions like the Max Planck Society, the Hermann von Helmholtz Association, the Fraunhofer Society, and the Leibniz Association provide funding and research positions in science and industry. This short list reflects only a choice of the various funding opportunities in Germany, providing an entire overview of all institutions and programmes including their specific target groups, funding requirements, etc. would be far beyond the scope of this article. The focus of this article is on the national and international funding opportunities provided by the German Research Foundation. For information about the other institutions, the interested reader is referred to the individual homepages, or to the Research in Germany portal (www.research-in-germany.de).

The German Research Foundation (Deutsche Forschungsgemeinschaft – DFG) is the self-governing organisation for science and research in Germany, and the main national funding organisation in the field of basic research. The DFG promotes research in all fields of science and the humanities. Some numbers and statistics about the amount and distribution of DFG research funding, particularly in the field of chemistry, are given in Sections 2 and 3. The DFG is internationally active, by promoting cross-border cooperation between researchers, fostering international collaborations, the mobility of researchers, and the internationalization of German universities. It actively encourages international research collaborations and maintains partnerships and relations with a large number of partner organizations all over the world – which is also valid for the field of chemistry. Support for international cooperation and exchange by the DFG is provided for individuals by specific grant programs, or by coordinated programs which are described in Section 2. Joint proposals, with two or more partners from different countries, follow in general the principle of mutual responsibility. Researchers working in Germany apply to the DFG while their partners abroad apply for funding at their respective partner organizations (see Section 3).

The aim of this article is to introduce selected examples of the funding portfolio of the DFG, which support international scientific collaboration and projects. The general program introduction is illustrated by examples of funded research in the field of chemistry. With this insight, national and international scientists are informed and encouraged to use these options to

establish or intensify their international networking or to apply for funding for research stays and visits in Germany or abroad.

2. DFG Research Funding Options

The DFG offers a large funding portefolio from Individual Grants Programs to Coordinated Programs for scientists from the graduate up to the senior level. A brief overview of DFG's research funding in the field of chemistry is given in Scheme 1. Related to the total DFG funding budget, chemical research accounts for 7%, all natural sciences have a proportion of about 26%. [1] Funding is not only offered to German scientists, also foreign researchers may be supported, if they fulfill the specific requirements of the respective programs. (For details about purpose, extent or requirements for all the programs described below, the interested reader is referred to http://www.dfg.de/en/research_funding/programmes/index.html.)

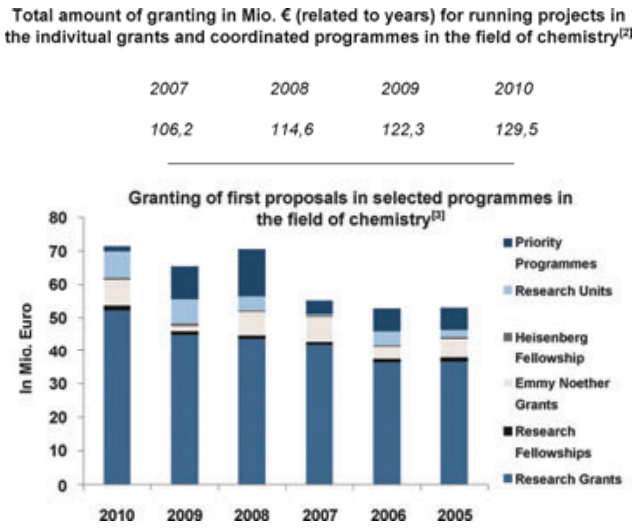

Scheme 1: Selected numbers and statistics on DFG's research funding in the field of chemistry.

2.1 Individual Grants Programs

Within the Individual Grants Programs the **Research Grants*** ("Einzelantrag") are the central funding form supported by the DFG. [2] Funding is provided from the doctorate research level upwards for a research project on a specific, defined topic for a limited time period. The project is carried out at a German research institution and enables international cooperation. The **Research Fellowships*** ("Forschungsstipendien") support young scientists at their postdoc level, and provide a basic fellowship for a research stay abroad for up to 2 years. Between 2005 and 2011 a total of 243 research fellowships (first proposals) were funded by the DFG in the field of chemistry (Figure 1). The USA was the host country in almost 50% of cases, followed by the United Kingdom (20%), Canada (7%), Switzerland (5%), and France (4%).

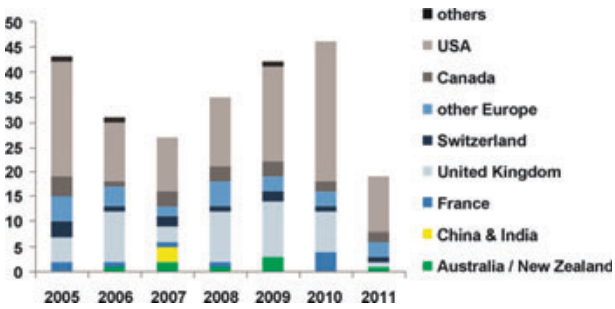

Figure 1: Number of funded research fellowships (first grants) in the field of chemistry between 2005 and 2011 (status July). Different colors indicate the various host countries. [3]

The two most prominent and prestigious individual grants and fellowships are named by two eminent researchers of the last century – Emmy Noether and Werner Heisenberg. The **Emmy Noether Program*** provides funding for outstanding researches with 2-4 years of postdoctoral and international experience to establish an independent junior research group for up to five years. In the natural sciences a total of 248 Emmy Noether proposals were funded between 1999 and 2010, which corresponds to an average funding rate of 38%. [3] 28% (on average) of the candidates came from the field of chemistry (Figure 2). The **Heisenberg Fellowship*** provides funding for 5 years for outstanding researchers who qualified for a professorship (by Habilitation, Emmy Noether, or junior professorship, etc.). Since 1978 a total of 173 Heisenberg candidates have been supported in chemistry, thereof 85% come from the chemical subdisciplines of "Molecular Chemistry" (51%), and "Physical and Theoretical Chemistry (34%). The other subdisciplines were each 5-6% ("Biological Chemistry", "Polymer Research"), and 2% ("Chemical Solid State Research", "Analytical Research"), respectively. [3]

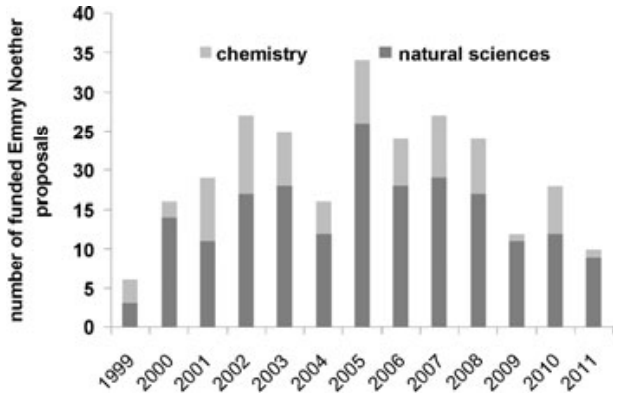

Figure 2. Number of funded Emmy Noether first grants in the field of chemistry compared to all natural science fields between 1999 and 2011 (state June 2011).[3]

2.2 Coordinated Programs

The Coordinated Programs include four main funding options: **Collaborative Research Centers - CRC*** ("Sonderforschungsbereiche - SFB") represent long-term (max. 12 years) university research centers, where a cross-disciplinary research program is performed. The traditional CRC is applied at one

* *funding also for foreign scientists under specific requirements

university, the CRC/Transregio is jointly applied by generally up to 3 universities, where also international partners can contribute (see Table 1). The **Research Training Groups - RTG*** ("Graduiertenkollegs - GRK") are established by universities for doctoral research with a structured program and may last up to 9 years. A specific form of the RTGs, the International RTGs provide joint doctoral training programs between universities abroad and from Germany. **Priority Programs - PP*** ("Schwerpunktprogramme - SPP") enable a collaborative networked research over several locations in an emerging field of science and are established for a period of six years. Once the program is established, the DFG announces a call for proposals. The **Research Units - RU*** ("Forschergruppen - FOR") comprise a team of researchers working together on a research project which, in terms of thematic focus, duration, and finances, extends beyond the funding options available under the Individual Grants Program or Priority Program. They generally last six years and often contribute to establishing new research directions. Funding opportunities for Research Units are subject to the same principles as Research Grants. Numbers of currently funded chemical projects in the respective coordinated programs are summarized in Table 1.

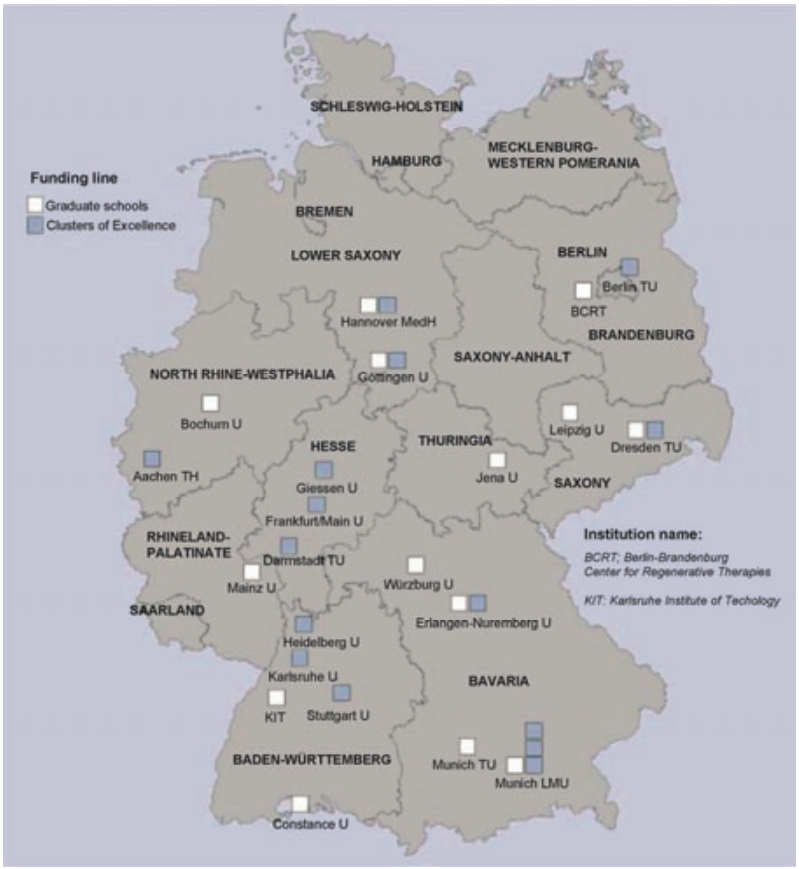

Figure 3. Graduate Schools and Clusters of Excellence of the German Excellence Initiative currently running (map kindly provided by C. Brück, DFG)

Table 1. Number of currently running Collaborative Research Centers (CRC), Research Training Groups (RTG), Priority Programs (PP), and Research Units (RU) in the field of chemistry.[3] In parentheses, the number and location of international partners is given.[a]

Chemical Subfield	CRC	RTG	PP	RU
Molecular Chemistry	3	7 (2 JP, 1 CH, 1 NL)	6 (USA, NL, F, I, BE, SK, RU, TH)	2 (1 CH)
Chemical Solid State Research	3	1 (NL)	3 (1 CH)	1
Physical and Theoretical Chemistry	4 (1 CN)	2 (1 USA)	1	6 (1 UK)
Analytical Chemistry	1	1	1 (USA)	1
Biological Chemistry	4	2 (1 SE)	2	3
Polymer Research	3	3 (1 ROK, 1 F)	1 (ES)	3
Total	18	16	14	16

[a] BE: Belgium, CA: Canada, CH: Switzerland, CN: China, ES: Spain, F: France, GB: United Kingdom, I: Italy, IE: Ireland, JP: Japan, NL: Netherlands, ROK: South Korea, RU: Russian Federation, SE: Sweden, SK: Slovakia, TH: Thailand, USA: United States.

2.3 Excellence Initiative (ExIn)

In addition to the programs mentioned in the previous Sections, in 2005 Germany started the Excellence Initiative. This nationwide competition among higher education institutions was established, to strengthen their research capacity and make them more attractive to highly qualified scientists from all over the world. 1,9 billion € were invested between 2006 and 2011, additional €2,7 billion will be provided for a second period from 2012 to 2017.[4] The initiative offers three funding lines: 1) **Graduate Schools** promote the education of young scientists. 2) **Clusters of Excellence**, which are internationally visible research hubs, and offer research positions for PhD studies, postdocs, junior professors, and professors. 3) **Institutional Strategies** promote top-level university research to enhance the institutions' international competitiveness. Currently 15 Clusters of Excellence and 14 Graduate Schools deal with chemical research topics (Figure 3). Corresponding funding for the first and second line in the field of chemistry amounts to 59.4 Mio €. [1]

3. Examples of Bi-/Multilateral International Funding Programs

3.1. Examples of European Programs

The network **ERA-Chemistry** was founded in the year 2004 with the aim to substantially develop and implement programs for transnational collaboration in the field of chemistry in Europe thereby significantly contributing to the creation of a harmonized European Research Area (see www.erachemistry.net). ERA-Chemistry is a network of national research funding organisations throughout Europe and was supported by the European Commission between 2004 and 2008. All activities of ERA-Chemistry are centered on the initiation of joint European research programs and the facilitation of international collaboration in curiosity-driven research in chemistry. Apart from the organization of research conferences, symposia, and workshops for scientists and/or administrators ERA-Chemistry has launched two Thematic Calls and four thematically open calls within the Open Initiative (see Table 2). Nine national funding agencies have already participated in the Open Initiative which is launched once per year, allowing scientists from these nations to collaborate with each other in bilateral or trilateral collaborative arrangements. The program follows a two-stage procedure, involving pre-proposals and full proposals. All proposals are subject of a joint peer-review and joint decision process of the funding organizations involved.

It is the purpose of ERA-Chemistry to establish the Open Initiative on a long-term perspective, to improve its procedures and to attract more Partners in Europe to participate. Moreover, ERA-Chemistry has the aim to intensify its collaboration with other European organizations in chemistry in order to significantly strengthen European chemistry, to provide efficient and easily available programs for transnational collaboration and to promote young scientists.

Table 2. Number of proposals and funding rates in the ERA-Chemistry program calls. [3]

Initiative[a]	Involved funding partners	Number of pre-proposals [b]	Number of invited full proposals[c]	Number of funded projects (success rate)
TC 2005	10	82	35	9 (26%)
TC 2007	12	36	22	13 (59%)
OI 2008	7	97	41	10 (24%)
OI 2009	7	50	26	8 (31%)
OI 2010	6	71	26	7 (27%)

[a] TC 2005: Thematic call 2005: "*Hierarchically organized chemical structures: from molecules to hybrid materials*"; TC 2007: "*Chemical activation of CO_2 and CH_4*" OI: Open Initiative

Apart from ERA-Chemistry, the DFG offers **specific bi-/trilateral funding programs** with corresponding European partner organizations, such as the French Agence Nationale de la Recherche (ANR), the Dutch Technologiestichting STW, or the trilateral cross-border D-A-C-H funding program offered by the research councils of Germany, Austria, and Switzerland. Proposals in these programs can be submitted anytime within the regular program for national proposals. Provision of a complete statistical overview bi-/trilateral programs funded to date is beyond the scope of this article, therefore only some examples are presented: Under the D-A-C-H umbrella 11 bi-/trilateral projects have jointly been funded since 2009. With French partners, almost 30 joint projects have been supported since 2009. In the same period the DFG financed about 10 grants to initiate and intensify the bilateral cooperation between research groups of these two countries.[3]

3.2 Examples of Funding Programs Jointly Organized with Partner Institutions from Overseas

One of DFG's major funding partners in the "International Collaboration in Chemistry" (ICC) program is the **U.S. National Science Foundation (NSF)**. Since 2005 joint calls for collaborative research proposals are announced once a year to establish new bilateral projects between investigators in Germany and in the United States. Applicants are asked to submit a joint proposal. The complete peer-review process, including selection of reviewers and decision-making is jointly carried out by NSF and DFG. Since 2005, out of 177 proposals 44 have been granted.[3] Due to the great success of the program, applicants will also have the opportunity in 2012 to submit joint proposals.

In 2007 an international Committee on Chemistry Research Funding (CCRF) was established under the umbrella of the **"International Union of Pure and Applied Chemistry" (IUPAC)**. The consortium of research funders aims at a better support to promote chemical basic research collaborations. As a consequence a first multilateral Call for Proposals in Polymer Chemistry was launched in late 2009. The goal of this pilot call was to establish an efficient transnational funding program in chemistry, with a minimum of bureaucracy for the applicants, and to establish best practices for future calls of this type. This call was supported by the Polymer Division of IUPAC and 7 national funding organizations. A joint call secretariat at the IUPAC was established, to enable a more efficient administration of the 28 multilateral proposals from a total of 88 applicants. Based on written peer-reviews an international panel of 12 eminent scientists gave the final funding recommendations. As a result seven proposals were announced for funding. In four of these a total of six German research groups are involved. The members of the CCRF intend to further continue and to intensify their activities. Therefore, further international calls in the chemical sciences can be expected in the coming years.

The DFG has a successful research collaboration with **China** which is underlined and supported by the Sino-German Center for Research Promotion (SGC), jointly founded in 2000 by the National Natural Science Foundation of China (NSFC) and the DFG (http://www.sinogermanscience.org.cn/). One example for projects currently running with China is the CRC/Transregio 61,

where the University of Münster, the Chinese Academy of Sciences, the National Center for Nano Science & Technology, and the Tsinghua University in Beijing are involved (Table 1). Since 2007 almost 15 grants have been funded to initiate international cooperation between China and Germany in the field of chemistry. With **Japan**, the DFG partners with the Japan Society for the Promotion of Science (JSPS) in the field of chemistry. Joint chemical projects since 2007 include about 10 individual projects, and an International RTG (see Table 1).

4. Summary and Perspectives

The aim of this article was to give a brief overview on funding programmes supported by the DFG with a special focus on options for international activities. As an example, numbers and statistics on projects funded in the field of chemistry were illustrated, a discipline where collaborative research is common practice. The presented data, make no claim to be complete, nevertheless, they allow some interpretation, such as delineation of trends.

The increase in structured PhD education programs, established by (International) Research Training Groups and the Graduate Schools strengthened the internationalization of Germany's scientific chemical education. This is underlined by a study on behalf of the German Chemical Society, which revealed that during the last ten years the proportion of international students obtaining a German PhD degree has increased from 5% in 1998 to 25-30% in 2007-2009.[5] In contrast, the total number of finished PhDs decreased from about 2200 in 1998 to about 1500 in 2009. In this context, a corresponding number of German graduates who obtained their PhD abroad would be interesting, unfortunately such data was not available.

Of the total number of first grant research fellowships funded in 2010, 13% were in the field of chemistry. This proportion is much higher compared to other interdisciplinary and internationally orientated natural sciences, such as geosciences (2%) or physics (6%)[3] (Figure 1). The proportion of chemical Emmy Noether grants and Heisenberg fellowships on the total number of funded first grants in 2010 was in the range of 12% and 15%, respectively. These funding rates are similar to those of the geoscientific and physical disciplines.[3] Collaborative activities between German and international chemical research groups are reflected by the great variety of coordinated research projects (see Table 2). The main collaboration partners from overseas are the United States, Japan, or China. In Europe groups from Great Britain, France, Switzerland, or the Netherlands mainly cooperate with Germany in chemical research (see also Section 3).

An intensification of the international collaboration described is not exclusive for the chemical sciences, but a major future objective of the DFG. As stated by its president Matthias Kleiner the international orientation of DFG activities is "to strengthen existing international collaborations between researchers, institutions and funding organizations as well as systematically identify and tap into new potentials for cooperation".[6] The long-term goal is to "pave the way to joint research areas", which is, according to Kleiner, "the highest integration level of scientific cooperation". Therefore collaboration with other internationally working funding agencies, such as the Humboldt Foundation, or the DAAD will be expanded. "International cooperations shall be particularly intensified with scientifically dynamic countries and regions. Of great interest for science in Germany are, therefore, the countries of the European Union, especially Austria, Switzerland, France, Great Britain, the Netherlands, and Poland, as are the USA and Canada, Israel and Japan, as well as Brazil, China, India, and Russia".[6]

Sibylle Grandel works at the DFG in the BMBF-funded project "International Research Marketing" and is associated to the group "Chemistry and Process Engineering".

E-Mail: sibylle.grandel@dfg.de

Acknowledgements:

I thank all my colleagues from the Chemistry and Process Engineering group for their fruitful contributions and proof reading, in particular Markus Behnke, Bernd Giernoth, Johanna Kowol-Santen and Kathrin Winkler.

[1] DFG, Förder-Ranking 2009, Institutionen – Regionen – Netzwerke, WILEY-VCH, Weinheim, ISBN 978-3-527-32746-1, 2009, p. 16.

[2] DFG, Jahresbericht 2010, Aufgaben und Ergebnisse, 2011, p. 164 (www.dfg.de).

[3] DFG, Internal Statistical Data and Management Reports, status July 2011.

[4] http://www.dfg.de/foerderung/programme/exzellenzinitiative/allgemeine_informationen/index.html

[5] GDCh, Chemiestudiengänge in Deutschland – Statistische Daten 2009, 2010, p.6.

[6] DFG press releases, No. 34 (13.7.2011). Working together for Research –Transparent – Internationa. Annual Press Conference in Berlin, 2011.

A New Molecular Architecture for Molecular Electronics

Anna Cattani-Scholz, Kung-Ching Liao, Achyut Bora, Anschuma Pathak, M. Krautloher, B. Nickel, Jeffrey Schwartz, Marc Tornow, Gerhard Abstreiter

1. Introduction

Our goal is to integrate fundamental surface science and interface synthesis chemistry with novel device architecture that is underpinned by an analysis of device physics to build next-generation molecular scale transistors with application to microelectronic devices. The promise of molecular electronics has been based on organic thin films in devices devised and studied so far. Organic thin film transistors (OTFTs) most commonly use pentacene as the semiconductor in these devices; pentacene-based OTFTs have carrier mobilities in the range of 1 cm^2/Vs and on-off ratios between 10^6 and 10^8 [1] which may rival the performance of amorphous silicon transistors. There are, however, major drawbacks of pentacene-based OTFTs, including processing issues and grain boundary limitations[2] poor sub-threshold performance and large positive threshold voltages. In order to truly realize the promise of molecular electronics, where active devices are of the scale of molecules, new device architectures must be devised where molecular control of the structure is key. We propose to create new molecular architectures based on organized growth of surface-attached organic semiconductors on nanoscale devices through directed regular stacking of bifunctional oligoarenes and organometallic complex linkers. Our new architecture eliminates the need for superdeposited pentacene or other organic semiconductors by synthesizing ordered, truly molecular devices based on new concepts of device physics that employ our unique ways to build ordered arrays of aromatics.

Our efforts are based on the application of organophosphonate chemistry as an alternative to silanization for covalent surface modification, specifically of silicon semiconductor based devices.[3,4] In particular, we have been able to prepare anthracene derivatives and analogs and to convert them to phosphonic acids by standard routes (Figure 1). We have demonstrated the growth of high quality monolayers of organics that are capped on each end by a phosphonate group, accomplished by the T-BAG method (tethering by aggregation and growth) using solvent mixtures.[5] Moreover we have learned how to generate three-dimensional, organized multilayers using techniques of coordination chemistry (Figure 2).

In this contribution we report on our preliminary investigation about the thin film properties of these novel organo-phosphonate SAMs on Si substrates using several analysis techniques, including AFM and X-ray reflectivity. In view of electrical passivation and transport properties we finally discuss first impedance spectroscopy characterization in electrolyte solution and electrical characterization in a vertical setup using a Hg top electrode.

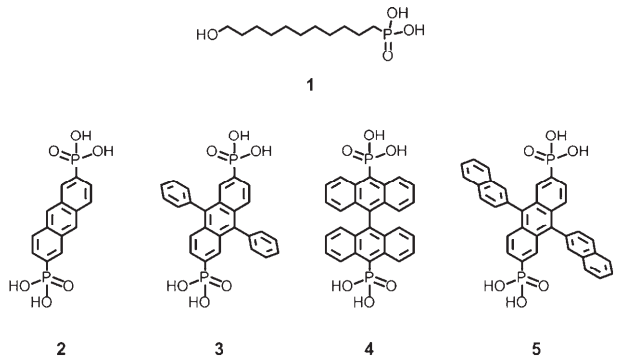

Figure 1. Chemical structure of 11-hydroxyundecylphosphonic acid (**1**) and of the anthracene derivatives 2,6-diphosphono-anthracene (**2**), 9,10-diphenyl-2,6-diphosphonoanthracene (**3**), 10,10'-diphosphono-9,9'-bianthracene (**4**), and 9,10-dinaphthyl-2,6-diphosphono-anthracene (**5**).

2. Preparation of Organophosphonate Three-Dimensional, Organized Multilayers on Silicon Oxide

This procedure involved the synthesis of two difunctional phosphonic acids and the formation of a monolayer SAMP of each on a silicon oxide/silicon wafer. This was accomplished by a simple solvent draw-down process called the T-BAG method.[5] After the SAMP was formed it was exposed briefly to vapor of titanium tetra(tert-butoxide), which gives a titanium di(tert-butoxide)-phosphonate complex on the distal surface of the SAMP. Because of the residual reactivity of the remaining tert-butoxide groups in the coordination sphere of the Ti, this complex can serve as a linker to join together two equivalents of a phosphonic acid, and because the coordination about the Ti gives rise to a net linear arrangement of these two equivalents of phosphonate, order in the monolayer SAMP is translated to the

second layer, giving a structurally ordered, three-dimensional duplex (Figure 2). Multi-monolayer structures were prepared using 2,6-diphosphonoanthracene (**2**) and 9,10-diphenyl-2,6-diphosphonoanthracene (**3**).

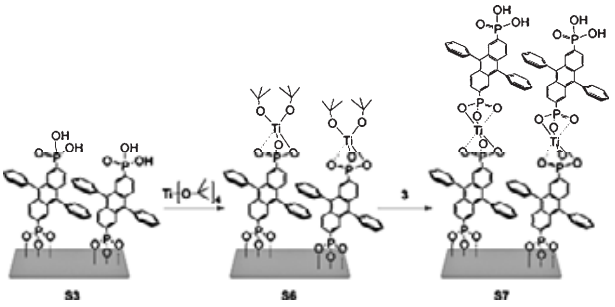

Figure 2. Synthesis of the duplex of 9,10-diphenyl-2,6-diphosphonoanthracene (**3**).

2,6-Bis(diethylphosphono)-9,10-diphenylanthracene (**6**). 2,6-Dibromo-9,10-diphenylanthracene (**7**) (2 mmol) was dissolved in flash distilled THF (70mL) under argon at -78 °C. tert-Butyllithium (Aldrich, 1.7 M, 2.5 mL, 4.25 mmol, 2.1 equiv.) was slowly injected through a rubber stopper using a glass syringe, and the resulting orange solution was allowed to stir for 30 minutes at -78 °C and then 1 hour at -20 °C. The solution was cooled back to -78 °C, and diethyl chlorophosphonate (Aldrich, 97%, 0.64 mL, 4.4 mmol, 2.2 equiv.) was added. The reaction mixture was allowed to stir first for 3 hr at -78 °C and then for 12 hr at room temperature. The resulting yellow mixture was concentrated under reduced pressure, and the recovered solid was purified by chromatography on a silica column (20% ethyl acetate/hexane eluent) affording a yellow product (Yield 94%). ^{1}H NMR (CDCl3, 500 MHz, 298K): δ = 8.29 (d, ^{3}J (H,P) = 17.00 Hz, 2H), 7.80 (d, ^{3}J (H,H) = 5.15 Hz, 2H), 7.65-7.55 (m, 8H), 7.45 (d, ^{3}J (H,H) = 6.35 Hz, 4H), 4.10-4.04 (m, 8H), 1.24 (dd, ^{3}J (H,H) = 6.65 Hz, ^{3}J (H,H) = 6.55 Hz, 12H) ppm; ^{13}C NMR ($CDCl_3$, 125 MHz, 298K): δ = 139.3, 137.4, 133.5, 133.4, 131.1, 131.0, 130.0, 129.9, 128.8, 128.2, 128.1,128.0, 126.6, 125.3, 125.2, 125.1, 62.3, 62.3, 16.3, 16.3 ppm; ^{31}P NMR ($CDCl_3$, 202 MHz, 298K): δ = 18.48 ppm; HRMS (ESI-TOF) for $C_{34}H_{37}O_6P_2$: Calc'd 603.2060 (M+H)+; found m/z 603.2064.

9,10-Diphenyl-2,6-diphosphonoanthracene (**3**). Bromotrimethylsilane (Aldrich, 97%, 1.2 ml, 6 mmol, 6 equiv.) was added to a solution of 2,6-bis(diethylphosphono)-9,10-diphenylanthracene (1 mmol) suspended in 25 mL of anhydrous methylene chloride under argon. The reaction mixture was stirred overnight, then anhydrous methanol (1.2 mL) was added, and the mixture was stirred for an additional 6 hours. The solvent was removed under reduced pressure, and the crude product was dissolved in methanol (10 mL). The solution was filtered through a filter aid packed on a fritted filter disk. The filtrate was concentrated under reduced pressure, and the recovered solid was recrystallized from ethanol, affording the bright yellow product (Yield 98%). 1H NMR (CD_3OD, 500 MHz, 298K): δ = 8.31 (d, ^{3}J (H,P) = 16.90 Hz, 2H), 7.76 (dd, ^{3}J (H,H) = 9.00 Hz, ^{3}J (H,H) = 3.65 Hz, 2H), 7.69-7.61 (m, 8H), 7.48 (d, ^{3}J (H,H) = 7.60 Hz, 4H) ppm; ^{13}C NMR (CD_3OD, 125 MHz, 298K): δ = 140.4, 139.1, 132.9, 132.8, 132.3, 132.1, 131.5, 131.1, 131.0, 130.0, 130.0, 129.3, 128.5, 128.4, 126.4, 126.3 ppm; ^{31}P NMR (CD_3OD, 202 MHz, 298K): δ = 15.42 ppm; HRMS (ESI-TOF) for $C_{26}H_{21}O_6P_2$: Calc'd 491.0808 (M+H)+; found m/z 491.0806. Diphosphonic acids **2**, **4**, and **5** were prepared similarly.

2.1. Preparation of the SAMP Duplexes of 3 on Silicon Oxide [8]

SAMPs of 3 were grown from 5 μM solutions in THF. Direct quartz crystal microgravimetry showed the molecular loading to be 0.24 nmol/cm^2. The SAMP-coated substrate (**S3**) was then placed in a deposition chamber that was equipped with two stopcocks for exposure either to vacuum or to vapor of titanium tetra(tert-butoxide) (Strem). The chamber was evacuated to 10^{-3} torr for 15 min. Samples were then exposed to vapor of Ti(O^{t}Bu)$_4$ at 10^{-3} torr for 12 minutes with active evacuation. This procedure was repeated in duplicate. Samples were then evacuated at 10^{-3} torr for 15 min. to allow for complete reaction to adduct **S6**, which was also measured by QCM to have an areal density 0.24 nmol/cm^2. Adduct **S6** was then dipped into a 10 μM solution of **3** in methanol for 2 hr to give duplex **S7**, which was then washed with methanol under sonication and measured by QCM for areal density (0.22 nmol/cm^2). Similar procedures were used to make duplex structures of **2**.

3. Characterization

Organophosphonate monolayers have been extensively characterized by a variety of techniques, such as contact angle measurements, X-ray reflectivity, ellipsometry and X-ray photoelectron spectroscopy (XPS).[4,9] However, no extensive studies on the electrochemical properties of the organophosphonate monolayers, in terms of resistive and capacitive behaviors in electrolytes, have been carried out so far. In this sense we have investigated the electrochemical properties of monolayers of 11-hydroxyundecylphosphonic acid (**1**) and of the anthracene derivatives **2**, **3**, and **4** on silicon/silicon oxide electrodes by using impedance spectroscopy. The resistive and capacitive behaviors have been quantitatively measured in aqueous electrolytes, near neutral pH. Complementary surface analysis by AFM and XRR is presented as supporting characterization, demonstrating the quality of the investigated molecular layer systems.

3.1. Thin Film Properties

Fig. 3 shows representative topography images of the molecular layer surfaces of self-assembled monolayers (SAMs) of 11-hydroxyundecylphosphonic acid (**1**) and 9,10-diphenyl-2,6-diphosphonoanthracene (**3**) acid precursors on p-doped (boron, 10^{18} cm^{-3}) silicon surfaces coated with a thin (~1 nm) silicon

oxide layer. Contact angle, AFM nanolithography and ellipsometry evidenced the homogeneity of the formed monolayers, and their thickness was determined to be 1.13+/-0.09 nm and 0.82+/-0.07 nm, respectively. The surfaces were overall homogeneous and free of pin holes. Locally, spots of larger thickness could be observed that may be assigned to residual multilayers. The surface roughness of the samples was measured for a scan area 5 µm x 5 µm and compared to that of the bare substrate. The root mean square (rms) values of roughness were found to be 0.21 nm, and 0.23 nm respectively, which was very close to 0.19 nm for the bare substrate. Complementary x-ray reflectivity measurements have been performed to determine the thickness and the scattering length density of the SAM layers of **2**, **3**, **4**, and **5** (Table 1).

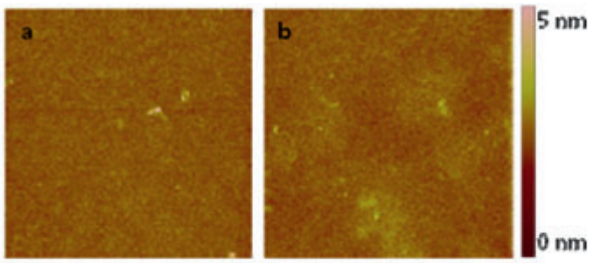

Figure 3. AFM topography of self-assembled monolayers of (a) 11-hydroxyundecylphosphonic acid (**1**) and (b) 9,10-diphenyl-2,6-diphosphonoanthracene (**3**). Image size is 5 µm ×5 µm.

	Monolayer of **2**	Monolayer of **3**	Monolayer of **4**	Monolayer of **5**
molecular volume [Å^3]	255	400	409	481
box volume [Å^3]	481	1294	853	1861
SLD_{box} [10^{-6}Å^{-2}]	9.6	5.5	8.8	4.7
SLD_{exp} [10^{-6}Å^{-2}]	8.0	4.2	7.8	5.1
thickness [Å]	7.0	8.0	8.1	9.1

Table 1. Calculated molecular volumes and experimental scattering length densities for monolayers of 2,6-diphosphono-anthracene (**2**), 9,10-diphenyl-2,6-diphosphonoanthracene (**3**), 10,10'-diphosphono-9,9'-bianthracene (**4**), and 9,10-dinaphthyl-2,6-diphosphono-anthracene (**5**), as obtained from X-ray reflectivity measurements.

To judge the packing efficiency, we have calculated the molecular volumes of the molecules using first the VABC method[10] and second a van der Waals box model, i.e., we have estimated the minimum volume of a rectangular box which includes the molecule (Table 1). The experimental scattering length densities SLD_{exp} match closely with the density obtained from the box model SLD_{box}. For the thickness, we obtain 0.70 nm, 0.80 nm, 0.81 nm, and 0.91 nm, respectively; this is about half of the full length of the molecules. This excludes an upright orientation of the molecules. Improvement of the coverage, i.e. initial grafting density, might induce a more upright orientation of the molecules. Interestingly, x-ray studies on 2,6-diphosphonoanthracene (**2**) bilayers[11] show that the addition of the second layer results in a rather vertical orientation of both layers presumably for steric reasons.

3.2. Electrochemical Impedance Spectroscopy

Fig. 4 displays a representative impedance measurement of a Si/SiO_2 substrate with and without 11-hydroxyundecyl-phosphonic acid (**1**) monolayer at V_{bias} = 0V. The recorded Bode spectra are analyzed according to the basic equivalent circuit models shown in Fig. 5. The data for the unfunctionalized sample are consistent with a simple series of one resistor and one capacitor (α). Herein, the lead resistances of the bulk semi-conductor and the electrolyte, as well as the capacitances of the semiconductor space charge region, the oxide layer and the Helmholtz layer are merged. While this circuit clearly oversimplifies the realistic situation we find that the obtained numerical values, in particular in comparison to the SAM-functionalized case, can describe the system well and do capture the main changes after coating. The oxide thickness derived from the oxide capacitance can be estimated to d=1.68 nm, in very good agreement to the thickness determined by ellipsometry d_{opt}= (1.62 +/- 0.06) nm.

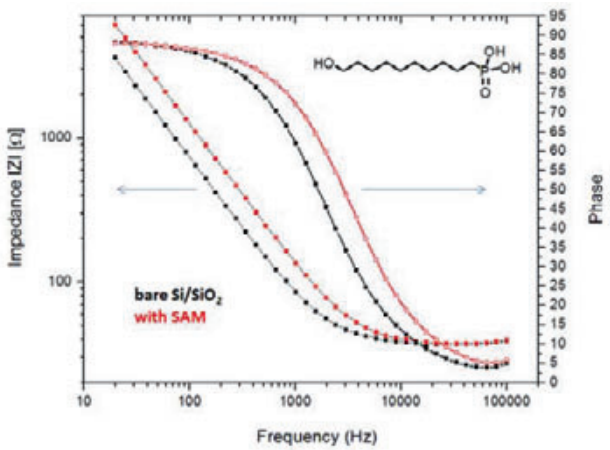

Figure 4. Bode plot of the impedance (absolute value |Z| and phase) as function of frequency, for a Si/SiO2 sample with (red) and without (black) a 11-hydroxyundecyl phosphonate monolayer coating. All shown symbols/lines are experimental data.

After functionalization of the silicon/silicon oxide electrodes with 11-hydroxyundecylphosphonic acid (**1**) both impedance curves shift to higher frequencies as expected for an additional capacitance C_{SAM}, in series, lowering the total capacitance and thereby increasing the cut-off frequency. To model this behavior we introduced an additional RC element to the equivalent circuit in Fig. 5 (β) and obtained C_{SAM}=2.64 μF/cm^2.

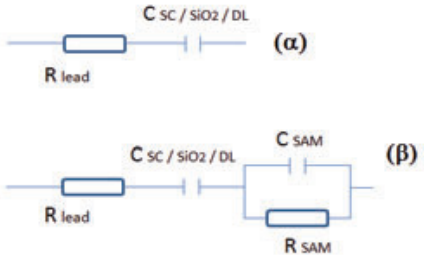

Figure 5. Equivalent circuits used to model the impedance data, R_{lead}: lead resistance of bulk semiconductor and electrolyte. $C_{SC/SiO2/DL}$: total series capacitance of semiconductor space charge layer (SC), oxide layer (SiO_2) and Helmholtz double layer (DL). R_{SAM} and C_{SAM} are the resistance and capacitance of the self-assembled monolayer, respectively.

Herein, we kept $C_{SC/SiO2/DL}$ fixed during the fitting procedure. The result is in good agreement with previously determined capacitance values for alkylphosphonates on titanium oxide and alumina.[12] The thickness of the monolayer calculated with a dielectric constant ε = 2.7 is obtained as d_{SAM} = 0.9 nm, a somewhat lower value than the one measured by ellipsometry and AFM scratching (1.1 nm).

Significantly higher capacitances around 7 to 10 μF/cm^2 were found for anthracene biphosphonic acid based films at 0V bias, with parallel resistances of the same order of magnitude as for the aliphatic SAM (data not shown). Further measurements are currently under investigation, in order to better evaluate the contribution of structural defects (pinholes), conformational rearrangements (stacking, tilting), and of electron delocalization effects (polarizability, dipole formation) to the overall capacitive properties of this new class of aromatic hybrid systems, in particular addressing the controlled growth of novel bilayer stacks by using metal ion coordination centers.[11]

4. Electrical Transport Characterization

The electrical transport through SAM molecules deposited on Si/SiO_2 surfaces was investigated by measuring the current-voltage (I-V) characteristics using a two terminal configuration, where a degenerately doped p-Si substrate was used as one electrode and a hanging Hg drop was used as another electrode (Fig. 6-a). The usage of a Hg drop as one electrode facilitates formation of a quick and reliable contact on the SAM with reproducible contact area and negligible risk of metal penetration through the SAM due to the high surface tension of Hg.[13] We have studied aliphatic as well as aromatic SAMs having identical end groups.

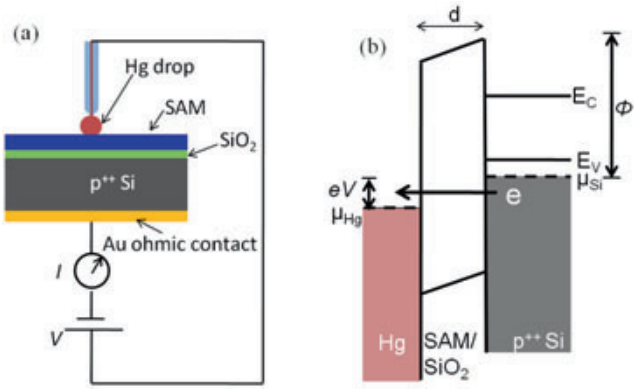

Figure 6. Schematic of (a) electrical characterization using a hanging Hg drop as top electrode and (b) respective tunnel barrier model under an applied bias V (not to scale). Note that the Si chemical potential is located within the valence band due to degenerate doping.

Figure 7 shows current density vs. voltage curves for 9,10-diphenyl-2,6-diphosphonoanthracene (**3**) SAMs in comparison to a model aliphatic compound 1,4-diphosphonobutane (purchased from Acros Organics). Each experimental data shown here were obtained by averaging over around 30 *J-V* plots measured at different positions of a given sample. Since the total thickness of the SAM and the SiO_2 was about 2nm, tunnelling of charge carriers could be a prevailing transport mechanism. Hence, we modelled our system within the framework of non-resonant tunnelling through a trapezoidal barrier consisting of the SAM and the SiO_2 (Fig. 6-b), fitting the measured *J-V* data to Simmons' equation[14]

$$J = \frac{e}{2\pi h d^2}\left[\left(\phi - \frac{V}{2}\right)e^{-\frac{4\pi d}{h}\sqrt{2\alpha . m_e\left(\phi - \frac{V}{2}\right)}} + \left(\phi + \frac{V}{2}\right)e^{-\frac{4\pi d}{h}\sqrt{2\alpha . m_e\left(\phi + \frac{V}{2}\right)}}\right]$$

where ***d***= effective barrier width, ***Φ*** = barrier height (***Φ*** > ***V***) and ***α*** is a correction factor to account for a non-ideal barrier shape and effective electron mass, taking ***Φ*** and ***α*** as fitting parameters. The measured *J-V* data for both SAMs can be excellently described within this model. We observed differences of barrier heights depending upon the bias polarity, which is expected for dissimilar electrode materials. The barrier heights for the 1,4-diphosphonobutane acid SAM were found to be much higher (3.63 eV and 3.18 eV at positive and negative biases to Si, respectively) than those for the 9,10-diphenyl-2,6-diphosphono-anthracene (**3**) SAM (0.95 eV and 0.69 eV). This observation can

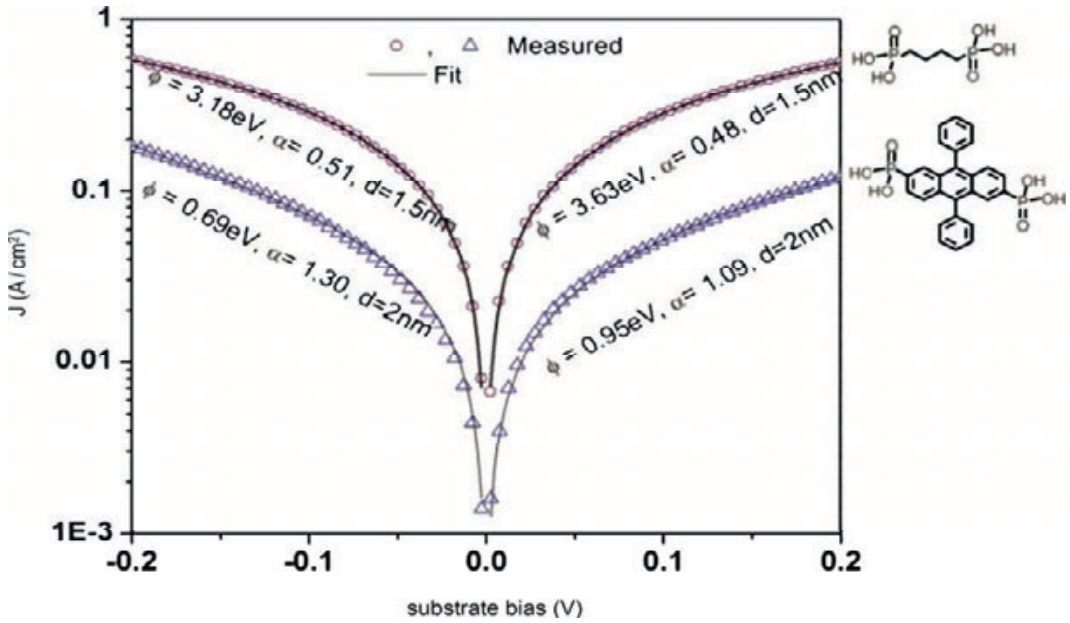

Figure 7. Absolute value of the current density as a function of substrate bias for 1,4-diphosphonobutane (top curve) and 9,10-diphenyl-2,6-diphosphonoanthracene (**3**) (bottom curve) SAMs on highly p-doped Si (10^{20} cm^{-3}). Open symbols are measured data and lines are model fits, with several of the fitting parameters displayed.

be explained by the fact that the height of the barrier would depend on the molecular orbital level energies of the SAM molecules. As supported by DFT calculation the aliphatic SAM precursors have a much larger energy gap between their highest occupied molecular orbital (HOMO) and lowest unoccupied molecular orbital (LUMO), compared to the aromatic one comprising a conjugated electron system. Details of this analysis will be published separately.

Summary

Understanding the electronic transport through layered systems comprising organic functional layers in direct contact to semiconductor surfaces is of major importance for future applications in nanoelectronics, photovoltaics and sensors. We report on the successful deposition of self-assembled monolayers (SAMs) of alkyl and aryl phosphonates onto silicon/silicon oxide substrates. These SAMs further served as a basis for the preparation of novel three-dimensional, organized bilayers of anthracene diphophonates, using techniques of coordination chemistry under controlled conditions by deposition of organometallic linkers onto the monolayers. We have characterized the mono- and bilayer systems on planar surfaces by AFM and XRR measurements. Furthermore the electrochemical properties of the organophosphonate monolayers, in terms of resistive and capacitive behaviors, were quantitatively analyzed by impedance spectroscopy. Finally we discuss preliminary electrical characterization data of aliphatic as well as aromatic organophosphonate systems in vertical transport using a metal top electrode.

Zusammenfassung

Für zukünftige Anwendungen in der Nanoelektronik, Photovoltaik und Sensorik ist ein grundlegendes Verständnis des elektronischen Transports durch Strukturen aus organischen Funktionsschichten in direkter Verbindung mit Halbleiteroberflächen von herausragender Bedeutung. Wir berichten über die erfolgreiche Deposition selbst-assemblierter Monolagen („self-assembled monolayers", SAMs) aus Alkyl- und Arylphosphonaten auf Si/SiO_2-Substraten. Diese SAMs dienen uns u.a. als Grundlage für die Präparation neuartiger, dreidimensionaler, geordneter Doppelschichten aus Antracen-Diphosphonaten. Hierfür kommen Techniken der Koordinationschemie unter kontrollierten Bedingungen zum Einsatz, bei welchen vor der zweiten SAM-Beschichtung organometallische Linker auf die Monolagen deponiert werden. Wir haben die Mono- und Doppellagensysteme auf planaren Oberflächen mit Hilfe von AFM und XRR-Messungen charakterisiert. Weiterhin konnten wir quantitative Analysen von elektrochemischen Impedanzspektroskopie-Messungen durchführen und so die Organophosphonat-Monolagen in Bezug auf ihre resistiven und kapazitiven Eigenschaften charakterisieren. Schließlich diskutieren wir erste elektrische Charakterisierungen von aliphatischen und aromatischen Organophosphonatsystemen in einem vertikalen Transportexperiment, bei welchem die Monolagen mit einer oberen Metallelektrode kontaktiert wurden.

Jeffrey Schwartz [1)*] *is Professor at the Department of Chemistry at Princeton University.*

Email: jschwart@princeton.edu

Marc Tornow [2)] *is Professor at the Institut für Halbleitertechnik at the Technische Universität Braunschweig.*

Email: m.tornow@tu-bs.de

Anna Cattani-Scholz [3)*] *is research assistant at the Zentrum für Nanotechnologie und Nanomaterialien at the Walter Schottky Institute of the Technical University München.*

Email: cattani@wsi.tum.de

** corresponding authors*

Working departments of coauthors: K.-C. Liao [1)], A. Bora [2)], A. Pathak [2)], M. Krautloher and B. Nickel [4)], G. Abstreiter [3)]

Addresses:

[1)] Department of Chemistry, Princeton University, Princeton, NJ 08544, USA

[2)] Institut für Halbleitertechnik, Technische Universität Braunschweig, Hans-Sommer-Str. 66, 38106 Braunschweig, Germany

[3)] Zentrum für Nanotechnologie und Nanomatrialien, Walter Schottky Institut, Technische Universität München, Am Coulombwall 4a, 85748 Garching, Germany

[4)] Department of Physics & CeNS, Ludwig-Maximilian Universität München, München, Germany

Project description & Acknowledgement

In order to truly realize the promise of molecular electronics, where active devices are of the scale of molecules, new device architectures must be devised where molecular control of the structure is key. The work presented here builds on our ability to synthesize and characterize self-assembled monolayers and multilayers of active molecules by incorporating them into new device architectures. Our efforts are based on the application of organophosphonate chemistry as an alternative to silanization for covalent surface modification, specifically of silicon semi-conductors based devices.

The authors gratefully acknowledge funding by the DFG (grants AB 35/8-1, TO 266/2-1), by the NSF (CHE-0924104), by the Braunschweig International School of Metrology IGSM, and by the Nanosystems Initiative Munich.

[1] D. J. Gundlach, Y. Y. Lin, T. N. Jackson, S. F. Nelson, D. G. Schlom, *IEEE Electron Device Lett.* **1997**, *18*, 87-89.

[2] M. Shtein, J. Mapel, J. B. Benziger, S. R. Forrest, *Appl. Phys. Lett.* **2002**, *81*, 268-270.

[3] A. Cattani-Scholz, D. Pedone, F. Blobner, J. Schwartz, M. Tornow, L. Andruzzi, *Biomacromolecules* **2009**, *10*, 489–496.

[4] A. Cattani-Scholz, D. Pedone, M. Dubey, S. Neppl, B. Nickel, P. Feulner, J. Schwartz, G. Abstreiter, M. Tornow, *ACS Nano* **2008**, *2*, 1653-1660.

[5] E. L. Hanson, J. Schwartz, B. Nickel, N. Koch, M. F. Danisman, *J. Am.Chem. Soc.* **2003**, *125*, 16074-16080.

[6] K.-C. Liao, A. G. Ismail, L. Kreplak, J. Schwartz, I. G. Hill, *Adv. Mater.* **2010**, *22*, 3081-3085.

[7] P. Hodge, G. A. Power, M. A. Rabjohns, *Chem. Commun.* **1997**, 73-74.

[8] J. E. McDermott, Ph. D. thesis, Princeton University, **2007**.

[9] M. Dubey, T. Weidner, L. J. Gamble, D. G. Castner, *Langmuir* **2010**, *26*, 14747-14754.

[10] Y. H. Zhao, M. H. Abraham, A. M. Zissimos, *J. Org. Chem.* **2003**, *68*, 7368-7373.

[11] A. Cattani-Scholz, K-C. Liao, A. Bora, C. Hundschell, A. Pathak, B. Nickel, J. Schwartz, G. Abstreiter, M. Tornow, "*Electrochemical Characterization of Self-Assembled Organophosphonate Monolayers and their Three-Dimensional Organized Bilayers on Silicon/Silicon Oxide Electrodes*", **2011**, in preparation.

[12] H. Klauk, U. Zschieschang, J. Pflaum, M. Halik, *Nature* **2007**, *445*, 745-748.

[13] H. Haick, D. Cahen, *Acc. Chem. Res.* **2008**, *41*, 359-366.

[14] J. G. Simmons, *J. Appl. Phys.* **1963**, *34*, 2581-2590.

Chemical Methods for the Generation of Graphenes and Graphene Nanoribbons

Jan M. Englert, Andreas Hirsch, Xinliang Feng, Klaus Müllen

Synthetic carbon allotrope chemistry is currently among the most rapidly growing topics in materials chemistry. The youngest and at the same time probably the most promising representative of new carbon allotropes is graphene. In this article we outline our recent contributions to chemical graphene formation and functionalization.

1. Introduction

In recent years graphene being the youngest representative of the growing family of synthetic carbon allotropes has attracted overwhelming attention due to outstanding and unprecedented physical and materials properties, such as novel magneto-transport and high charge carrier mobility in the ballistic regime at temperatures up to 300 K. Structurally, these single sheets of graphite can be considered as a mother of all expanded aromatic carbon modifications and they have been considered for a very long time to be an exclusively theoretical material. The first preparation of single graphene layers succeeded in 2004 *via* a straightforward mechanical exfoliation of graphite using a scotch tape. This method, however, is not suitable for mass production, which on the other hand is required when targeting large scale practical applications of graphene. In principle, there are two major strategies to prepare graphene or graphene derived nanoforms, namely, the top-down exfoliation of graphite and *de novo* bottom up approaches using suitable small precursor molecules that can be condensed to extended two-dimensional conjugated π-systems. We report here on our recent investigations in both directions, a) the wet-chemical functionalization and exfoliation of graphite leading to free as well as covalently and non-covalently functionalized graphene and b) the cyclodehydrogentation of oligophenyl precursors as a highly versatile bottom-up strategy for the formation of atomically well defined graphene nanoribbons.

2. Exfoliation of Graphite

In order to generate individualized graphene sheets out of graphite the most obvious obstacle is to overcome the strong π/π interaction adhering them in graphite. On the other hand, graphene can undergo also pronounced interactions with substrates, which initially enabled generation of single layer graphene (SLG) from highly ordered pyrolytic graphite (HOPG) by sticky tape exfoliation in 2004.[1] With suitable post-processing the extrinsic corrugation of the substrate can be further utilized to improve the single layer yield of mechanical exfoliation on very large areas.[2]

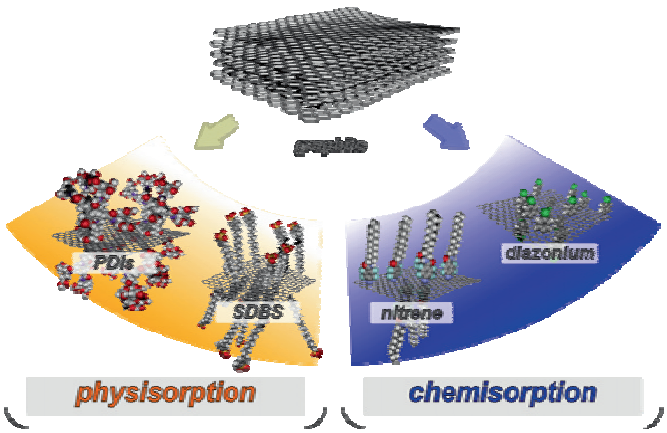

Figure 1. Wet chemical top down approaches for the generation of graphene sheets out of graphite. Non-covalently functionalized graphene mediated by surfactants such as amphiphilic perylenediimides or SDBS (left) and covalently functionalized graphene generated, for examples, by reactions with nitrenes or diazonium salts (right).

The cohesive energy gained by stacking graphene sheets onto each other was experimentally determined to be as high as 61 meV/C-atom.[3] Similar challenges had to and still have to be met for debundling and "unmeshing" carbon nanotubes, which share the hexagonal sp2-carbon network with graphene but present a convex outer surface. This significantly reduces the areal interaction and facilitates exfoliation.. A promising approach to the target of exfoliation was to search for solvents balancing the cohesive energy term, which could enable the generation of meta-stable dispersions of graphene, CNTs and other carbon based nanostructures by application of ultrasonication.[4] In the case of CNTs these considerations led to the identification of a series of lactam- or lactone based solvents providing appreciable concentrations of dissolved carbon nanotubes.[5] Consequently, in

2008, this concept has been applied microcrystalline graphite, where most effective solubilization after sonication and centrifugation was found for those liquids that match a surface tension of 40-50 mJ m^{-2}. Among the most prominent representatives of these solvents are N-methylpyrrolidone (NMP), N-cyclohexylpyrorlidone (CHP), benzylbenzoate (BBZ), γ-butyrolacton (GBL). These effectively reduce the energetic penalty connected with dissolution of the graphite by balancing the graphene/graphene interactions.[6]

Encouraged by these findings we and other groups went forward aiming for advanced noncovalent stabilization techniques.[7] Next to the direct ultrasound aided solvent exfoliation of graphite an alternative is taking advantage of the hydrophobic effect using suitable surfactants. While doing so the entropy penalty for the solvent, in particular water is kept low due to the formation of surfactant cages around the material to be dispersed. Obviously, in order to fully exploit the hydrophobic effect the use of very polar media, at best water, is mandatory in the first place. Graphite does not constructively interact with the water phase unless it is subjected to ultrasonication in the presence of dissolved detergents. While the use of commercially available detergents like SDBS, SDS or bile salts enable e.g. ultracentrifugation based purification protocols[8] and large scale liquid phase production of graphene, specialized π-detergents permit solution bound spectroscopies. Our previous investigations on carbon nanotube dispersions suggested the use of electron deficient amphiphilic or bolaamphiphilic perylenediimide (PDI) surfactants (Scheme 1),[9-11] which can undergo pronounced π-π stacking interactions with carbon nanotubes in water.[12]

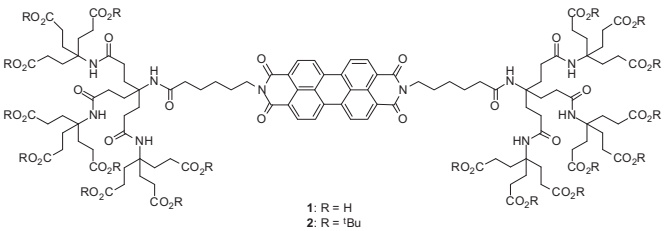

Scheme 1. Bolaamphephilic perylenediimide (PDI) equipped with two 2nd generation Newkome dedrimers. The watersoluble moiety **1** is obtained after quantitative acidic deprotection of **2**.

The features of these amphiphiles, namely dendrimer mediated solubility in water, characteristic absorption and emission properties in the visible light region together with high fluorescence quantum yields paved the way to an in depth understanding of carbon nanotube dispersion, individualization and doping.[13] We expected that our experience with carbon nanotube dispersion studies will provide insight into solution phase graphite exfoliation. Indeed, we could show that dendronized amphiphilic perylenes such as **1** (Scheme 1) are able to exfoliate graphite in water.[9] The characteristic spectroscopic properties of PDIs such as **1** allowed for the characterization and quantification of the perylene/graphene interaction. In particular pronounced π-π-stacking interactions were observed as demonstrated by efficient emission quenching - even upon resonant laser excitation of the PDI.[10]

Although graphite is chemically rather inert it has been known for a long time that it can undergo a series of reactions providing graphite intercalation compounds (GICs). GICs may be considered salts of the amphoteric carbon host classified as *donor* or *acceptor* compounds depending on the electronic nature of the guest which is to be intercalated. Intercalation usually occurs in a stoichiometric fashion forming ordered layers of the guest located parallel to the graphene sheets, which in turn increases the carbon/carbon interlayer distance and thus, depending on the stage of the GICs, virtually reduces or completely removes the π/π interaction in the crystal. On the other hand, ionic or dipolar interactions are introduced at the same time stemming, for example, from electron transfer from the guest to the carbon host or *vice versa*. Acceptor GICs of strong oxidizing acids like sulfuric acid or ferric chloride are known to form after charge transfer from the sheets to the guest.[14] The opposite situation, namely an electron transfer onto the graphene sheet, was found when for the first time potassium was intercalated into graphite crystals to form a first stage donor-GIC.[15] Evidence for dissolved negatively charged graphene generated from the potassium GIC KC_8 was found after the treatment with polar aprotic solvents under inert atmosphere.[16] According to this approach we came up with the concept of a balanced combination of intercalation combined with coulomb driven exfoliation and repulsion. This opens the door for wet chemical functionalization of the electronically activated graphene sheets *via* recombination with reactive addends. In the following two sections these new developments in non-covalent and covalent graphene functionalization will be outlined.

2.1. Surfactant Aided Exfoliation

The surfactant based exfoliation in biocompatible nontoxic and *green* solvents like water is one of the most promising routes to large scale production of cost efficient graphene dispersions. However, it remains challenging to carry out a reliable bulk analysis of the degree of exfoliation and of the determination of the number of layers in the resulting dispersed particles. As a consequence, a model system that reflects the dispersion properties of graphene without sacrificing spectroscopic insight was required. Expanded polyaromatic molecules like hexa-*peri*-benzocoronenes (HBC) can offer monodispersity with precisely defined absorption and emission features while resembling many of the aggregation phenomena of graphite. Thus it can be anticipated that detergents and dispersion protocols which yield a high amount of HBC monomer in aqueous solution also would result in appreciable yields of graphene monolayers. First investigations based on commercially available surfactants such as sodium dodecylbenzenesulfonate (SDBS), sodium cholate (SC) and sodium deoxycholate (SDC) (Scheme 2) were carried out in our laboratories and revealed significant differences in material uptake and individualization efficiencies.

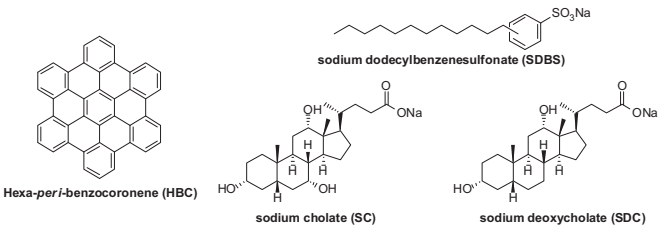

Scheme 2. Structural representation of hexa-*peri*-benzocoronene (HBC), sodium dodecylbenzenesulfonate (SDBS), sodium cholate (SC) and sodium deoxycholate (SDC)

While the highest overall material uptake could be observed in amphiphilic SDBS dispersions, the use of SDC on the other hand led by far to the highest degrees of individualization. Individualized HBC molecules could easily be identified by their characteristic emission pattern and quantified by fluorescence lifetime analysis. In contrast, when graphite was used for surfactant assisted exfoliation into graphene, solution based bulk analytical access is not easily provided with such surfactants due to the lack of descriptive optical properties either of graphene or the detergent itself. With the use of chromophors such as perylenes as part of the surfactant structure these shortcomings can be overcome. By doing so also enhanced interactions with graphene layers can be achieved. Besides the ultrasound based exfoliation of graphite down to high quality single graphene layers in water, also electronic communication between the perylene-anchor and graphene could be investigated. This is manifested in quantitative fluorescence quenching in the solid phase that can be explained in terms of electron or energy transfer of the photoexcited $S_{n>0}$ state into the graphene conduction band (photoinduced n-doping of graphene) or by fast filling of the electron vacancy in the photoexcited PDI S_0 level by a graphene valence band electrons (photoinduced p-doping of graphene).[10] Ground state p-doping of carbon nanotubes like CNTs by PDIs has been carefully investigated[13] and justifies the assumption of latter process being the reason for the efficient quenching of the PDI emission after deposition. The pronounced interaction of graphene and the perylene moiety in turn even allowed the acquisition of a resonantly enhanced Raman spectrum of the PDI/graphene complex which, without the strong interaction, would just result in superimposition of the weak Raman signal by the strong emission pattern of the PDI.

2.2. Covalent Bulk Functionalization of Graphene

The procedures to generate solutions or dispersions of graphene in water or special solvents discussed so far rest on non-covalent interactions. The oldest known approach to generate soluble graphite or graphene however is based on oxidative covalent chemistry (Fig. 2).[17] As early as in 1860 oxidation of graphite powder carried out by Brodie allowed to produce oxidized material which resembles the properties of presently known graphene oxid (e.g. swelling in water). The water solubility is mediated by the presence of a myriad of oxygen containing functional groups like carboxyl-, carbonyl-, epoxide and alcohol groups including defects (holes) in the sheets.[18] These randomly formed functionalities are the reason for the easy dissolution of graphite oxide into single layer graphene oxide in water or solvents of comparable polarity.[19] These functional groups greatly disturb the aromatic hexagonal carbon network of the graphene basal planes. Attempts to regenerate the initial order by various reduction agents like e.g. hydrazine treatment[20] or physically via thermal annealing[21] so far failed. Anyway, the carboxylic acid groups attached to the carbon framework resemble very useful and versatile anchors for further functionalization by means of organic chemistry. Another possibility for graphite functionalization is the direct treatment with very "hot" reagents such as hydrogen plasma, fluorine gas or radicals. Evidence was provided that a large amount of sp^3-defects was introduced this way, which is indicative of successful addend binding. In the case of the treatment with atomic hydrogen even the perfunctionalization, namely, the formation of graphane was discussed.[22] Recently also azomethin ylides[23] or benzynes[24] provided covalently functionalized graphene *via* cycloaddition reactions and finally edge selective functionalization have be achieved by Friedl-Crafts like acylation routes.[25]

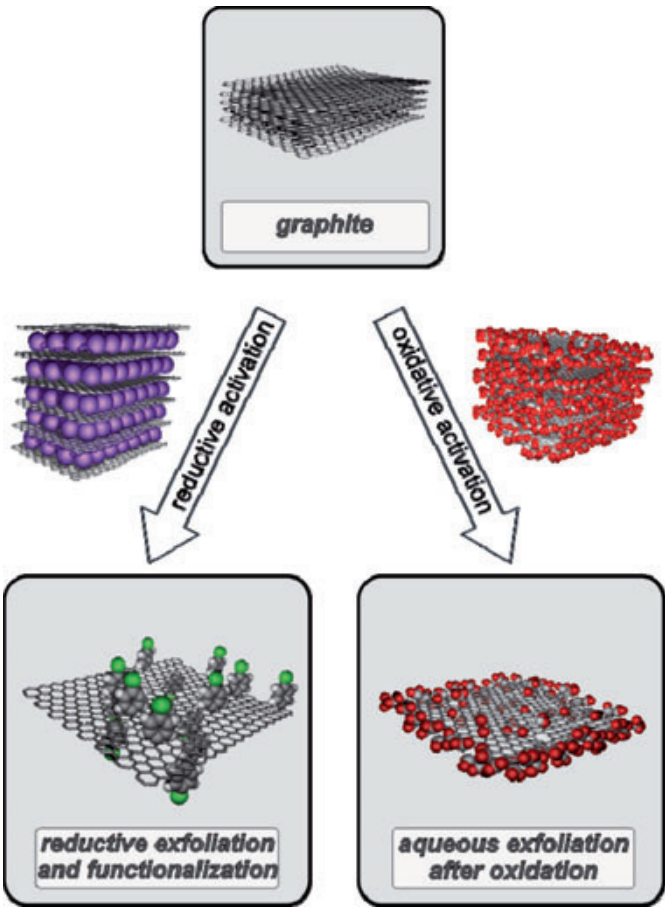

Figure 2. Covalently functionalized graphene by oxidation of graphite leading to graphene oxide (right) or via the recombination of potassium GICs with acitved addends such as diazonium salts (left).

One very versatile approach for covalent carbon allotrope functionalization is aryl diazonium based derivatization. So far diazonium cations have been used to successfully functionalize e.g. carbon nanotubes, graphite surfaces or even glassy carbon materials.[26] The reactants can be activated through thermal shock, host material electron transfer or electrochemically. We have recently reported on the first wet chemical graphene functionalization by the reaction of aryl diazonium compounds with *in situ* activated, exfoliated and reduced graphene.[27] Reduced graphene sheets were obtained from spontaneously dissolved GICs which have been synthesized in solutions of liquid sodium/potassium alloys in 1,2-dimethoxyethane (DME) as inert and electride/alkalide stabilizing solvent. Working in DME in contrast to the more commonly used liquid ammonia (classical Birch conditions) offers the opportunity of working at room temperature and also allows using most diazonium compounds in solutions because DME does not decompose the labile diazonium moiety. After addition of the diazonium salt to the dispersion of reduced and exfoliated graphene sheets functionalization takes place accompanied by fast nitrogen evolution. The functionalized material can be recovered by means of spin-casting, filtration or dip-coating for spectroscopy and microscopic characterization. High-resolution transmission electron microscopy (HRTEM) allowed for the observation of amorphous domains among crystalline areas in the flake's surface. After introduction of heteroatom markers into the diazonium salt addends additional characterization by elemental and chemical analysis through EDX and XPS was accomplished. The aryl moiety was found to exhibit typical emission patterns and could be quantified by thermogravimetry. Annealing of the material at 1000°C under inert gas allowed for the complete regeneration of the hexagonal carbon network which is in stark contrast to graphene oxide materials as up to now no possibility exists to heal hole defects which are generated during the cleavage of the addends. This complete reversibility is combined with the possibility of varying both the nature of the addend and the degree of functionalization to a large extend. Hence, these new graphene modification protocols open the door to a broad variety of functional and processable graphenes with tailored properties.

3. Directed Synthesis of Graphene Nanoribbons

Graphene nanoribbons (GNRs), which are narrow and straight stripes of graphene, are expected to exhibit quantum confinement and edge effects which make them attractive for the fabrication of nanoelectronic devices. In general, all GNRs with width smaller than 10 nm show the semiconducting property, while zigzag-type GNRs are always metallic.[28, 29] Therefore, the band gap of GNRs can be effectively tailored through the control of their width and edge structure. Due to the localized states at the edges, zigzag GNRs can allow spin-polarized electron transport, which makes them interesting for application in spintronics.[30]

A number of top-down methods have been devised to fabricate GNRs. They were initially produced by physical methods such as high resolution electron beam lithography.[31] Later, chemical means like liquid exfoliation of graphene with the assistance of functional polymers,[32] controlled plasma etching of graphene[33] and unzipping of carbon nanotubes[34, 35] in solution and on surface have been proposed to prepare GNRs with widths down to 5 -10 nm which is needed to bring about semiconducting characteristics with high on/off transistor operations. Due to the abundant availability of CNTs, the longitudinal unzipping of multiwalled CNTs may offer a feasible production of GNRs on a large scale. However, all these approaches fail to control the size and edge structure and thus only provide poorly defined graphene materials.

In order to achieve GNRs with defect-free edges and widths below 5 nm, a bottom-up synthetic strategy starting from small aromatic building blocks has been established in the past few years.[36-38] In this approach, the final GNRs are exclusively determined by the type and shape of precursor monomers employed. Actually, this strategy has been widely adopted to build up extended PAHs of different size, symmetry and periphery together with various functional substituents.[39,40] Structurally well-defined PAHs with carbon numbers up to 222 have been synthesized and fully characterized in the past decade.[41] These graphene-type molecules show tailorable optoelectronic properties which are dependent upon the size and edge structure. They also display interesting supramolecular behaviour at different length scales in solution, in bulk and on surfaces which leads to promising applications in molecular electronics and organic electronics.[42] Typically, two-step syntheses are involved to make GNRs. In the first step, the monomers need to be coupled covalently for yielding pre-organized polyphenylene precursors that have a (2D) planar projection without any overlapping of benzene rings. In the second step, intramolecular cyclcodehydrogenation associated with planarization has to be carried out to furnish the final GNRs. This synthetic strategy has been firstly developed for solution synthesis for which the solubility of precursors and compatibility with the reaction conditions need to be considered. Very recently, we and co-operators hypothesized that a catalytic surface may also provide a platform for the GNR and graphene synthesis with atomic precision.[43] In this way, the processing of single GNRs can be facilitated by performing the reaction on the surface. Therefore, in the following two sections, we will demonstrate the synthesis of GNRs in solution and on surfaces, respectively.

3.1. Solution synthesis of GNRs

As we discussed above, the solution synthesis of GNRs will firstly rely on the build up of oligo/poly-phenylene precursors. Afterwards, the *Scholl*-type intramolecular oxidative cyclodehydrogation in the presence of Lewis acids and oxidants is typically employed to produce GNRs. The use of the weaker Lewis acid $FeCl_3$ renders a sufficient oxidation potential for C-C bond formation during cyclodehydrogenation.[40] Other oxidant systems such as $AlCl_3/CuCl_2$,[44] $PhI(OOCCF_3)_2/BF_3.Et_2O$[45] and DDQ/H^+ [46] can also be used for this purpose. In an early case, the Diels-Alder reaction was demonstrated for the synthesis of

soluble branched polyphenylenes with high molecular weight.[36] However, the presence of three structural isomeric units within precursor polymers caused by the irregular Diels-Alder cycloaddition can not allow the generation of final GNRs with the singly defined conformation. Nevertheless, the $FeCl_3$ mediated cyclodehydrogenation afforded a black, insoluble powder with graphite-like appearance. Raman, infrared spectroscopy and high-resolution transmission electron microscopy (HR-TEM) further disclose that the final materials possess graphite-type features. Later, one-dimensional linear GNRs (**6**) were obtained by oxidative cyclodehydrogenation of hexaphenylbenzene-type polymers (**5**) derived from a sterically hindered Suzuki-Miyaura coupling between 1,4-diido-2,3,5,6-tetraarylbenzene (**3**) and the bis-boronic ester of hexaphenylbenzene (**4**) (Scheme 3).[37] Gel-permeation chromatography (GPC) analysis indicates a number-average molecular weight of $Mn=1.39*10^4$ g/mol with a low polydispersity value of PD=1.2, which is further confirmed by MALDI-TOF mass spectroscopy. After $FeCl_3$ based cyclo-dehydrogenation, a black solid was produced which dissolves well in common organic solvents. This fact can be attributed to the introduction of a large number of branched alkyl chains located at the adjacent position of the aromatic periphery, which are known to reduce the aggregation in solution. High cyclodehydrogenation efficiency can be confirmed based on the mass analysis and UV-vis spectroscopy. The TEM study on a solid film of GNRs reveals a well-ordered stacking of the graphene layers with a π-stacking distance of 0.34 nm, suggesting that the GNRs prone to stack together as similar to the behaviour of graphene. After drop-casting the solution of **6** on the HOPG surface, single objects of GNRs with lengths from 8 to 12 nm can be clearly visualized by means of scanning tunnelling microscopy (STM). Therefore, this result clearly demonstrates that the bottom-up organic synthesis can serve as a powerful protocol for fabricating GNRs with well-defined structure.

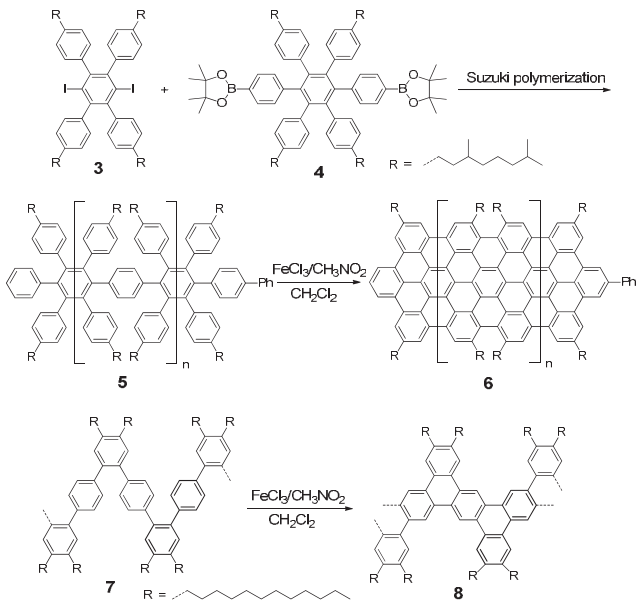

Scheme 3. Synthesis of linear (**6**) and kinked (**8**) graphene nanoribbons.

It should be however noted that it remains a great challenge to achieve long GNRs by using the above methods which generally suffer from the difficulty of obtaining high molecular weight polyphenylene precursors. To overcome this obstacle in the polymerization step, very recently, we improved the concept by introducing nonrigid kinked polyphenylene backbones. This strategy led to a significantly increased solubility of polyphenylene systems (Scheme 3).[38] The precursors **7** can be prepared by the microwave assisted Suzuki polycondensation of ortho-dibromobenzenes and benzene-1,4-dibornonic esters. For polymer **7** with solubilising dodecyl chains, GPC analysis with polystyrene (PS) standards indicates an average molecular weight of Mn=9900 g/mol with a polydispersity index as low as 1.40. MALDI-TOF mass suggests that molecular weight up to 20000 g/mol can be detected. Thereby, full dehydrogenation of polyphenylenes with a length of more than 40 nm is possible upon the treatment of $FeCl_3$ mediated Scholl reaction. The perfectly defined nanoribbons **8** are still soluble in common organic solvents, which make further structural characterizations and processing of GNRs from solution possible.

3.1. Surface synthesis of GNRs

Albeit great progress has been achieved in the wet chemical synthesis of GNRs by means of the bottom-up strategy, several obstacles may obstruct its general applicability. One particular problem is the re-aggregation of graphitic structures during the cyclodehydrogenation step which always leads to the difficulty of regenerating single graphene species. Therefore, further processing of aggregated GNRs is necessary in order to uncover their intrinsic electronic and optic properties. Like the solution exfoliation of graphite and HBC with the assistance of surfactants which has been discussed in Section 2, the exfoliation of GNRs by means of covalent and non-covalent methods are being pursued in our groups. It is also the motif of our joint project that fully exfoliated single GNR objects can be readily accessed in solution environment or on surfaces. And eventually we expect to gain further structural information of GNRs and push forward to electron transport studies of single GNR.

An alternative approach to the synthesis of GNRs by the "stitching up" of oligophenylene precursors associated with intramolecular cyclodehydrogenation and planarization is performed directly on a metallic surface that can provide a catalytic role on stabilizing intermediates and lowing the energy barrier of these reactions.[43] For this approach, the precursor monomers should be firstly deposited on the surface with monolayer coverage via sublimation. Afterwards, these carefully selected molecular building blocks should react with each other via two thermal activation steps. During the first thermal treatment, the dehalogenated intermediates of monomers contain enough thermal energy to diffuse along the surface and form polymer chains through radical addition. In the second heating process which is normally carried out below 500 °C, the thermally mediated intramolecular cyclodehydrogenation will take place and generate final GNRs on the surface. For instance, the intermolecular coupling of 10,10'-dibromo-9,9'-bianthryl (**9**)

on a gold surface can be realized through a thermal annealing at 200 °C (Scheme 4).[43] The surface-stabilized biradical species form single covalent C-C bonds to furnish linear polymer precursors. The second step of thermal treatment to 400 °C induces intramolecular cyclodehydrogenation of polymer precursors, which can be monitored under the STM. Apparently, as demonstrated in Scheme 4b and 4c, the topology of resulting GNRs is exclusively governed by the precursor monomer utilized. STM simulations are perfectly consistent with experimental images, confirming the reaction products are atomically precise N=7 GNRs with fully hydrogen-terminated armchair edges (Scheme 4c). High monolayer density coverage of GNRs on gold surface can be achieved, and no obvious structural defects can be observed in GNRs, which can not be accessed by the present top-down approaches. A simple "chip-to-chip press" method suggests that the GNRs can be readily transferred from gold films onto a SiO_2 substrate.

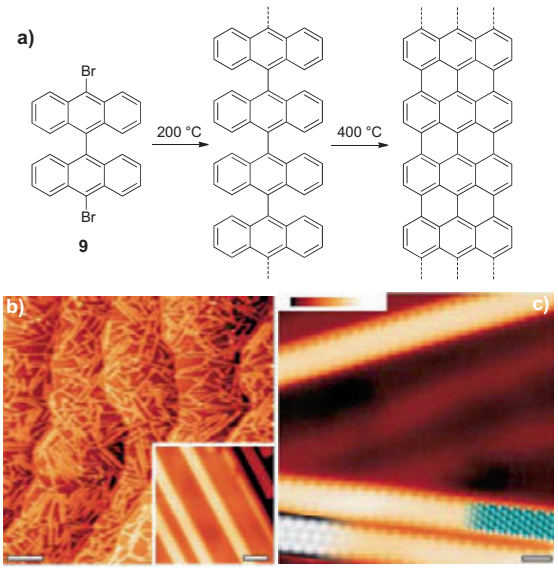

Scheme 4. Surface synthesis of straight graphene nanoribbons (N=7). a) reaction scheme from bianthryl monomer (9) to GNRs. b) overview of STM image after cyclodehydrogenation at 400 °C. c) High resolution STM image of the GNRs. (Copyright Nature 2010 publishing group)

This renders a possibility to build up electronic devices on such GNRs. Raman spectra of these GNRs both on gold and SiO_2 surface reveal the specific vibrational modes that arise from their defined edge and low dimensionality. In addition, this surface-mediated synthesis approach allows the fabrication of graphene with much more complex architectures. For instance, a chevron-type GNRs with pure armchair edge structure and three-fold GNR junction based on two different monomers can be also efficiently produced.[43] Moreover, extended nanographene[47] and porous graphene[48] nanostructures have been demonstrated by this synthetic approach starting from defined oligophenylene precursors. There is no doubt that the surface-mediated bottom-up approach will provide a route to GNRs with engineered chemical and physical properties. It is also our aim within this project to realize the synthesis of novel graphene architectures including the theoretically predicted graphene quantum dots, boron/nitrogen-doped graphenes, and GNRs with zigzag edge peripheries.

Summary

Chemical entries into the constantly growing general field of graphene can be categorized in two major classes. On the one hand there is the category of top-down approaches starting from easily available graphite sources following the exfoliation route and on the other hand there is the bottom up technique offering atomic precision of produced materials by means of organic synthesis. The top-down approach - capable to produce large amounts of graphenes - is further divided into two strategies resting on different binding interactions. Non-covalent functionlization by surfactants and suitable solvents provides defect free few and single layer graphene in processable dispersions which may be used for all kinds of coating techniques from spray- to simple dip-coating. The exfoliation efficiency of surfactants can be tailored allowing them to fulfill more than their sole dispersion purpose by implementation of electron donating/accepting units. If covalent functionalization is utilized while walking down the "top-down track" one usually does not obtain defect free material as defects in the form of sp^3-carbon centers are introduced into the graphene lattice. However GICs offer the possibility to minimize possible σ-lattice damage during reductive activation of the parent graphite stack. The obtained reductively exfoliated negatively charged graphene sheets can successively be functionlized by mild organic oxidants leading to covalent bond formation between the sheets and addend to be introduced.

When control about local atomic structure is concerned e.g. in order to define exact optical and electronic properties for narrow graphene nanoribbons, the bottom-up synthetic strategy has to be chosen. Both solution and surface synthesis have been revealed for the successful generation of polyphenylene precursors and following graphene nanoribbons upon intramolecular cyclodehydrogenation process. For both cases, the topology and edge periphery of GNRs are strongly governed by the precursor monomers utilized. Suzuki-type polymerization enables one to synthesize polyphenylene precursors in solution. The introduction of a kinked-backbone and attachment of suitable alkyl chains at specific positions can improve the solubility of final GNRs in organic solvents which are essential for further solution processing and structural characterizations. Regarding the surface-mediated synthesis of GNRs, the precursor monomers with functional halogen groups must be firstly deposited on the surface with monolayer coverage, and then a two step thermal activation process must be performed. While the low temperature treatment in the first step generates the polyphenylene chains via radical addition, a higher temperature is required to fully planarize the precursor by eliminating the hydrogen and affords atomically precise GNRs on the surface. Naturally, extending the width of GNRs by selecting expanded precursor monomers should pave the way to tailoring and engineering the

architectures and properties of GNRs. This will finally bridge the bottleneck of current top-down synthesis of GNRs by means of lithography and chemical etching of graphene.

Zusammenfassung

Die chemischen Zugänge zum ständig wachsenden Forschungsgebiet Graphen können in zwei große Unterkategorien zusammengefasst werden. Einerseits sind die „top-down"-Vorgehensweisen zu nennen, welche, ausgehend von leicht verfügbarem Graphit, der Exfoliationsmethodik folgen, während andererseits die „bottom-up"-Ansätze die atomare Präzision der präparativen organischen Chemie nutzen. Der „top-down"-Ansatz – geeignet zur kostengünstigen Herstellung von großen Mengen an Graphen – kann weiter in zwei unterschiedliche Strategien unterteilt werden, welche auf den jeweils ausgenutzten Wechselwirkungstypen beruhen. Die nichtkovalente Funktionalisierung durch oberflächenaktive Stoffe oder geeignete Lösungsmittel kann genutzt werden, um defektfreies, in flüssiger Form prozessierbares Graphen in großem Maßstab zu erzeugen, das in fast jeder denkbaren Beschichtungsroutine zum Einsatz kommen kann. Durch chemische Veränderungen im Aufbau der verwendeten Tenside kann deren Effektivität gezielt angepasst werden, was wiederum die Möglichkeit eröffnet, Funktionalität über die reine Dispergierungswirkung hinaus einzuarbeiten – beispielsweise durch Implementierung von elektronendonierenden oder -aufnehmenden Untereinheiten. Sollte im Zuge eines „top-down"-Ansatzes die kovalente Funktionalisierung zum Einsatz kommen, wird in der Regel kein störstellenfreies Material generiert, da während der Funktionalisierung sp^3-Kohlenstoffzentren in das Graphengitter eingebaut werden. Jedoch erlauben Graphit-Interkalationsverbindungen (GICs) die Minimierung möglicher σ-Gerüstschäden während der reduktiven Aktivierung des Ausgangsgraphits. Die erhaltenen reduktiv exfoliierten Graphenschichten können anschließend mit organischen Oxidationsmitteln versetzt werden, was zur Knüpfung neuer Bindungen zwischen den einzuführenden organischen Addenden und der zu funktionalisierenden Schicht führt.

Wenn Kontrolle über die lokale atomare Struktur erreicht werden soll, beispielsweise um exakte optische und elektronische Eigenschaften von dünnsten Graphen-Nanostreifen (GNS) einzustellen, so muss eine „bottom-up"-Strategie gewählt werden. Sowohl lösungs- als auch oberflächenbasierte Synthesemethoden wurden zur Herstellung von Polyphenylen-Vorläufermolekülen eingesetzt, wobei nach intramolekularer Cyclodehydrierung ebenfalls Graphen-Nanostreifen erhalten werden konnten. In beiden Fällen hängt die Topologie sowie die Randstruktur der GNS stark von den verwendeten Vorläufermolekülen ab. Suzuki-artige Polymerisation erlaubt die Synthese der Vorläufer in Lösung. Die Einführung eines geknickten Phenylgerüsts sowie die Verknüpfung mit geeigneten Alkylketten an bestimmten Positionen kann die Löslichkeit der letztendlich erhaltenen GNS deutlich verbessern, was essentiell für die weitere Prozessierung und Strukturaufklärung ist. Bei der oberflächenvermittelten Synthese von GNS muss das halogenhaltige Vorläufermonomer erst dünnschichtig, wenn möglich in einer Monolage, abgeschieden werden und durchläuft dann zwei weitere thermisch aktivierte Prozesse. Im ersten Schritt werden bei niedriger Temperatur Polyphenylenketten über radikalische Addition aneinander gebunden. Anschließend sind höhere Temperaturen notwending, um eine vollständige Planarisierung dieser Ketten zu erreichen. Die Eliminierung von Wasserstoff führt schließlich zu den atomar vordefinierten GNS auf der Oberfläche. Natürlich sollte durch Wahl größerer Vorläufermoleküle der Weg zu maßgeschneiderten Architekturen und Eigenschaften der GNS geebnet werden können. So sollten schließlich die Problematiken der momentan verwendeten „top-down"-Verfahren, welche auf lithographischen und chemischen Ätztechniken beruhen, überwunden werden können.

Andreas Hirsch *[1*] is Professor for Organic Chemistry at the University Erlangen-Nürnberg. His research interests are the chemistry of synthetic carbon allotropes such as fullerenes carbon nanotubes and graphene as well as supramolecular and nanochemistry.*

Email: andreas.hirsch@chemie.uni-erlangen.de

*Jan M. Englert [2], Xinliang Feng [3], Prof. Klaus Müllen [3]**

** corresponding authors*

Addresses:

[1] University Erlangen-Nürnberg, Henkestrasse 42,D-91054 Erlangen, Germany

[2] ZMP-Institute of Advanced Materials and Processes, Dr.-Mack Str. 81, 90762 Fürth, Germany

[3] Max Planck Institute for Polymer Research, Ackermannweg 10, 55128 Mainz, Germany

Acknowledgement

We thank the "Deutsche Forschungsgemeinschaft (DFG)" (Directed synthesis of graphene nanoribbons – 559148), The Interdisciplinary for Molecular Materials (ICMM) and the Graduate School Molecular Science (GSMS) for financial support.

[1] K. Novoselov, A. Geim, S. Morozov, D. Jiang, Y. Zhang, S. Dubonos, I. Grigorieva, A. Firsov, *Science* **2004**, *306*, 666; A. K. Geim, K. S. Novoselov, *Nat. Nanotechnol*. **2007**, *6*, 183.

[2] S. Pang, J. M. Englert, H. N. Tsao, Y. Hernandez, A. Hirsch, X. Feng, K. Müllen, *Adv. Mater*. **2010**, *22*, 5374.

[3] R. Zacharia, H. Ulbricht, T. Hertel, *Phys. Rev*. *B* **2004**, *69*, 155406.

[4] S. E. Skrabalak, *Phys. Chem. Chem. Phys*. **2009**, *11*, 4930.

[5] C. A. Furtado, U. J. Kim, H. R. Gutierrez, L. Pan, E. C. Dickey, P. C. Eklund, *J. Am. Chem. Soc*. **2004**, *126*, 6095; S. Giordani, S. D. Bergin, V. Nicolosi, S. Lebedkin, M. M. Kappes, W. J. Blau, J. N. Coleman, *J. Phys. Chem. B* **2006**, *110*, 15708; B. J. Landi, H. J.

Ruf, J. J. Worman, R. P. Raffaelle, *J. Phys. Chem. B* **2004**, *108*, 17089; T. Hasan, V. Scardaci, P. Tan, A. G. Rozhin, W. I. Milne, A. C. Ferrari, *J. Phys. Chem. C* **2007**, *111*, 12594.

[6] Y. Hernandez, V. Nicolosi, M. Lotya, F. M. Blighe, Z. Sun, S. De, I. T. McGovern, B. Holland, M. Byrne, Y. K. Gun'Ko, J. J. Boland, P. Niraj, G. Duesberg, S. Krishnamurthy, R. Goodhue, J. Hutchison, V. Scardaci, A. C. Ferrari, J. N. Coleman, *Nat. Nanotechnol*. **2008**, *3*, 563.

[7] J. Malig, N. Jux, D. Kiessling, J.-J. Cid, P. Vázquez, T. Torres, D. M. Guldi, *Angew. Chem.* **2011**, *123*, 3623; *Angew. Chem. Int. Ed*. **2011**, *50*, 3561; X. An, T. Simmons, R. Shah, C. Wolfe, K. M. Lewis, M. Washington, S. K. Nayak, S. Talapatra, S. Kar, *Nano Lett.* **2010**, *10*, 4295; A. Ghosh, K. V. Rao, S. J. George, C. N. R. Rao, *Chem. Eur. J*. **2010**, *16*, 2700.

[8] A. A. Green, M. C. Hersam, *Nano Lett.* **2009**, *9*, 4031.

[9] J. M. Englert, J. Röhrl, C. D. Schmidt, R. Graupner, M. Hundhausen, F. Hauke, A. Hirsch, *Adv. Mater*. **2009**, *21*, 4265.

[10] N. V. Kozhemyakina, J. M. Englert, G. Yang, E. Spiecker, C. D. Schmidt, F. Hauke, A. Hirsch, *Adv. Mater*. **2010**, *22*, 5483.

[11] C. D. Schmidt, C. Böttcher, A. Hirsch, Eur. *J. Org. Chem*. **2007**, 5497.

[12] C. Backes, C. D. Schmidt, K. Rosenlehner, F. Hauke, J. N. Coleman, A. Hirsch, *Adv. Mater*. **2010**, *22*, 788; C. Backes, C. D. Schmidt, F. Hauke, A. Hirsch, *Chem. Asian. J*. **2011**, *6*, 438; C. Backes, C. D. Schmidt, F. Hauke, C. Böttcher, A. Hirsch, *J. Am. Chem. Soc.* **2009**, *131*, 2172; C. Backes, F. Hauke, A. Hirsch, *Adv. Mater.* **2011**, *23*, 2588.

[13] C. Ehli, C. Oelsner, D. M. Guldi, A. M. -Alonso, M. Prato, C. Schmidt, C. Backes, F. Hauke, A. Hirsch, *Nat. Chem*. **2009**, *1*, 243.

[14] W. Rüdorff, H. Schulz, *Z. Anorg. Allg. Chem*. **1940**, *245*, 121.

[15] K. Fredenhagen, H. Suck, *Z. Anorg. Allg. Chem*. **1929**, *178*, 353.

[16] C. Vallés, C. Drummond, H. Saadaoui, C. Furtado, M. He, O. Roubeau, L. Ortolani, M. Monthioux, A. Pénicaud, *J. Am. Chem. Soc*. **2008**, *130*, 15802; A. Catheline, C. Valles, C. Drummond, L. Ortolani, V. Morandi, M. Marcaccio, M. Iurlo, F. Paolucci, A. Penicaud, *Chem. Commun*. **2011**, *47*, 5470.

[17] L. Staudenmaier, *Ber. Dtsch. Chem. Ges.* **1898**, *31*, 1481; W. S. Hummers, R. E. Offeman, *J. Am. Chem. Soc*. **1958**, *80*, 1339; B. Brodie, *Ann. Chim. Phys*. **1860**, *59*, 466.

[18] W. Gao, L. B. Alemany, L. Ci, P. M. Ajayan, *Nat. Chem.* **2009**, *1*, 403; K. Erickson, R. Erni, Z. Lee, N. Alem, W. Gannett, A. Zettl, *Adv. Mater*. **2010**, *22*, 4467.

[19] H. P. Boehm, A. Clauss, G. O. Fischer, U. Hofmann, *Z. Naturforsch. B* **1962**, *17*, 150.

[20] S. Stankovich, D. A. Dikin, R. D. Piner, K. A. Kohlhaas, A. Kleinhammes, Y. Jia, Y. Wu, S. T. Nguyen, R. S. Ruoff, *Carbon* **2007**, *45*, 1558.

[21] V. Kohlenschütter, P. Haenni, *Z. Anorg. Chem*. **1918**, *105*, 121.

[22] J. O. Sofo, A. S. Chaudhari, G. D. Barber, *Phys. Rev. B* **2007**, *75*, 153401; D. C. Elias, R. R. Nair, T. M. G. Mohiuddin, S. V. Morozov, P. Blake, M. P. Halsall, A. C. Ferrari, D. W. Boukhvalov, M. I. Katsnelson, A. K. Geim, K. S. Novoselov, *Science* **2009**, *323*, 610.

[23] M. Quintana, K. Spyrou, M. Grzelczak, W. R. Browne, P. Rudolf, M. Prato, *ACS Nano* **2010**, *4*, 3527.

[24] X. Zhong, J. Jin, S. Li, Z. Niu, W. Hu, R. Li, J. Ma, *Chem. Commun.* **2010**, *46*, 7340.

[25] E.-K. Choi, I.-Y. Jeon, S.-Y. Bae, H.-J. Lee, H. S. Shin, L. Dai, J.-B. Baek, *Chem. Commun*. **2010**, *46*, 6320.

[26] P. Allongue, M. Delamar, B. Desbat, O. Fagebaume, R. Hitmi, J. Pinson, J.-M. Saveant, *J. Am. Chem. Soc*. **1997**, *119*, 201; M. S. Strano, C. A. Dyke, M. L. Usrey, P. W. Barone, M. J. Allen, H. Shan, C. Kittrell, R. H. Hauge, J. M. Tour, R. E. Smalley, *Science* **2003**, *301*, 1519.

[27] J. M. Englert, C. Dotzer, G. Yang, M. Schmid, C. Papp, J. M. Gottfried, H.-P. Steinrück, E. Spiecker, F. Hauke, A. Hirsch, *Nat. Chem.* **2011**, *3*, 279.

[28] V. Barone, O. Hod, G. E. Scuseria, *Nano Lett.* **2006**, *6*, 2748-2754.

[29] K. Nakada, M. Fujita, G. Dresselhaus, M. S. Dresselhaus, *Phys. Rev. B* **1996**, *54*, 17954.

[30] N. Tombros, C. Jozsa, M. Popinciuc, H. T. Jonkman, B. J. Van Wees, *Nature* **2007**, *448*, 571.

[31] M. Y. Han, B. Ozyilmaz, Y. Zhang, P. Kim, *Phys. Rev. Lett.* **2007**, *98*, 206805.

[32] X. L. Li, X. R. Wang, L. Zhang, S. W. Lee, H. J. Dai, *Science* **2008**, *319*, 1229.

[33] X. Wang, H. J. Dai, *Nat. Chem.* **2010**, *2*, 661.

[34] D. V. Kosynkin, A. L. Higginbotham, A. Sinitskii, J. R. Lomeda, A. Dimiev, B. K. Price, J. M. Tour, *Nature* **2009**, *458*, 872.

[35] L. Jiao, L. Zhang, X. Wang, G. Diankov, H. J. Dai, *Nature* **2009**, *458*, 877.

[36] J. Wu, L. Gherghel, M. D. Watson, J. Li, Z. Wang, C. D. Simpson, U. Kolb, K. Müllen, *Macromolecules* **2003**, *36*, 7082.

[37] X. Yang, X. Dou, A. Rouhanipour, L. Zhi, H. J. Räder, K. Müllen, *J. Am. Chem. Soc.* **2008**, *130*, 4216.

[38] L. Dössel, L. Gherghel, X. Feng, K. Müllen, *Angew. Chem.* **2011**, *123*, 2588; *Angew. Chem. Int. Ed.* **2011**, *50*, 2540.

[39] X. L. Feng, V. Marcon, W. Pisula, M. R. Hansen, J. Kirkpatrick, D. Andrienko, K. Kremer, K. Müllen, *Nat. Mater*. **2009**, *8*, 421.

[40] W. Pisula, X. L. Feng, K. Müllen, *Adv. Mater.* **2010**, *22*, 3634.

[41] C. D. Simpson, J. D. Brand, A. J. Berresheim, L. Przybilla, H. J. Räder, K. Müllen, *Chem. Eur. J.* **2002**, *8*, 1424.

[42] W. Pisula, X. L. Feng, K. Müllen, *Chem. Mater.* **2011**, *23*, 554.

[43] J. Cai, P. Ruffieux, R. Jaafar, M. Bieri, T. Braun, S. Blankenburg, M. Muoth, A. P. Seitsonen, M. Saleh, X. Feng, K. Müllen, R. Fasel, *Nature* **2010**, *466*, 470.

[44] P. Kovacic, C. Wu, R. W. Stewart, *J. Am. Chem. Soc.* **1960**, *82*, 1917.

[45] B. T. King, J. Kroulik, C. R. Robertson, P. Rempala, C. L. Hilton, J. D. Korinek, L. M. Gortari, *J. Org. Chem.* **2007**, *72*, 2279.

[46] T. S. Navale, K. Thakur, R. Rathore, *Org. Lett.* **2011**, *13*, 1634.

[47] M. Treier, C. A. Pignedoli, T. Laino, R. Rieger, K. Müllen, D. Passerone, R. Fasel, *Nat. Chem.* **2010**, *3*, 61.

[48] M. Bieri, M. Treier, J. Cai, K. Aït-Mansour, P. Ruffieux, O. Gröning, P. Gröning, M. Kastler, R. Rieger, X. Feng, K. Müllen, R. Fasel, *Chem. Commun.* **2009**, 6919.

Interfacial Electron Transfer Energetics Studied by High Spatial Resolution Tip-Enhanced Raman Spectroscopic Imaging

Xiao Wang, Dai Zhang, Yuanmin Wang, Papatya Sevinc, H. Peter Lu, Alfred J. Meixner

Interfacial electron transfer (ET) in TiO_2-based systems is important in artificial solar energy harvesting systems, catalysis, and in advanced oxidative waste water treatment. The fundamental importance of ET processes and impending applications make the study of interfacial ET a promising research area. Photo-excitation of dye molecules adsorbed on the surface of wide band gap semiconductors, such as TiO_2, results in the injection of electrons from the dye molecules to the conduction band of the semiconductor or energetically accessible surface electronic states. Using Raman spectroscopy and ensemble-averaging approaches, the chemical bonding and vibrational relaxation of the ET processes have been extensively studied. However, due to the complexity of the interfacial ET energetics and dynamics, significant questions remain on characterizing the source of the observed complexities. To address these important issues, we have applied advanced spectroscopic and imaging techniques such as confocal and tip-enhanced near-field Raman as well as photoluminescence spectroscopic and topographic imaging. Here we explore single surface states on TiO_2 as well as the interfacial electronic coupling of alizarin to TiO_2 single crystalline surfaces.

1. Introduction

nterfacial electron transfer (ET) plays a central role in dye-sensitized solar cells, photocatalysis, environmental chemistry, surface chemistry, and molecular electronics.[1] A model dye-sensitized semiconductor system is represented in Figure 1. The forward electron transfer (FET) kinetics in various dye-TiO2 systems has typical half-times ranging from femtoseconds to several hundred picoseconds.[2] When the adsorbed molecule is strongly bound close to the TiO_2 surface, then rapid FET is expected. In the so-called wide-band limit, Franck-Condon factors do not matter for FET and the transfer rate is primarily controlled by the electronic coupling.[3] Following FET, the injected electron relaxes and is localized to sub-band states. Backward electron transfer (BET) from the semiconductor to the oxidized dye molecules often follows. Compared to ultrafast FET processes, BET processes take longer, with lifetimes ranging from sub-nanoseconds to several milliseconds.[4] The wide timescale variation is most likely associated to the inhomogeneous molecular surface bonding and vibrational relaxation energy barriers for the back electron transfer; although, other contributions can be from the existence of trap states and non-Brownian electron diffusion in semiconductors. Furthermore, the dynamics of the BET processes are also often multiexponetial and stretched exponential.[4b, 5]

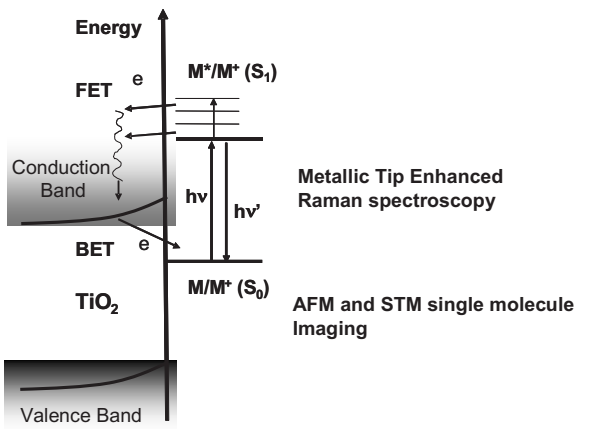

Figure 1. Diagram of interfacial electron transfer processes for the dye-sensitized TiO_2 system.

Designing an efficient solar energy harvesting system entails controlling the rate of the BET process in order to generate long-lived charge-separated states. Characterization of the electron trap

and localized states are important because these states play a regulating role in BET dynamics and, in turn, the fluorescence dark-state lifetimes of the oxidized dye molecules. An efficient dye-sensitized TiO_2 solar cell system should have fast forward electron transfer from the dye excited state to the semiconductor conduction band, and a slow backward electron transfer so that the excess electron has a higher probability of conversion to electricity.

We have used confocal and tip-enhanced high-resolution near-field luminescence and Raman imaging spectroscopy to analyze the interfacial charge transfer energetics down to the single site and single-molecule level, well beyond the spatial resolution of the optical diffraction limit.[6] We intend to extend our Raman spectral analysis to obtain the vibrational relaxation energy, surface bonding, and molecular vibronic coupling information in order to dissect the interfacial electron transfer energetics. Near-field scanning optical microscopy makes use of the strongly enhanced electric field around a sharp metal tip under laser illumination. In a near-field Raman spectroscopic measurement, the excitation field is locally significantly enhanced by a combination of an electrostatic lightning-rod effect and a tip-plasmon excitation induced by the laser field. The spatial resolution achievable with this technique is determined primarily by the apex radius and the shape of the metallic tip, and the signal-to-noise ratio is defined by the strength of the field-enhancement effect. We have made significant advances towards using near-field Raman spectroscopic mapping to analyze interfacial electron transfer on the TiO_2 surfaces.[6]

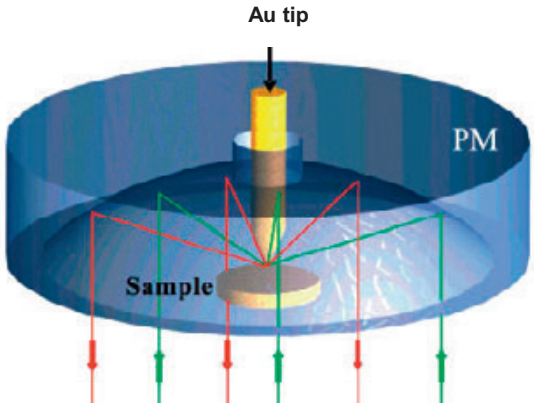

Figure 2. Schematic illustration of a parabolic-mirror-assisted confocal ultramicroscope. A sharp Au tip is adjusted into the center of diffraction limited focus as created by an incident radially polarized laser beam. Laser illumination is applied in a radially polarized mode to obtain a well defined field distribution in the focal volume. The tip serves as an optical antenna providing intense local electromagnetic (EM) field enhancement at the tip apex for local excitation and emission to the optical far-field.

We have applied a special near-field spectroscopic imaging microscopy to characterize the dye-sensitized TiO_2 single crystal surfaces, and we were able to demonstrate ~15-nm spatial resolution on the correlated topographic and Raman spectroscopic images.[6] This is the first time that a single-molecule near-field Raman spectroscopic imaging has been done for dye-sensitized TiO_2 systems. All the measurements were performed with a home-built parabolic mirror-assisted near-field optical microscope.[7] A typical configuration of the microscope is illustrated in Figure 2. The sample is illuminated from above by a parabolic mirror which generates a diffraction limited excitation spot on the sample surface and in return efficiently collects the scattered and reflected photons and directs them onto a confocal detection system consisting of an avalanche photodiode (APD) and a spectrograph equipped with a CCD-detector for spectral analysis. For perfect polarization control in the focal volume, the parabolic mirror is illuminated with an aperture filling radially polarized laser mode. For super-resolution optical imaging and topographic recording the tip is brought through the axial hole in the parabolic mirror and precisely centred into the focus. The tip-sample distance is kept to about 3 nm by a shear-force feed back loop.

2. Imaging of single TiO2-surface states and interfacial electronic coupling

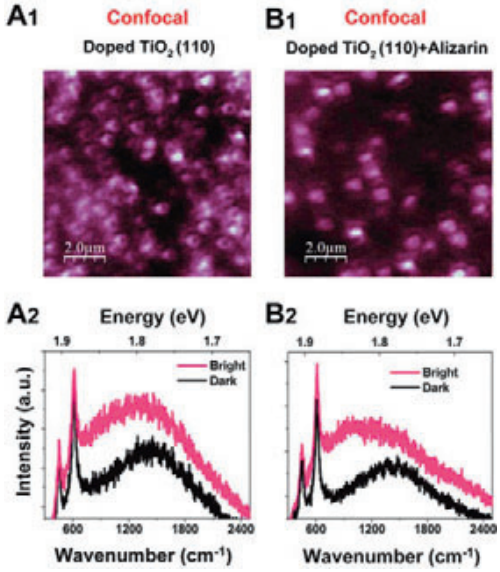

Figure 3. Optical response of the abundant surface states of the Nb-doped rutile TiO_2 (110) surface. (A1) Confocal imaging and (A2) Raman/luminescence spectra of TiO_2 (110) surface. (B1) Confocal imaging and (B2) Raman/luminescence spectra of TiO_2 (110) surface with alizarin (1 μM).

Panels A1 and B1 in Figure 3 show confocal images of the Nb-doped rutile TiO_2 (110) surface under the conditions of without (A) and with alizarin (B), respectively. Most of the hot spots in the confocal image (without the tip) in Figure 3A1 show as donut-shape features, and only a small number of them show as circular or ellipsoidal-shaped spots. Such different diffraction limited fluorescence excitation patterns can only be observed when single quantum systems are raster scanned through the field distribution of a tightly focused radially polarized laser beam.

Since the excitation rate is proportional to the square of the projection of the transition dipole moment D onto the electric field E as

$$R_{exc} \propto \left|\vec{D} \cdot \vec{E}\right|^2$$

Distinct excitation patterns are observed if single quantum systems, such as a single molecule, defects, or surface states are imaged, revealing their orientation and the dimensionality of their optical transition. We have calculated the optical patterns of quantum systems with one dipole moment, two perpendicular dipole moments, or three perpendicular dipole moments excited by radially polarized laser beams as shown in Figure 4. Only for quantum systems with a two dimensional transition dipole moment as recently found for excitons in quantum dots[8] we can observe circular patterns. Here the ring patterns suggest that the transition dipole moment of the surface states can assume two perpendicular orientations with the same probability and both lying in the surface plane.[8] This is consistent with recent quantum-chemical calculations which suggest that O-vacancy formation in rutile Ti(110) surface results in two excess electrons occupying 3d orbitals on Ti atoms neighboring the vacancy.[9]

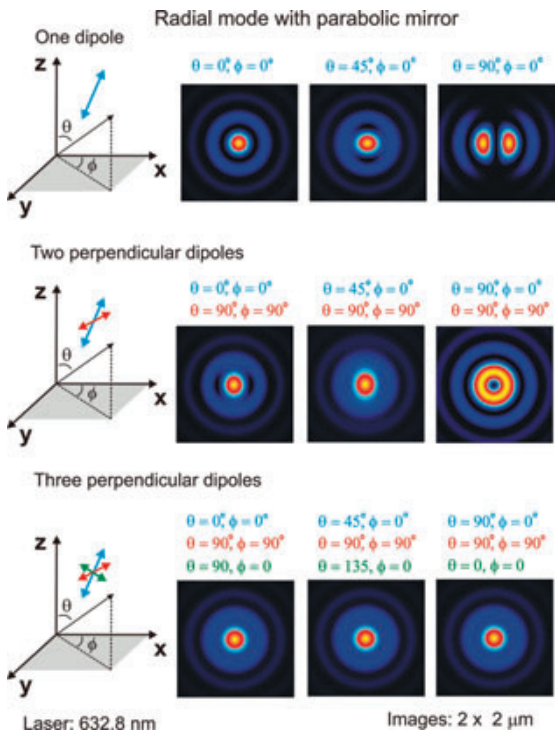

Figure 4. Calculated optical patterns of quantum systems with one dipole moment, two perpendicular dipole moments and three perpendicular dipole moments excited by radially polarized laser beams with parabolic mirror. The intensity in each figure is normalized individually.

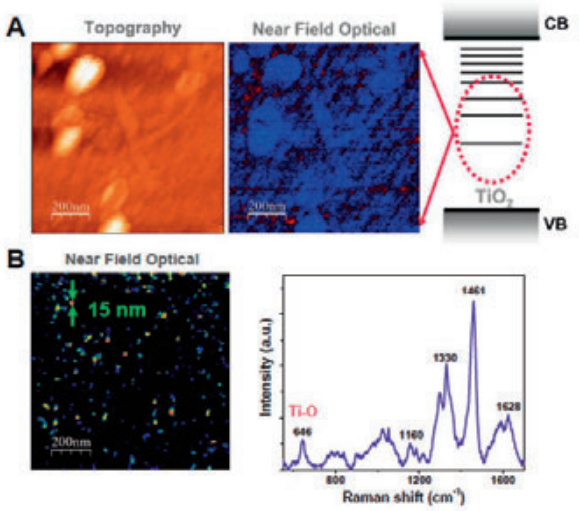

Figure 5. (A) Simultaneously obtained topographic and near field optical images of a clean Niobium-doped rutile TiO_2 (110) surface. Single surface states localized at the sub-domain boundaries can be clearly observed. (B) For the Alizarin adsorbed TiO_2 surface, resonance Raman spectrum (using 532 nm laser excitation) with the Ti-O peak at 646 cm^{-1} provides the evidence of the strong electronic coupling at the interface.

Surface states have been demonstrated to play important roles in interfacial electron transfer process.[10] Their density and energy distributions are the possible parameters that affect the charge transfer pathways. We have used TiO_2/alizarin, a typical model system with strong electronic coupling,[11] to probe these parameters. However, as shown in Figure 3B1 and 3B2, we observed less hot spots and inhomogeneous imaging patterns (ellipsoidal shaped and donut-shape) and clear blue-shifts in the photoluminescence background of the spectra comparing with the TiO_2 only crystal surface. These observations can be interpreted by the intensity difference of the electronic coupling between TiO_2 and alizarin molecules.[6]

The feasibility of using the near-field Raman imaging analysis for TiO_2 single crystal systems is demonstrated in Figure 5. Brightly luminescent spots arise from localized surface states which are distributed mainly along the sub-domain boundaries as evidenced in the superimposed topographic (in blue) and near-field optical (in red) image (Figure 5A). The interfacial electronic molecule-substrate coupling has been characterized by probing the molecule-perturbed surface states distribution and the associated specific Raman vibrational modes. Figure 5B shows the high resolution (15 nm) surface states imaging (left) and the Raman spectrum of the Alizarin adsorbed TiO_2 surface (right). We observed a direct evidence of the formation of the Alizarin-TiO_2 charge transfer complex: besides the normal vibrational modes from Alizarin, we also observed a new Raman peak at 646 cm^{-1}, which is a typical Ti-O stretching mode from a bridging Ti-O-C bond [11-12] The strong C-O stretching at 1330 cm^{-1} reveals that the Alizarin-TiO_2 charge transfer complex forms primarily through the hydroxyl groups of Alizarin and a Ti atom of TiO_2 surface.

3. Surface states, electronic coupling, charge delocalization at the interface, and their roles in interfacial ET dynamics

In a solar energy conversion system such as a dye-sensitized solar cell, one of the key parameters that limit the photo electrical conversion efficiency is the charge transport inside the semiconductor electrode. Due to its complexity, energetically trapping, thermally activated detrapping, and Non-Brownian electron diffusion have been proposed to describe the charge transport process in the semiconductor. To improve the charge transport efficiency of TiO_2 electrodes, single crystal TiO_2 nanowires, polycrystalline TiO_2 nanowires, and TiO_2 nanotubes have been applied in solar cells. However, it was demonstrated that electron transport rate of these materials can be as slow as in TiO_2 nanoparticle because the surface traps almost dominate the charge transport pathways[10] indicating the important role of surface states in charge transport.

Surfaces states on rutile TiO_2 (110) surface have been investigated and visualized by traditional approaches such as scanning tunneling microscopy.[13] The physical nature of surface states have been attributed to bridging oxygen vacancies or interstitial Ti-atoms.[14] We suggest that the single surface states revealed by our nanoscale imaging are originated from the bridging oxygen vacancies, which can be deduced from the donut-shape optical patterns under radial polarized mode laser excitation because only for quantum systems with a two dimensional transition dipole moment can give circular optical patterns. On the basis of a quantum-chemical calculation,[9] O-vacancy formation in rutile Ti(110) surface results in two excess

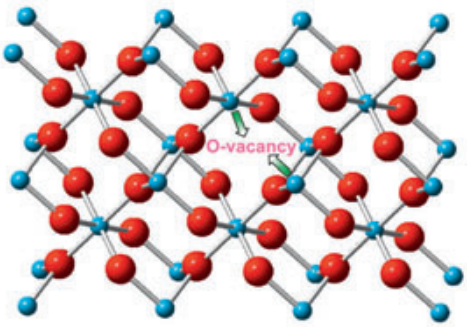

Figure 6. Conceptual view of the O-vacancy on rutile TiO_2 surface. The structure is plotted by ball and stick model (Red: O; Blue: Ti). Because there are two excess electrons occupying 3d orbital of two neighboring Ti atoms, two transition dipole moments will occur under laser excitation. The two arrows show the direction of the dipole moments.

electrons occupying 3d orbitals on Ti atoms neighboring the vacancy. With laser excitation, electrons at the valence band can be excited to higher energy states, for example, trap states below the conduction band. Considering the spatial configuration of the O-vacancy and the two adjacent Ti atoms, there should be two possible transition dipole moments with an angle close to vertical. A conceptual view is shown in Figure 6. Actually, the real angle between the two transition dipole moments may be affected by the local structural distortion.

As the electron trap center, surface states on rutile TiO_2 (110) surface has been proved to be active chemical reaction centers. Toward the potential applications as electron traps for photogenerated electrons, dye molecule (such as alizarin) perturbed surface states in TiO_2 is a critical research topic. The strength of the electronic coupling between dye and TiO_2 significantly affects the charge transfer rate at the interface. Driven by a strong electronic coupling, electrons can directly delocalize from the highest occupied molecular orbital of the dye molecule to the trap center of TiO_2 in forming the interfacial charge transfer complexes. This will make efficient electron injection for a dye-sensitized TiO_2 system. In addition, as a model system, many experiments and calculations also focus on the fundamental understanding of the surface chemistry and physics of TiO_2 surface by investigating the diffusion, adsorption, dissociation, and reaction of molecular Oxygen, H_2O, and related species on the TiO_2 single crystal surface.[15] These efforts actually also base on a thorough understanding of the electronic structure of the semiconductor surface.

Summary

Interfacial electron transfer energetics has been probed using nanoscale confocal and tip-enhanced near-field photoluminescence and Raman imaging and spectroscopy. Single surface states on clean and Alizarin-doped TiO_2(110)surfaces as well as strong electronic coupling at the alizarin/TiO_2 interfaces have been demonstrated by exploring the imaging and spectroscopic characters. Our results help for the understanding of fundamental processes in solar energy conversion, photocatalysis, and molecular electronics.

Zusammenfassung

Elektronenübertragungsprozesse zwischen Farbstoffen und einer Halbleiteroberfläche wurden mittels hochauflösender konfokaler und spitzenverstärkter nahfeld-optischer Raman- und Lumineszenz-Mikroskopie untersucht. Es konnten sowohl einzelne lumineszierende Oberflächendefekte bei undotierten als auch bei Alizarin-dotierten Oberflächen als auch eine starke elektronische Kopplung zwischen Alizarin und der TiO_2(110)-Oberfläche beobachtet werden. Unsere Resultate tragen zu einem besseren Verständnis der Photovoltaik, der Photokatalyse und der molekularen Elektronik bei.

Xiao Wang [1)#], *is PhD student and working with Alfred Meixner and Dai Zhang.*

Email: xiao.wang@uni-tuebingen.de

#: These authors contributed to the work equally.

Dai Zhang [1)#] *is junior research group leader working with Alfred Meixner.*

Email: dai.zhang@uni-tuebingen.de

#: These authors contributed to the work equally.

Yuanmin Wang [2)] *is postdoctoral fellow working with H. Peter Lu.*

Email: yuawang@bgsu.edu

Papatya C. Sevinc [2)] *is a PhD-student working with H. Peter Lu.*

Email: psevinc@bgsu.edu

H. Peter Lu [2)]*, Ohio Eminant Scholar is Full Professor of Chemistry at the Bowling Green State University.*

Email: hplu@bgsu.edu

** corresponding author*

Alfred J. Meixner [1)*] *is full Professor for Physical Chemistry at the University of Tübingen.*

Email: alfred.meixner@uni-tuebingen.de

** corresponding author*

Addresses:

[1)] *University of Tübingen, Auf der Morgenstelle 18, 72076 Tübingen, Germany*

[2)] *Bowling Green State University, Center for Phytochemical Sciences, Deoartment of Chemistry, Bowling Green, OH 43403 USA*

Acknowledgements:

Lu acknowledges the support from the Basic Energy Science of Department of Energy (grant DE-FG02-06ER15827) and the Division of Chemistry of National Science Foundation (grant CHE-0822694) of the United States; Meixner acknowledges the support from the DFG, project ME 1600/11-1, Germany

1] a) B. Oregan, M. Gratzel, *Nature* **1991**, *353*, 737-740; b) C. Joachim, M. A. Ratner, *Proc. Natl. Acad. Sci. USA* **2005**, *102*, 8801-8808; c) P. V. Kamat, *J. Phys. Chem. C* **2007**, *111*, 2834-2860.

[2] a) J. Asbury, E. Hao, Y. Wang, H. Ghosh, T. Lian, *J. Phys. Chem. B* **2001**, *105*, 4545-4557; b) Y. Gao, Y. Georgievskii, R. Marcus, *J. Chem. Phys.* **2000**, *112*, 3358; c) R. Huber, J. Moser, M. Grätzel, J. Wachtveitl, *Chem. Phys.* **2002**, *285*, 39-45; d) P. Kamat, *J. Phys. Chem. B* **2002**, *106*, 7729-7744; e) A. Barzykin, M. Tachiya, *J. Phys. Chem. B* **2002**, *106*, 4356-4363.

[3] R. Ernstorfer, S. Felber, W. Storck, E. Galoppini, Q. Wei, F. Willig, *Res. Chem. Inter.* **2005**, *31*, 643-647.

[4] a) V. Biju, M. Micic, D. Hu, H. P. Lu, *J. Am. Chem. Soc.* **2004**, *126*, 9374-9381; b) Y. Wang, X. Wang, S. K. Ghosh, H. P. Lu, *J. Am. Chem. Soc.* **2009**, *131*, 1479-1487; c) Y. M. Wang, X. F. Wang, H. P. Lu, *J. Am. Chem. Soc.* **2009**, *131*, 9020-9025.

[5] L. J. Guo, Y. M. Wang, H. P. Lu, *J. Am. Chem. Soc.* **2010**, *132*, 1999-2004.

[6] P. C. Sevinc, X. Wang, Y. Wang, D. Zhang, A. J. Meixner, H. P. Lu, *Nano Lett.* **2011**, *11*, 1490-1494.

[7] a) D. Zhang, U. Heinemeyer, C. Stanciu, M. Sackrow, K. Braun, L. E. Hennemann, X. Wang, R. Scholz, F. Schreiber, A. J. Meixner, *Phys. Rev. Lett.*, **2010**, *104*, 56601; b) X. Wang, D. Zhang, K. Braun, H. J. Egelhaaf, C. J. Brabec, A. J. Meixner, *Adv. Funct. Mater.*, **2010**, *20*, 492-499.

[8] A. I. Chizhik, A. M. Chizhik, D. Khoptyar, S. Ba r, A. J. Meixner, *Nano Lett.* **2011**, *11*, 1131-1135.

[9] B. J. Morgan, G. W. Watson, *J. Phys. Chem. C* **2010**, *114*, 2321-2328.

[10] a) E. Enache-Pommer, *Phys. Chem. Chem. Phys* **2009**, *11*, 9648-9652; b) E. Enache-Pommer, J. E. Boercker, E. S. Aydil, *Appl. Phys. Lett.* **2007**, *91,* 113116; c) K. Zhu, N. R. Neale, A. Miedaner, A. J. Frank, *Nano Lett.* **2007**, *7*, 69-74.

[11] D. Pan, D. Hu, H. Lu, *J. Phys. Chem. B* **2005**, *109*, 16390-16395.

[12] L. C. T. Shoute, G. R. Loppnow, *J. Chem. Phys.* **2002**, *117*, 842-850.

[13] A. C. Papageorgiou, N. S. Beglitis, C. L. Pang, G. Teobaldi, G. Cabailh, Q. Chen, A. J. Fisher, W. A. Hofer, G. Thornton, *Proc. Natl. Acad. Sci. USA* **2010**, *107*, 2391.

[14] a) C. M. Yim, C. L. Pang, G. Thornton, *Phys. Rev Lett*, **2010**, *104*, 36806; b) S. Wendt, P. T. Sprunger, E. Lira, G. K. H. Madsen, Z. Li, J. O. Hansen, J. Matthiesen, A. Blekinge-Rasmussen, E. Laegsgaard, B. Hammer, *Science* **2008**, *320*, 1755.

[15] a) M. Rasmussen, L. Molina, B. Hammer, *J. Chem. Phys.* **2004**, *120*, 988-997; b) S. Wendt, R. Schaub, J. Matthiesen, E. Vestergaard, E. Wahlstrom, M. Rasmussen, P. Thostrup, L. Molina, E. Lægsgaard, I. Stensgaard, *Surf. Sci.* **2005**, *598*, 226-245.

Water Oxidation

Water Oxidation in the Context of the Energy Challenge: Tailored Transition-Metal Catalysts for Oxygen-Oxygen Bond Formation

Antoni Llobet and Franc Meyer

Understanding water oxidation mechanisms: The power of two cooperating metal centers.

1. Introduction

The energy demand for the year 2050 is expected to be in the range of 30-50 TW,[1] which is a huge amount of energy that cannot be covered by today's energy resources. Further, given the increase in the rate of CO_2 production and the dramatic consequences this increase has for our planet,[2] any additional energy should preferably come from carbon-neutral renewable sources and mainly from solar energy,[3] Today's energy problem[4] needs to be solved urgently in order not only to be able to maintain the lifestyle of our developed societies, but also to attain decent living standards in developing countries. The foreseeable increase in worldwide energy utilization has to come necessarily from environmentally friendly and sustainable sources, so that future generations can still enjoy living on planet earth.

Hydrogen is a clean energy vector that has attracted substantial attention from energy related industrial and car making corporations. H_2-based technology is already quite developed and can be used to provide electricity to a house or car, and it can also produce hot water or run a domestic central heating. Particularly interesting is the Personal Power Plant (P3) concept that was put forward in 1994 by Honda[5] and more recently by Audi.[6] This concept is reminiscent of the computer revolution that took place in the 80's when the centralized main frame computers were substituted at home with local and independent Personal Computers (PC). An important advantage of H_2 technology is that it can be used independently of the precise situation of the earth rotational period.

While the storage and use of hydrogen has already been achieved with a significant degree of success and sees rapid further improvement,[7] the question of a sustainable hydrogen source still remains to be answered.[8] In fact, besides being utilized as fuel itself, solar hydrogen is also considered the key to a large-scale production of other renewable fuels such as the conversion of lignocellulosic biomass or the reduction of CO_2 to methanol.[9] One particularly attractive solution for generation of molecular hydrogen consists of water splitting by sunlight, as shown in Figure 1. That is sunlight is used to promote a thermodynamically uphill reaction where water is transformed into molecular oxygen and hydrogen. The inverse reaction then forms water and renders back the harvested sunlight energy that can be transformed into heat and/or electricity with no net molecular loss or byproduct formation. This scheme represents an example of the concept of storing energy into chemical bonds. Using water as a raw material certainly is the most sustainable option for providing the electrons that are required for generating any non-fossil fuel.

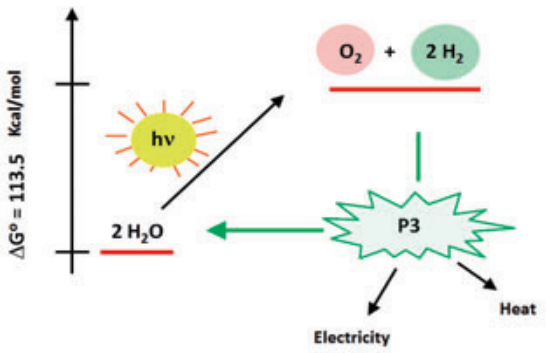

Figure 1. Sunlight water splitting and the P3 concept

Even though sunlight has sufficient energy to promote the water splitting reaction shown in Figure 1, the uncatalyzed reaction is extremely slow and essentially does not take place. Actually the interaction of sunlight with water occurs solely at a vibrational level, and thus it only produces heat. Therefore alternative schemes need to be developed in order to couple the elementary steps of light harvesting, charge separation, electron transfer and finally splitting of water. From a chemical view point the water splitting reaction can be written as two half reactions, namely

(i) water oxidation to O_2

$$2\,H_2O \longrightarrow O_2 + 4\,H^+ + 4\,e^- \qquad (1)$$

(ii) proton reduction to H_2

$$2\,H^+ + 2\,e^- \longrightarrow H_2 \qquad (2)$$

The water oxidation reaction (equation 1) is a thermodynamically demanding reaction since E^{o}=1.23 V (vs. NHE) at pH 0. It is also of enormous molecular complexity from a mechanistic perspective, since formally it involves the removal of four protons and four electrons from two water molecules, together with the formation of an oxygen–oxygen bond. The present research project is aimed at the development and mechanistic understanding of transition metal complexes capable of acting as efficient water oxidation catalysts (WOCs).

Nature has been using water and sunlight as a source of energy in its photosynthetic processes in green plants and algae for a long time. The photosynthetic process can be summarized according to equation 3:

$$6\,CO_2 + 6\,H_2O \xrightarrow{h\nu} C_6H_{12}O_6 + 6\,O_2 \qquad (3)$$

Incidentally, nature uses a similar strategy as the water splitting depicted in Figure 1 in the sense that electrons and protons are extracted from water to form dioxygen. In photosynthesis, however, the reductive equivalents and protons are coupled to NADPH formation and subsequent CO_2 reduction - to in the end form carbohydrates, $C_6H_{12}O_6$. Nature uses a sophisticated polynuclear Ca-Mn_4 complex as an oxygen evolving catalyst (OEC), which is situated in photosystem II (PSII). Recently substantial efforts have been directed at elucidating the OEC-PSII structure and the biological water oxidation mechanism.[10,11] Low molecular weight OEC models are contributing significantly to this endeavor, since they do not only provide critical information regarding the potential mechanism/s that operate at the photosynthetic OEC, but may also lead to efficient artificial catalysts that are part of the energy challenge solution.[9] In fact, water oxidation is currently recognized as one of the bottlenecks for photoproduction of hydrogen from water and sunlight.

2. The Joint Project

Various transition metal complexes have recently been described that are capable of oxidizing water to dioxygen,[12] but very few mechanistic studies have yet been performed.[13] However, proper understanding of the potential reaction pathways as well as the deactivation channels is crucial in order to come up with a sufficiently rugged and efficient catalyst that can be used technologically for a commercial water splitting cell. The majority of the well-studied systems are currently based on Ru complexes. Most Ru WOCs share a common feature, namely, the intermediacy of ruthenium-oxo species in which the metal center is formally in a high oxidation state. This high oxidation state species for dinuclear complexes can then potentially follow three fundamentally different pathways depending on how the O-O bond is formed, as depicted in Figure 2.

One of the best studied and most active dinuclear Ru water oxidation catalysts to date is the Ru-Hbpp system (Hbpp = 3,5-bis(2-pyridyl)pyrazole) developed in one of our laboratories (Llobet group).[14] It consists of a dinucleating anionic pyrazolate scaffold that serves as a backbone to position the two Ru metal centers in close proximity. In *in,in*-{[Ru^{II}(trpy)(H_2O)]$_2$(μ-bpp)}$^{3+}$ (**1**) two ancillary trpy ligands (trpy = 2,2':6,6'-terpyridin) occupy additional coordination sites to leave two positions within the bimetallic pocket for water binding (Figure 3). This places the two O atoms in a favourable distance of 2.48 Å. Upon treatment with four equivalents of the 1e$^-$ oxidant Ce^{IV} the (II,II) species **1** is oxidized to the (IV,IV) oxidation state, which advances to an intermediate that finally evolves dioxygen. Labelling experiments with $H_2{}^{18}O$ and kinetic studies unambiguously revealed that this system operates according to the intramolecular I2M mechanism.[15]

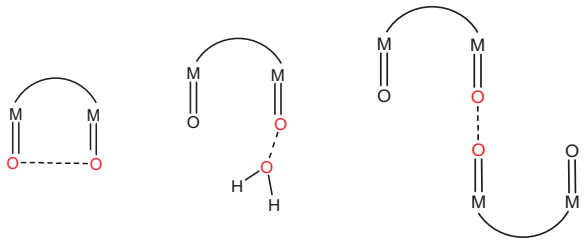

Figure 2. Potential reaction pathways for the formation of oxygen-oxygen bonds assisted by dinuclear transition metal complexes. Left: intramolecular interaction of two MO units, I2M; Center: water nucleophilic attack, WNA; Right: bimolecular I2M.

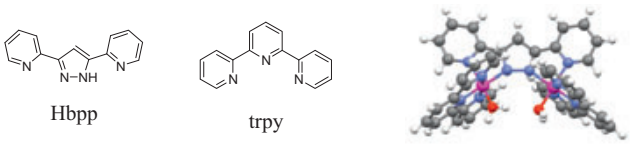

Figure 3. Left: bis(bidentate) Hbpp ligand. Center: ancillary trpy ligand. Right: calculated structure of *in,in*-{[Ru^{II}(trpy)$_2$(H_2O)]$_2$(μ-bpp)}$^{3+}$. Color code: Ru, pink; N, blue; O, red; C, gray; H, white.

At present, the optimized turn-over-number (TON) of catalyst **1** is more than 500. This calls for further modification of the dinucleating scaffold in order to obtain more rugged and even more efficient systems. Routes to a diverse array of multidentate pyrazole-based ligands have been developed in one of our laboratories (Meyer group),[16] including the bis(terdentate) Hbbp scaffold (Hbbp = 3,5-bis(2-bipyridyl)pyrazole) that can be viewed as an expanded version of Hbpp (Figure 4).[17] It thus suggested itself to team up for the development of improved pyrazole-bridged diruthenium water oxidation catalysts.

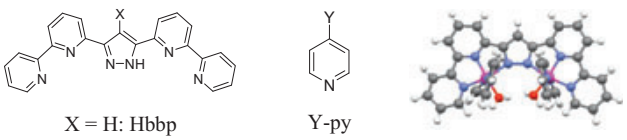

Figure 4. Left: bis(terdentate)X-Hbbp family of dinucleating ligands. Center: substituted monodentate pyridyl ligands. Right: calculated structure of a representative diruthenium complex, {[Ru^{II}(py)$_2$(H_2O)]$_2$(μ-bbp)}$^{3+}$. Color code: Ru, pink; N, blue; O, red; C, gray; H, white.

The main aim of the joint project is to obtain a T understanding of the different factors that influence the O-O bond formation in dinuclear water oxidation catalysts. To achieve this goal a family of highly preorganized binucleating pyrazolate based ligands and their diruthenium complexes such as the one shown in Figure 4 are synthesized and studied in great detail. The different X- and Y-substitutents on the bbp scaffold as well as on the py ligands, respectively, provide a handle for tuning the redox properties of the metal centers, which also allows to potentially control the mechanism through which the water oxidation reaction proceeds. Further the X substituent can be used to attach an anchoring group that would permit to heterogenize the catalyst system. Fixation of the individual catalyst species on a heterogeneous support is expected to avoid potential bimolecular catalyst deactivation reactions as well as the undesired intermolecular I2M type of mechanism. Initial results for the highly preorganized new diruthenium complexes jointly developed in the two participating laboratories are promising.

Summary

Water oxidation (WO) catalysis is a research field that presently experiences a tremendous upsurge. The interest for this field is dual and stems from the fact that WO is the reaction that takes place at the oxygen evolving complex in photosystem II and is a key reaction for the design of new energy conversion schemes and of future scenarios for sustainable energy supply. In the present collaborative project we merge the complementary expertise of two groups to synthesize and study a new family of bimetallic transition metal complexes capable of acting as WO catalysts. The findings contribute to a more thorough understanding of the different potential reaction mechanism through which this important reaction can proceed. It thus represents fundamental work that is needed in order to progress toward the discovery of rugged and efficient water oxidation catalysts.

Zusammenfassung

Die Wasseroxidations(WO)-Katalyse ist ein Forschungsfeld, das derzeit aus vielfältigen Gründen einen enormen Aufschwung erlebt. Zum einen ist die WO jene chemische Reaktion, die am Sauerstoff entwickelnden Komplex des Photosystems II stattfindet; zum anderen handelt es sich um eine fundamentale Reaktion im Zusammenhang mit neuen Szenarien zur Energiekonversion und zur nachhaltigen Energieversorgung. Im hier skizzierten Kooperationsprojekt bringen wir die komplementären Fachkenntnisse zweier Forschungsgruppen zusammen, um eine neue Familie von maßgeschneiderten bimetallischen Übergangsmetallkomplexen zu synthetisieren und zu untersuchen, die als WO-Katalysatoren wirken. Die daraus gewonnenen Erkenntnisse tragen zu einem besseren Verständnis der verschiedenen möglichen Reaktionsmechanismen bei, nach denen diese wichtige chemische Reaktion verlaufen kann. Es handelt sich somit um grundlegende Arbeiten, die von Wert sein werden, um zielgerichtete Fortschritte bei der Entwicklung von robusten und effizienten Wasseroxidations-Katalysatoren zu erreichen.

Antoni Llobet [1] *is professor of chemistry at the Universitat Autònma de Barcelona and Group Leader at the Catalan Institute for Chemical Research in Tarragona (Spain).*

Email: allobet@iciq.es

Franc Meyer [2] *is professor of inorganic chemistry at the Georg-August-University Göttingen (Germany) since 2001.*

Email: franc.meyer@chemie.uni-goettingen.de

Addresses:

[1] *Institute of Chemical Research of Catalonia (ICIQ), Avinguda Paisos Catalans 16, E-43077 Tarragona, Spain*

[2] *Institute of Inorganic Chemistry, Georg-August-University, Tammannstrasse 4, D-37077 Göttingen, Germany.*

Acknowledgements:

Funding of this joint project by the German Research Foundation (DFG) and the Spanish Ministeria de Ciencia e Innovacion (MICINN) in the framework of the ERA Chemistry program is gratefully acknowledged.

[1] a) Basic Research Needs for the Hydrogen Economy; A report from the Basic Energy Sciences Workshop on Hydrogen Production, Storage and Use; Department of Energy; WashingtonDC, **2003**; b) Solar Energy Utilization Workshop **2005,***Basic Science Needs for Energy Utilization* (US Dept of Energy, WashingtonDC).

[2] K. Caldeira, A. K. Jain, M. I. Hoffert, *Science* **2003**, *299*, 2052.

[3] "Energy: the 50-year plan" by Nancy McGuire. Web of the ACS (www.acs.org.; First appeared on September 13th, 2004).

[4] A. Witze, *Nature* **2007**, *445*, 14.

[5] http://www.alt-energy.info/hydrogen-power/hondas-home-hydrogen-fueling-station/. January 24th, 2008.

[6] http://www.naikontuning.com/noticias_nt/2011/05/13/audi-balanced-mobility-el-e-gas-project-a-metano/. May 13th, 2011

[7] a) L. Schlapbach, A.Züttel, *Nature* **2001**, *414*, 353; b) H. Lee, J.-W. Lee, D. Y. Kim, J. Park, Y.-T. Seo, H. Zeng, I. L. Moudrakovski, C. I. Ratcliffe, J. A. Ripmeester, *Nature* **2005**, *434*, 743.

[8] a) N. Armaroli, V. Balzani, *Angew. Chem.* **2007**, *119*, 52; *Angew. Chem. Int. Ed*. **2007**, *46*, 52; b) S. His, in "Hydrogen: An Energy Vector for the Future", *Panorama*, 2004, IFP-Information, France; c) J. S. Connolly, *Photochemical Conversion and Storage of Solar Energy*, Academic Press, New York, **1981**; d) *Energy Resources through Photochemistry and Catalysis* (Ed.: M. Grätzel), Academic Press, New York, **1983**; e) T. N. Verziroglu, F. Barbir, *Int. J. Hydrogen Energy* **1992**, *17*, 391.

[9] H. Dau, C. Limberg, T. Reier, M. Risch, S. Roggan, P. Strasser, *ChemCatChem* **2010**, *2*, 724.

[10] a) W. Lubitz, E. J. Reijerse, J. Messinger, *Energy Environ. Sci.* **2008,** *1*, 15; b) J. Barber, *Inorg. Chem.* **2008**, *47*, 1700; c) Y. Umena, K. Kawakami, J.-R. Shen, N.Kamiya, *Nature* **2011**, *473*, 55.

[11] a) J. P. McEvoy, G. W. Brudvig, *Chem. Rev.* **2006**, *106*, 4455-4483; b) M. Haumann, P. Liebisch, C. Müller, M. Barra, M. Grabolle, H. Dau, *Science* **2005**, *310*, 1019.

[12] a) L. Duan, A. Fischer, Y. Xu, L. Sun, *J. Am. Chem. Soc.* **2009**, *131*, 10397; b) J. D. Blakemore, N. D. Schley, D. Balcells, J. F. Hull, G. W. Olack, C. D. Incarvito, O. Eisenstein, G. W. Brudvig, R. H. Crabtree, *J. Am. Chem. Soc.* **2010**, *132*, 6017; c) W. C, Ellis, N. D. McDaniel, S. Bernhard, T. J. Collins, *J. Am. Chem. Soc.* **2010**, *132*, 10990; d) D. K. Dogutan, R. McGuire, Jr., D. G. Nocera, *J. Am. Chem. Soc.* **2011**, *133*, 9178; e) Q. Yin, J. M. Tan, C. Besson, Y. V. Geletii, D. G. Musaev, A. E. Kuznetsov, Z. Luo, K. I. Hardcastle, C. L. Hill, *Science* **2010**, *328*, 342; f) F. Toma, A. Sartorel, M. Iurlo, M. Carraro, P. Parisse, C. Maccato, S. Rapino, B. R. Gonzalez, H. Amenitsch, T. D. Ros, L. Casalis, A. Goldoni, M. Marcaccio, G. Scorrano, G. Scoles, F. Paolucci, M. Prato, M. Bonchio, *Nat. Chem.* **2010**, *2,* 826.

[13] See for instance: a) J. J. Concepcion, M.-K. Tsai, J. T. Muckerman, T. J. Meyer, *J. Am. Chem. Soc.* **2010**, *132*, 1545; b) D. J. Wasylenko, C. Ganesamoorthy, M. A. Henderson, B. D. Koivisto, H. D. Osthoff, C. P. Berlinguette, *J. Am. Chem. Soc.* **2010**, *132*, 16094; c) S. Romain, L. Vigara, A. Llobet, *Acc. Chem. Res*. **2009**, *42*, 1944.

[14] a) C. Sens, I. Romero, M. Rodríguez, A. Llobet, T. Parella, J. Benet-Buchholz, *J. Am. Chem. Soc.* **2004**, *126*, 7798; b) J. Mola, E. Mas-Marza, X. Sala, I. Romero, M. Rodríguez, C.Viñas, T.Parella, A. Llobet, *Angew. Chem.* **2008**, *120,* 5914; *Angew. Chem. Int. Ed.* **2008**, *47*, 5830.

[15] a) S. Romain, F. Bozoglian, X. Sala, A. Llobet, *J. Am. Chem. Soc.* **2009**, *131*, 2768; b) F. Bozoglian, S. Romain, M. Z. Ertem, T. K. Todorova, C. Sens, J. Mola, M. Rodríguez, I. Romero, J. Benet-Buchholz, X. Fontrodona, C. J. Cramer, L. Gagliardi, A. Llobet, *J. Am. Chem. Soc.* **2009**, *131*, 15176.

[16] J. Klingele, S. Dechert, F. Meyer, *Coord. Chem. Rev.* **2009**, *253*, 2698.

[17] a) J. I. van der Vlugt, S. Demeshko, S. Dechert, F. Meyer, *Inorg. Chem.* **2008**, *47*, 1576; b) B. Schneider, S. Demeshko, S. Dechert, F. Meyer, *Angew. Chem.* **2010,** *122*, 9461; *Angew. Chem. Int. Ed.* **2010**, *49*, 9274.

Ammonoxidation

Ammonoxidised Lignins as Slow Nitrogen-Releasing Soil Amendments and CO_2-Binding Matrix

Falk Liebner, Georg Pour, José Maria de la Rosa Arranz, André Hilscher, Thomas Rosenau, Heike Knicker

Nitrogen (N) is a major nutrient element controlling the cycling of organic matter in the biosphere. Its availability in soils is closely related to biological productivity. In order to reduce the negative environmental impact, associated with the application of mineral N-fertilizers, the use of ammonoxidised technical lignins is suggested. They can act as potential slow N-release fertilisers which concomitantly may increase C sequestration of soils by its potential to bind CO_2. The idea of our study was to combine an improved chemical characterisation of ammonoxidised ligneous matter as well as their CO_2-binding potential, with laboratory pot experiments, performed to enable an evaluation of their behaviour and stability during the biochemical reworking occurring in active soils.

1. Introduction

Among today's crucial global socioeconomic and ecological issues, erosion by wind and water and the resulting soil degradation are most prominent ones. In many parts of the world, agricultural areas are insufficient to guarantee for adequate nutrition, in addition to a permanently growing population.

A major factor in maintaining soil productivity represents the replacement of N used for plant growth which is mostly achieved by the amendment of mineral fertilisers. However, the unintended costs to the environment and human health due to surplus and inefficient application are substantial. Runoff from farms can lead to contaminated surface and groundwater and ammonia and nitrous oxides released from fertilised cropland are considered as major source of air pollution and potent greenhouse gases. Thus, since fertilisation is essential, there is certainly an urgent need for the development of efficient and environmentally sustainable fertilisers that are able to slowly release their N in accordance with the needs of the plants.

A further matter of intensive current attention and debate is the global climate change. Taking large-area deforestation and extensive utilisation of fossil fuels as most probable reasons, both aspects have also caused a dramatic atmospheric increase in CO_2, the former by a decrease in the fixation of CO_2 in carbohydrates and the latter by release of CO_2 upon combustion of carbon-containing matter.

Current environmental research strategies focus on alternative energy sources, on effective landscape and soil rehabilitation to increase primary production and thus CO_2 fixation in renewable matter, and on the usage of CO_2 as a synthon in chemical processes. This chemical fixation is superior to a mere CO_2 storage or sequestration. The project "COBAL - CO_2 binding of ammonoxidised ligneous materials" (since 2008) within the framework of the ERA-chemistry call „Chemical activation of carbon dioxide and methane" and jointly funded by the German DFG and the Austrian FWF addresses these aspects.

Ammonoxidation of technical lignins or ligneous materials under mild conditions is proposed as an approach to mimic the natural humification process.[1] Technical lignins are by-products of the pulp and paper industry or of biorefinery processes which are so far almost exclusively "energetically used", i.e. burned. Upon ammonoxidation, ligneous matter reacts with aqueous ammonia and oxygen in suspension or solution under slightly elevated pressure and temperature. The N-enriched products are expected to be valuable humus substitutes, which are able to return N (amines, amides, carbamates) as well as C (lignin C and CO_2 bound as carbamates) to the soil and into mineralization cycles, stimulating microbial biomass production and hence soil development. Ammonoxidised lignins are likely to allow for a long-lasting fertilisation due to the presence of different types of N bonds that mineralise in soil at different rates. However, up to now, neither the mechanisms of N enrichment during ammonoxidation nor the chemical nature of the organic N or its behaviour in soils is well understood. Therefore, the investigation of N binding in different ammonoxidised lignins as well as their stability in soils where biological activity enforces high competition for the limited N sources has been a central task of the COBAL project. As the N moieties are crucial in interacting with CO_2, comprehension of their structure and their role in CO_2 fixation, both under the conditions of laboratory chemistry and the complex situation of soil environments goes hand in hand.

Further, a better understanding of the chemical constitution and properties of artificial and natural humic substances is generated.

2. Ammonoxidation of lignins and elucidation of different nitrogen binding

Amongst several theories on natural humification, the polyphenol theory is based on the assumption that low molecular phenolic and quinoid intermediates are formed by microbial lignin degradation products.[2] This is in line with the concept of our studies on ammonoxidation chemistry. 2,5-Dihydroxy-[1,4]benzoquinone (DHBQ) and methoxyhydroquinone (MHQ) were chosen as model compounds as they were the most likely intermediates to be formed if the humification process follows the polyphenol theory, i.e. oxidative, microbial degradation of lignin, and subsequent re-condensation of the reactive phenol and quinone intermediates under incorporation of N.

Analytical data, e.g. ^{15}N CPMAS NMR and XPS spectra, of the ammonoxidised model compounds and the ammonoxidised technical lignins Indulin AT (Pine kraft lignin; MeadWestvaco, Charleston, SC, USA), Sucrolin (autohydrolysis bagasse lignin; Illovo Sugar Ltd., Sezela, South-Africa) and Sarkanda grass soda lignin (Granit SA, Lausanne, Switzerland) are very similar, indicating the reaction sequence to proceed via a common key intermediate. To exploit the ^{15}N NMR technique, we used isotopic enrichment through ^{15}N-labelled aq. NH_4OH in many of our experimental approaches. The data suggest furthermore a far-reaching lignin degradation to MHQ-analogous low-molecular phenols at least under ammonoxidation conditions (100°, 5% aq. NH_4OH, 2 bar O_2).

DHBQ was shown to react with ammonia to 2,5-diamino-[1,4]benzoquinone (DABQ) already at slightly elevated temperature. Interestingly, DABQ and its N-methylated counterpart 2,5-bis(methylamino)-[1,4]benzoquinone were also isolated from the reaction mixtures of MHQ with aqueous ammonia and methyl amine, respectively. As the presence of DABQ in ammonoxidised technical lignins was also confirmed (2D-NMR) we accumulated sufficient evidence to propose (substituted) 2,5-diamino-[1,4]benzoquinones as key intermediates in the chemical alteration of ligneous materials caused by ammonia/amines under aerobic conditions. 2,5-Diamino-[1,4]benzoquinone can be perceived as a dimeric vinylogous amide as the two amino groups of the symmetric molecule are each located in β-position of an α,β,-unsaturated carbonyl moiety. This accounts for the peculiar reactivity of the compound which behaves more as an amide rather than an amine, and also the spectral data point to an amide. Another striking feature is the strong stabilisation of the molecule by H-bonds in acidic or neutral media and by resonance in alkaline medium (Scheme 1). Nevertheless, the intermediate DABQ disappears after longer ammonoxidation times as shown by UV/Vis and IR spectroscopy, and the structural elucidation of the reaction products is currently going on.

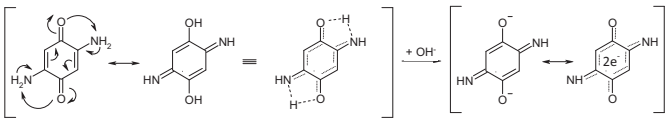

Scheme 1. Stabilisation of the dimeric vinyloguous amide 2,5-diamino-[1,4]benzoquinone by tautomerism and resonance.

3. CO_2 binding of ammonoxidised lignins and lignin model compounds

Several secondary amines are able to bind CO_2, mostly in the form of 2:1 complexes.[3] These compounds can be described both as addition products or ion pairs (dialkylammonium dialkylcarbamates, "dialcarbs"). The simplest candidate of this compound class, the dimethylamine - carbon dioxide complex (cf. Scheme 2), is a good example to reflect the complex structural-dynamic behaviour in these addition products. Many dialkylammonium dialkylcarbamates are room-temperature ionic liquids or room-temperature salts, but they may reversibly degrade into their gaseous components upon heating, and re-form upon cooling. They can thus be "distilled" in contrast to the conventional heterocycle-based ionic liquids.

Ammonoxidised lignins are supposed to bind CO_2 in carbamate complexes in an action mode similar to low-molecular weight secondary amines, especially if ammonia is (partially) replaced by amines. This is due to the content of alkylaminobenzoquinones, alkylamines and alkylamides, and has been confirmed for the ammonoxidised models 2,5-dihydroxy-[1,4]benzoquinone and methoxyhydroquinone. Both significantly increase the CO_2-binding ability of lightweight bacterial cellulose aerogels (8 mg cm^{-3}) when finely dispersed as nanoparticles inside the aerogel pore network. As mentioned, the content of dialkylamines and dialkylamides as CO_2-binding moieties in N-lignin is further increased using (di)methylamine instead of ammonia in the preparation of the N-lignins. Dialkylammonium (dialkyl)carbamates are stable compounds that can be stored without decomposition.

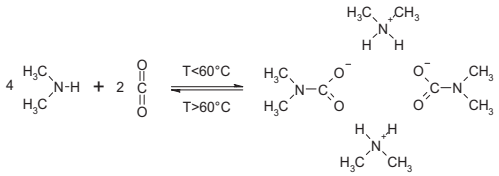

Scheme 2. Formation of the dimethylamine carbon dioxide ("Dimcarb") complex.

4. CO_2 binding of activated hydroxybenzo-quinones

Recently, it was demonstrated that not only lignoid phenols, but also cellulose is converted into 2,5-dihydroxy-[1,4]benzo-quinone structures upon aging, with those structures mainly contributing to residual chromophores and yellowing effects.[4,5] These findings are intriguing with respect to the current teaching

of natural humification, claiming those structures in humic substances to originate mostly from lignin and secondary metabolic products. Hydroxy-[1,4]benzoquinones have found no significant synthetic usage so far. This is due to their properties as potent chromophores and their tendency to undergo condensation and polymerisation reactions. This behaviour, which is preventive for synthetic utilization, renders them predestined for natural and artificial humification scenarios – and for the studies in the present project. Importantly, 2,5-dihydroxy-[1,4]benzoquinone structures exhibit a peculiar behaviour that has been neither recognised nor used so far. In weakly acidic to alkaline medium, 2,5-dihydroxy-[1,4]benzoquinones form symmetrical dianions highly stabilised by resonance (cf. Scheme 3), with the remaining non-substituted ring positions being able to attack carbon dioxide and carbonic acid derivatives, by analogy to biochemical pathways. Such carboxylation of 2,5-hydroxy-[1,4]benzoquinone in neutral medium is one of the very few examples of binding CO_2 under carbon-carbon bond formation. The resulting alicycles undergo fragmentation and rearrangements according to several pathways (Scheme 3).

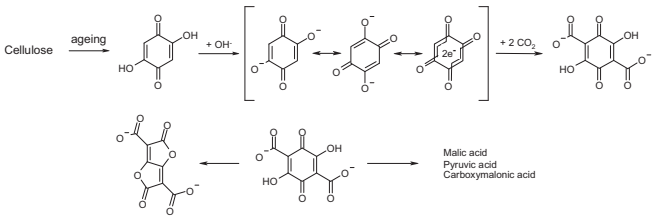

Scheme 3. 2,5-Dihydroxy-[1,4]benzoquinone and its proposed carboxylation reaction under alkaline conditions.

The main products are C_2-C_4 monoacids, oxoacids and diacids. The average CO_2-binding capacity of DHBQ at neutral pH is 1.86 equivalents. In contrast to the temporary binding of CO_2 by N functionalities such as in Dimcarb, the CO_2 binding by DHBQ-type compounds is permanent. In N-lignins, both binding modes are active.

5. Ammonoxidised lignins as slow N-release fertilizer

For the study of the effect of ammonoxidised lignin on plant growth, a series of pot experiments were conducted for two and a half months. In the first, material of a Terra rossa representing a typical agriculturally used soil of Mediterranean regions, was mixed with ^{15}N-enriched ammonoxidised lignin (Indulin and Sarkanda) on which grass seeds (Lolium perenne) were planted and grown in a greenhouse under controlled conditions based on an experimental design described in more detail by de la Rosa Arranz and Knicker.[6] The above-ground biomass production as well as the partitioning of the ^{15}N label among the plant, the microbial biomass and the soil was monitored as a function of incubation time. A high ^{15}N enrichment of 2.5 to 2.8 atom% was used to enable ^{15}N NMR spectroscopy of the soils amended with N-lignins. Their addition to the organic-matter-poor and calcareous soil increased its N content from 0.9 mg g^{-1}soil to 1.5 (^{15}N-Indulin) and 1.6 mg g^{-1} soil (^{15}N-Sarkanda). In order to account for possible N losses due to leaching, the bottom of the incubation pots were perforated to allow the exit of excess water after watering. For comparison, a control soil without any amendment and a soil mixed with $K^{15}NO_3$ were prepared. Because we expected a fast removal of the latter due to leaching, the starting ^{15}N concentration was 10 mg 100 g^{-1} soil.

Compared to the controls, the addition of $K^{15}NO_3$ resulted in a significant increase of the total above-ground plant yields. Most of the growth occurred during the first 18 days for the control and during 28 days for the fertilised samples. After that, the growth rate declined significantly which is best explained with the using-up of the bioavailable N pool. This assumption is supported by the fact that after one month incubation time less than 20% of the added ^{15}N ($^{15}N_{add}$) were recovered with the soil matrix, whereas a third was already incorporated into the above-ground plant biomass and no major increase was achieved until the end of the experiment. However, in spite of the low ^{15}N amendment, between 40% and 60% of $^{15}N_{add}$ were already lost after one month either due to leaching but possibly also by volatilisation. With the expectation that ammonoxidised lignins act as a slow release fertiliser and prevent fast N leaching they were applied in amounts in which $^{15}N_{add}$ was between 4 and 6 times higher than with the mineral fertiliser. This, however, did not result in higher above-ground biomass production. Not earlier than after 42 days (^{15}N-Indulin) and 58 days (^{15}N-Sarkanda) the accumulated harvest overran, but only slightly that of the unfertilised pots. In spite of the lower mass yields, the N concentrations were approximately 70% higher, suggesting that the above-ground shoots of the ^{15}N-lignin-added pots were considerably richer in proteins than those from the mineral fertilised pots.

After 58 days, less than 7% and 20% of $^{15}N_{add}$ of ^{15}N-Indulin und ^{15}N-Sarkanda were incorporated into the plant shoots. In the ^{15}N-Indulin experiment, most of the unused $^{15}N_{add}$ remained in the soil (80% of $^{15}N_{add}$), indicating that here, N was efficiently sequestered from fast release into the soil solution. The ^{15}N-Sarkanda lignin, on the other hand, showed a different picture. Here, already after 28 days of incubation only one-third of the $^{15}N_{add}$ were retained in the soil, most of which was recovered with the microbial biomass, as it was determined with the chloroform fumigation extraction methods.[7] The respective $^{15}N_{add}$ recovery with the microbial biomass for the ^{15}N-Indulin series was about 8%. Although for both experiments, the amount of ^{15}N retained in the soil matrix did not alter much until the end of the incubation, $^{15}N_{add}$ associated with the microbial biomass declined to less than 2%.

In order to obtain some more insights into the fate of the N-lignins during plant growth, the soil material of selected pots were dried and after removing the carbonates with HCl they were demineralised with hydrofluoric acid[8] to increase their sensitivity for solid-state ^{13}C and ^{15}N CPMAS NMR spectroscopy. The latter was further facilitated by the high ^{15}N enrichments. The solid-state ^{13}C CPMAS NMR spectra of the ^{15}N-lignins showed the typical lignin pattern[9] and the respective solid-state ^{15}N CPMAS NMR spectra demonstrated signals in the chemical

shift region assignable to pyrrole-type N (-145 to -245 ppm) (Figure 1), as well as considerable signal intensity in the chemical shift regions of aminobenzoquinones (-274 ppm), aminohydroquinones (-304 ppm), aromatic amines (-330 ppm) and ammonium (-358 ppm).[10,11] However, in the ^{15}N NMR spectra of the HF-treated soil material from the pot after 30 days of incubation those typical signals disappear in favour to a dominating signal around -260 ppm and a small intensity at -348 ppm, demonstrating a surprisingly fast transformation of the aromatic amino groups into peptide-type N, although some intensity remained in the chemical shift region assignable to pyrrole-type N. The signals at -260 and -348 ppm are also observed in the ^{15}N NMR spectrum of the soils amended solely with $K^{15}NO_3$ and are typical for organic N in biomass.[12]

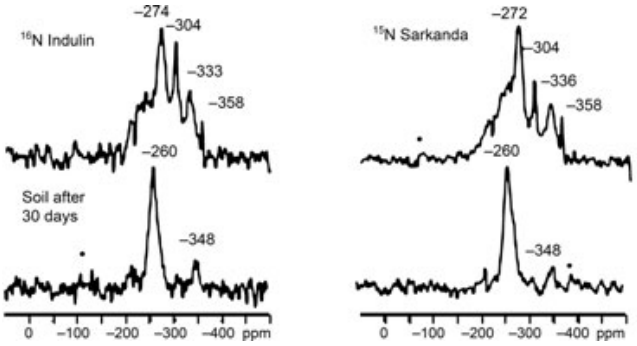

Figure 1. Solid-state ^{15}N CPMAS NMR spectra of the used ^{15}N-lignins and the HF-treated soils amended with ^{15}N-lignins and $K^{15}NO_3$ after one month of incubation. Asterisks indicate spinning side bands. The spectra were obtained at the Lehrstuhl für Bodenkunde, TU-München.

The shift of the ^{15}N signal intensity, thus, is most tentatively caused by the fast and efficient recycling of amino groups released from the lignin backbone for the build-up of new microbial biomass. The high $^{15}N_{add}$ recovery in the microbial biomass of the pots incubated for one month after amended with the ^{15}N-lignins supports this conclusion. With respect to soil organic C, the solid-state ^{13}C CPMAS NMR spectroscopy revealed no major alteration due to incubation.

For the next experiment, material of a Luvisol[13] derived from the experimental station Viehhausen of the TU-München was mixed with Indulin that beforehand was ammonoxidised with methylamine (P1) or dimethylamin (P2). These lignins, synthesized to increase the CO_2 binding potential, were compared to 2,5-diamino-[1,4]benzoquinone (P3) and 2,5-dihydroxy-[1,4]benzoquinone ammonoxidised with NH_3 (P5) and control soils with and without addition of KNO_3. Although the basic experimental set-up remained comparable to the first incubation, this time, leaching was not enabled and the N-addition via KNO_3 was approximately the same as for the other pots. The N content of the soil matrix was with 0.15% approximately twice as high as for the Terra rossa, which most tentatively contributed to a doubling of the yields with respect to the control of the first experiment. However, here the plant production could not be increased by KNO_3 addition. Comparable to the first experiment, the germination was retarded with P1 and P2 by 2 weeks and with P5 by at least one month. Whereas, relative to the control, after 8 weeks, P1 and P2 addition finally increased the harvest by more than a factor 2, P3 and P5 could not achieve this threshold.

The C/N ratio of the grass grown on the control pots confirmed that consumption of bioavailable N results in the production of low-protein plant biomass. Concomitantly, the high availability of KNO_3 resulted in grass shoots with a very low C/N (w/w) ratio of 5.6. The excess supply of mineral N, however, turned to a disadvantage which led to the death of grass plants after 2 months. Low C/N values were also detected for P1 and P2 (7) but increased to 20 until the end of the experiment, indicating that here, too, the availability of the N source declined after a first boost. Plant shoots from pots with P3 and P5 had C/N-values of around 10 and 6, respectively. Whereas no N loss was detected for the control approximately 23 and 32% of the KNO_3-N was lost, most of which already during the first two weeks. Comparably high losses of N_{add} were observed for the N-lignins and the N-model compounds. It seems that similar to the first experiment, a part of the "amino"-N which has been shown to behave as an amide (see above) was relatively quickly released from the aromatic backbone and subjected to N-cycling in the soil. Whereas the N-recoveries remained constant for P1 and P3, for P5, they decreased to 50% after 4 months.

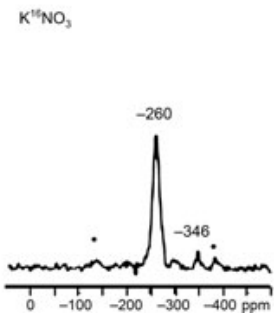

In order to test the assumption derived from the two pot experiments that in a soil system, some of the N of the ammonoxidised lignins, may be quickly mineralised, the concentrations of inorganic N were determined as a function of incubation time.[14] After two weeks, for the soils amended with P1, P2 and P3, 10% of N_{add} was recovered as NH_4^+. Since, here, ^{15}N-labelling was not applied, we were not able to obtain unbiased quantitative data about N partitioning into microbial biomass. After two months, the concentrations of extractable NH_4^+ decreased to values comparable to those determined for the control pots. Because neither an increase of the N loss nor a noteworthy transformation into nitrate was revealed, it can be assumed that after the first flush, the released N was used for plant growth, although some part was certainly incorporated into microbial remains that subsequently contributed to the soil organic matter pool. The model lignin P3 showed no major accumulation of NH_4^+ at any stage of the experiment and for P5, 18% of N_{add} was extracted as NH_4^+ after two weeks. Considering the low N-recovery of 68% for this sample, it seems that at least 50% of N_{add} have passed through the mineral stage before any plant growth occurred. Comparable to P1 and P2, the concentration of NH_4^+ were decreasing constantly during the experiment, either by the mechanisms discussed above or by

further N losses since only 50% of N_{add} were recovered in plant and soil after four months.

6. CO_2 binding of ammonoxidised Indulin in a soil respiration experiment

The impact of N-lignin addition on the CO_2-sequestration potential of soils was elucidated in a model experiment determining the respective CO_2-release of soil incubates with and without addition of N-Indulin in a Respicond Apparatus IV (A. Nordgren Innovations AB, Sweden). This was based on the idea that efficient CO_2 fixation by the N-lignins decreases the amount of CO_2 released during soil organic matter degradation. Nevertheless, we were aware that this experiment could only be a first approach, since lower CO_2-release rates can also be caused by i) a slower degradation of the added lignin, ii) by a possible inhibition of microbial activity or iii) by the opposite, namely an increased microbial growth due to higher amounts of substrate and N. For our experiment, we used a sandy and acid soil (pH: 4; Histic Humaquept from the Doñana National Park, Spain) to avoid possible CO_2 adsorption to the matrix. Materials of two horizons with different C contents (4% C and 2% C) were used with and without addition of N-Indulin and Indulin. All samples were inoculated with a bacterial mixture isolated from a gardening soil. After two and a half months of microbial degradation at 28°C, all vessels showed a comparable C loss of 5 to 6%, thus no major differences of the C-sequestration potential were observed.

Those results imply two major conclusions. First, the comparable degradation rates evidence that lignins are degraded at a rate comparable to natural soil organic matter. Second, CO_2 produced during soil organic matter degradation was not efficiently sequestrated by the added N-lignin under the used conditions. However, this may change under neutral or weak alkaline conditions under which CO_2 fixation according to the proposed mechanisms (schemes 1 and 2) is expected to be much more pronounced.

Summary

^{15}N CPMAS NMR and XPS spectra of ^{15}N labelled ammonoxidised technical lignins, methoxyhydroquinone and 2,5-dihydroxy-[1,4]benzoquinone were very similar, indicative for a reaction sequence proceeding via a common key intermediate. Therefore, (substituted) 2,5-diamino-[1,4]benzoquinones are proposed to be key intermediates of the chemical alteration of ligneous materials caused by ammonia or amines in the presence of oxygen. 2,5-Diamino-[1,4]benzoquinones are vinylogous amides which are highly stabilised by tautomery and resonance. Both ammonoxidised methoxyhydroquinone and 2,5-dihydroxy-[1,4]benzoquinone were confirmed to bind CO_2. 2,5-Dihydroxy-[1,4]benzoquinone was furthermore shown to react in alkaline medium with CO_2 to C_2-C_4 monoacids, oxoacids and diacids. Subjecting the ammonoxidised lignins to pot experiments resulted in a surprisingly fast formation of amides. During the first weeks at least a part of the N_{add} passes through the microbial biomass stage. The harvested plants showed an N enrichment caused by the amendment. Respiration experiments revealed comparable CO_2 production rates in soil incubated with and without N-lignins, possibly because microbial activity competed with CO_2 for the available N groups.

Zusammenfassung

^{15}N-CPMAS-NMR- und XPS-Spektren von ^{15}N-markierten, ammonoxidierten technischen Ligninen, Methoxyhydrochinon sowie 2,5-Dihydroxy-[1,4]benzochinon wiesen eine überraschende Ähnlichkeit auf, woraus auf eine Reaktionssequenz mit einem gemeinsamen Intermediat geschlossen wurde. Als Schlüsselverbindung der chemischen Modifizierung von ligninhaltigen Materialien durch Ammoniak oder Amine in Gegenwart von Sauerstoff wurden (substituierte) 2,5-Diamino-[1,4]benzochinone vorgeschlagen. 2,5-Diamino-[1,4]-benzochinone sind vinyloge Amide die durch Tautomerie und Resonanzeffekte in besonderem Maße stabilisiert werden. Sowohl Methoxyhydrochinon als auch 2,5-Dihydroxy-[1,4]benzochinon weisen nach Ammonoxidation ein erhöhtes Bindevermögen für CO_2 auf. Weiterhin konnte gezeigt werden, dass 2,5-Dihydroxy-[1,4]benzochinon in alkalischem Medium mit CO_2 zu C_2-C_4-Monocarbonsäuren, -oxosäuren und -disäuren reagiert. Topfexperiment zeigten, dass die Zugabe der ammonoxidierten Lignine zu einer überraschend schnellen Bildung von Amiden führt. Schon während der ersten Wochen wurde zumindest ein Teil des N_{add} in mikrobielle Biomasse eingebaut. Elementaranalysen bestätigten eine durch die Düngung verursachte N-Anreicherung im Grasmaterial. In Respirationsexperimenten wurden für Böden mit und ohne N-Lignin-Zugabe vergleichbare CO_2-Mengen freigesetzt. Eine mögliche Erklärung hierfür könnte die Konkurrenz zwischen Mikroorganismen und CO_2 um die verfügbaren N-Gruppen darstellen.

Acknowledgements

The financial support of the German DFG (projet: KN 463/9-1) and Austrian FWF through the project I154-N19 is gratefully acknowledged. The authors would like to thank E. Brendler, TU Bergakademie Freiberg, Germany, and J. Ralph, University of Wisconsin-Madison, USA, for recording some of the ^{15}N CPMAS and the 2D-NMR spectra. Furthermore, we thank H. Hesse and P. Streubel, University of Leipzig, Germany, for the X-ray photoelectron analyses. The IRNAS-CSIC, Spain, is gratefully acknowledged for providing access to their greenhouse, their respirometer as well as their laboratory facilities. Comparably, the Lehrstuhl für Zierpflanzenbau of the TU-München, Germany, is thanked for allowing us to use their Phytotrons.

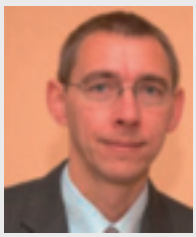

Falk Liebner [1] *is Assistant Professor and head of the group "Biomaterial Chemistry" at the University of Natural Resources and Life Sciences Vienna (BOKU), Dept. of Chemistry, Chair of Wood, Pulp and Fiber Chemistry.*

Email: falk.liebner@boku.ac.at

Georg Pour [1] *is PhD student at the University of Natural Resources and Life Science Vienna (BOKU), Dept. of Chemistry, Chair of Wood, Pulp and Fiber Chemistry.*

Email: georg.pour@boku.ac.at

José Maria de la Rosa Arranz [2] *is auxiliary researcher at the Nuclear and Technologic Institute of Portugal.*

Email: jmrosa@itn.pt

André Hilscher [3] *is PhD student at the Lehrstuhl für Bodenkunde of the Technische Universität München-Weihenstephan.*

Email: hilscher@wzw.tum.de

Thomas Rosenau [1] *is full professor and chair of Wood, Pulp and Fiber Chemistry at the University of Natural Resources and Life Sciences Vienna (BOKU), Dept. of Chemistry (since 2005).*

Email: thomas.rosenau@boku.ac.at

Heike Knicker [4] *is profesora de investigación (since 2008) at the Institute of Natural Resources and Agrobiology of Sevilla (IRNAS-CSIC) and apl. Professor at the Lehrstuhl für Bodenkunde, TU-München.*

Email: knicker@imase.csic.es

Addresses:

[1] *Konrad-Lorenz_Str. 24, A-3430 Tulln an der Donau*

[2] *Estrada Nacional 10, P- 2686-953, Sacavém*

[3] *Emil-Ramann-Straße 2, D-85354 Freising*

[4] *Avda. Reina Mercedes, 10, E-41012 Sevilla*

[1] F. Liebner, K., Fischer, J. Katzur, L. Böcker in *The Loess Plateau in Central China: Ecological Restoration and Management* (Ed.: UNESCO office Beijing), Tsinghua University Press, Springer, Beijing**, 2005**, pp. 183-207.

[2] M. Kästner, M. Hofrichter in *Biopolymers I* (Eds.: A. Steinbüchel, M. Hofrichter), Wiley-VCH, Weinheim, **2001**, pp. 349-378.

[3] W. Schroth, H.-D. Schädler, J. Andersch, *Z.. Chem.* **1989**, *29*, 129-135.

[4] T. Rosenau, A., Potthast, W. Milacher, A. Hofinger, P. Kosma, *Polymer* **2004**, *45,* 6437-6443.

[5] K. Kraintz, A. Potthast, U. Suess, T. Dietz, N. Nimmerfroh, T. Rosenau, *Holzforschung* **2009**, *63*, 647-656.

[6] J.M. de la Rosa Arranz, H. Knicker, *Soil Biol. Biochem.* **2011,** accepted.

[7] D.S. Jenkinson, D.S. Powlson, *Soil Biol. Biochem.* **1976**, *8,* 167-177.

[8} C.N. Gonçalves, R.S.D. Dalmolin, D.P. Dick, H. Knicker, E. Klamt, I. Kögel-Knabner, *Geoderma* **2003**, *116*, 373-392.

[9] H. Knicker, H.-D. Lüdemann, K. Haider, *Europ. J. Soil Sci.* **1997,** *48,* 431-441.

[10] K. A. Thorn, M.A. Mikita, *Sci. Total Environ.* **1992**, *113*, 67-87.

[11] M. Witanowski, L. Stefaniak, G.A. Webb. *Nitrogen NMR Spectroscopy*, Academic Press, London, **1993**.

[12] H. Knicker, *J. Environ. Qual.* **2000**, *29*, 715-723.

[13] H. Knicker, P. Müller, *Water Air Soil Poll.* **2006**, *6*, 235-260.

[14] J. C. Forster in *Microbiology and Biochemistry* (Eds.: K. Alef, P. Nannipieri), Academic Press, London, **1995**, pp. 49-121.

Carbamate Synthesis

Pd-N to Pd-O Rearrangement for a Carbamate Synthesis from Carbon Dioxide and Methane: A Density Functional and Ab Initio Molecular Dynamics Metadynamics Study

Philipp J. di Dio, Marc Brüssel, Kilian Muñiz, Rupashree Shyama Ray, Stefan Zahn, Barbara Kirchner

We investigated the key step of Pd-N to Pd-O rearrangement from a model catalytic cycle for the activation of carbon dioxide and methane with static quantum chemical calculations and metadynamics simulation. Our calculations show that different bottlenecks appear in the catalytic cycle but that the investigated rearrangement of the Pd-N to Pd-O bounded complex has a barrier $\Delta G^{\#}/\Delta F^{\#}$ of approximately 20 kJ mol^{-1} and is therefore accessible at ambient reaction conditions.

1. Introduction

Since the first isolation and characterization of a carbon dioxide-transition metal complex by Aresta in 1975,[1] the fixation and activation of carbon dioxide as a non-toxic, abundant, and inexpensive C_1 building block in organic synthesis was extensively studied by experimental as well as theoretical methods.[2] There are several transition and main-group metal complexes which are capable to engage in CO_2 fixation and subsequent chemical transformation. Usually, CO_2 can be activated within two different binding modes at the active site of a transition metal: The transition metal interacts with one C-O π-bond in a η^2-binding mode or a transition metal C-bond is formed in a η^1-binding mode (Figure 1).[3]

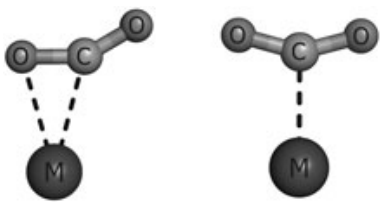

Figure 1. Ball-and-stick model illustrating the η^2-binding mode (*left*) and η^1-binding mode (*right*) of CO_2 with a transition metal M.

Both cases result in a non-linear CO_2 geometry and allow reactions of CO_2 with various substrates. In this way, coordinated CO_2 can be reacted to form methanol, formic acid, ureas, lactones, carboxylic acids etc.[4] Alternatively, CO_2 can be functionalized directly with organometallic reagents, for example in the synthesis of carboxylic acids.[5] Overall, a series of synthetic transformations is now available that demonstrates the usefulness of CO_2 as a C_1 building block. Particular interest in CO_2 fixation has recently been devoted to the condensation of this molecule with epoxides under metal catalysis.[6] Organic carbonates are widespread feedstocks for industrial synthesis. Therefore, an easy, cheap and save production process is desirable. While traditional routes for synthesizing organic carbonates usually involve the highly poisonous phosgene ($COCl_2$), several atom-economic reactions, where CO_2 reacts with peroxides in the presence of a metal catalyst, are now available (Figure 2).

Figure 2. A simple example of an epoxide reacting with CO_2 in the presence of a catalyst.

Although detailed description about the mechanisms and the reaction conditions for several catalytic CO_2 condensation reactions with epoxides has been accomplished,[6] most reactions still need vigorous reaction conditions and a further improvement of the catalysts is hence required.

Besides the CO_2 activation, the activation of C-H bonds is also of special interest to chemists. The direct functionalization of alkanes from small, simple, and inexpensive molecules like methane CH_4, ethane CH_3-CH_3, and toluene $C_6H_5CH_3$ leads to important synthetic precursors for academic synthesis and

industrial processes. This has been widely applied[7] and investigated[8] for different C-H bond types (C_{ar}-H, C_{sp2}-H, C_{sp3}-H, ...) and different metal complexes (Ni, Au, Pt, Pd, ...) forming different bonds (C-C, C-N, ...).[9]

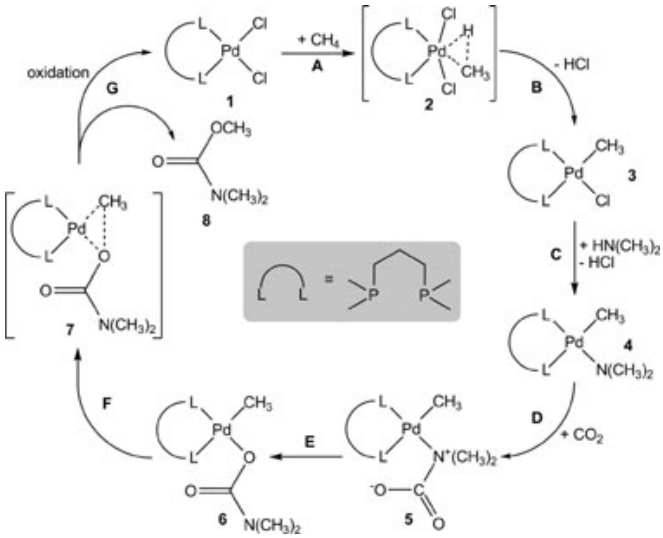

Scheme 1. Proposed and investigated catalytic cycle for the activation and fixation of CO_2 and CH_4 forming the methyl *N*,*N*-dimethylcarbamate **8** at the palladium catalyst **1**.

We currently pursue an approach to combine both carbon dioxide and methane activation within a single catalytic cycle, which is shown in Scheme 1 for a palladium catalyst **1** bearing the bis(dimethylphosphino)-propane ligand. In this proposed catalytic cycle, the reaction starts with methane activation (step **A**) through an intermediate **2** to form a palladium methyl complex **3** under concomitant loss of HCl. Exchange of the remaining anion at palladium for dimethylamine (step **C**) proceeds with loss of HCl and forms a palladium amide complex **4**. Since reductive elimination of trimethylamine from **4** is a slow process, addition of carbon dioxide should be kinetically feasible. This step **D**, the coordination of CO_2 to the amide ligand, was investigated previously with ab initio molecular dynamics simulations, in particular by metadynamics and thermodynamic integration.[10] The comparison between solvated and gas phase simulation gave insight into solvation effects. The results demonstrated that the CO_2 addition to **4** takes place with an activation barrier of approximately $\Delta F^{\#} = 45$ kJ mol^{-1}. The final catalytic cycle should then proceed through a series of steps including the rearrangement from **5** to **6** (step **E**), followed by reductive elimination through transition state **7**. This step liberates the carbamate product **8** and generates a palladium(0) catalyst state that upon reoxidation (step **G**) regenerates the initial catalyst **1**.

In the following, we investigate step **E** of the catalytic cycle in detail. This reaction comprises a rearrangement to generate an *N*,*N*-dimethylcarbamoyl ligand. After the computational details, we first give the results of the static quantum chemical calculations for the whole catalytic cycle, i.e., the reaction energies of every single step. Thereafter, we show and discuss the quantum chemical calculations of the transition state which leads from **5** to **6** (step **E**). Finally, we present metadynamics simulations of this rearrangement in carbon dioxide solution to investigate the dynamics and solvent effects in this reactions step.

2. Computational Details

For the static quantum chemical calculations the program package Turbomole 5.10[11] was used to optimize all structures reported in this paper. No symmetry or internal coordinate constraints were applied during optimizations. We used the B3LYP functional[12,13] and all calculations were carried out with the triple-ζ basis set def2-TZVPP[14] which includes a relativistic electron core potential for Pd.[15] The energy convergency criterion was 10^{-8} Hartree. For frequency calculations the program SNF 4.0 was chosen.[16] The simulations were carried out employing Born–Oppenheimer molecular dynamics simulations with Gaussian and plane waves using the program CP2k.[17] The temperature was set to 350 K controlled by Nosé–Hoover chain thermostats.[18] A time step of 0.5 fs was chosen and the DZVP-MOLOPT-SR-GTH basis set[19] with the GTH-BLYP-q*n* pseudopotentials[20] (H: $n = 1$; C: $n = 4$; N: $n = 5$; O: $n = 6$; Pd: $n = 18$) were used. The plane wave representation was truncated with a cutoff of 280 Ryd and the gradient corrected functional BLYP[12] with Grimme dispersion correction[21] was applied. The simulations box was taken from a previous work,[10] it contains one molecule of complex **5**/**6** with 59 additional CO_2 and has a box length of 1800 pm ($\rho = 0.85$ g cm^{-3}) with periodic boundary conditions. The technique of metadynamics simulations was explicitly described in a previous work.[10] The height of the Gaussian hills was lowered during the simulations (3.9, 1.32 and 0.26 kJ mol^{-1}). The time interval between adding two Gaussian hills was increased according to the lowering of the hills height ($2.5 \cdot 10^{-2}$, $5 \cdot 10^{-2}$ and $6 \cdot 10^{-2}$ ps). The hill width was fixed to 0.3 rad for the simulation. For all three collective variables the force constant was set 840.2 kJ mol^{-1} rad^{-2} and the fictional mass to 200 amu. The figures were generated with Matplotlib, which is a 2D plotting library for Python,[22] and VMD.[23]

3. Results and Discussion

In Table 1 we show the energies from static quantum chemical calculations for the step **E** of the catalytic cycle (Scheme 1), the reaction barrier for step **E** (**E-TS**), and the overall reaction energy for the whole cycle (Σ).

Table 1. Reaction energy of the step **E**, reaction barrier **E-TS** for the investigated step **E**, and reaction energy Σ of the whole catalytic cycle (Scheme 1).

	$\Delta E^{[a]}$	$\Delta G^{[a,b]}$
E	-84.2	-99.5
E-TS	22.5	22.4
Σ	-72.5	-48.7

[a] In kJ mol^{-1}. [b] At 298.15 K.

We find that the overall reaction energy is approximately -70 and -50 kJ mol^{-1} for ΔE and ΔG, respectively. The catalytic cycle is therefore exergonic, i.e., in the direction of the formation of **8** thermodynamically preferred. Unfortunately, the different reaction energies for the different steps may vary significantly and different bottlenecks may occur in the catalytic cycle. Future investigations of this and similar methane activation cycles must therefore concentrate on the critical steps.

A detailed description of metadynamics can be found in the literature[24] or in a previous work[10] wherein we investigated step **D**. Thus, we will present here only a short introduction. In the metadynamics approach, a set of collective coordinates (CC), which are functions of the atomic coordinates, is selected. Each CC has a corresponding collective variable (CV), which is coupled to its CC. The main idea is to explore the free energy surface (FES) only in the phase space of the CVs. The FES is reconstructed by gradually building a potential in the CVs space. This potential is referred to a history dependent potential in the CVs space. If the potential is converged, it corresponds (approximately) to the FES. The convergence of the potential is a very critical point achieved by sampling multiple reaction events. The CVs should fulfill the following two criteria: Firstly, they should provide a good description of the reaction, i.e., every characteristic and significant change during the reaction must be described by the CVs. Secondly, it should be possible to clearly distinguish with the values of the CVs the different structures and reaction pathways, i.e., in our case **5** and **6** must be uniquely described by their CV values. For different reaction pathways the same argument holds.

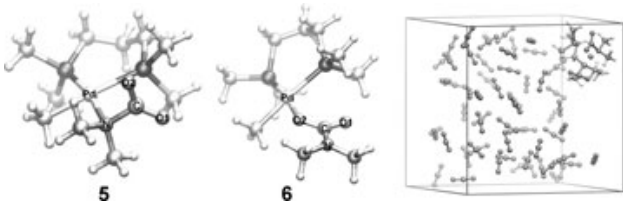

Figure 3. *left* and *center*: Atom labeling of molecules **5** and **6** for the definition of the collective variables displayed at a ball-and-stick picture. *right*: Snapshot of the simulation box with one molecule **5**/**6** and 59 CO_2 molecules.

In the present simulation three angles were selected as CVs, namely ∠(Pd-C-O1), ∠(Pd-C-O2), and ∠(Pd-C-N), see Figure 3 for atom labeling and the simulation box with **5**/**6** and 59 molecules CO_2. For the rearrangement **E** the distances r(Pd-O1), r(Pd-O2), and r(Pd-N) do also describe the reaction in a suitable way and might be a more intuitive choice for the reaction coordinate in the rearrangement. Unfortunately, the calculations with the distance CVs revealed additional reaction pathways during the simulation, namely dissociation of the amide ligand and carbon dioxide from the ligand. Like the distances, the angles are able to fulfill the criteria mentioned above in the same way. The different species are distinguishable by the values of the CVs and they provide a sufficient description of the reaction. Despite the usage of the distances, a dissociation of the amide ligand or the carbon dioxide becomes more difficult with the angles, i.e., several decomposition pathways are not easily accessible for the selected angle CVs and this leads to a better and more efficient exploration of the interesting parts of the FES. Therefore, the corresponding distances were not selected for the CVs but the angles, because the angles describe the reaction in the same way but with the advantage of time saving in the computationally expensive ab initio molecular dynamics simulations. The time saving occurs because the regions in the FES corresponding to the decomposition reactions (side reactions, not of our primary interest) need not to be sampled.

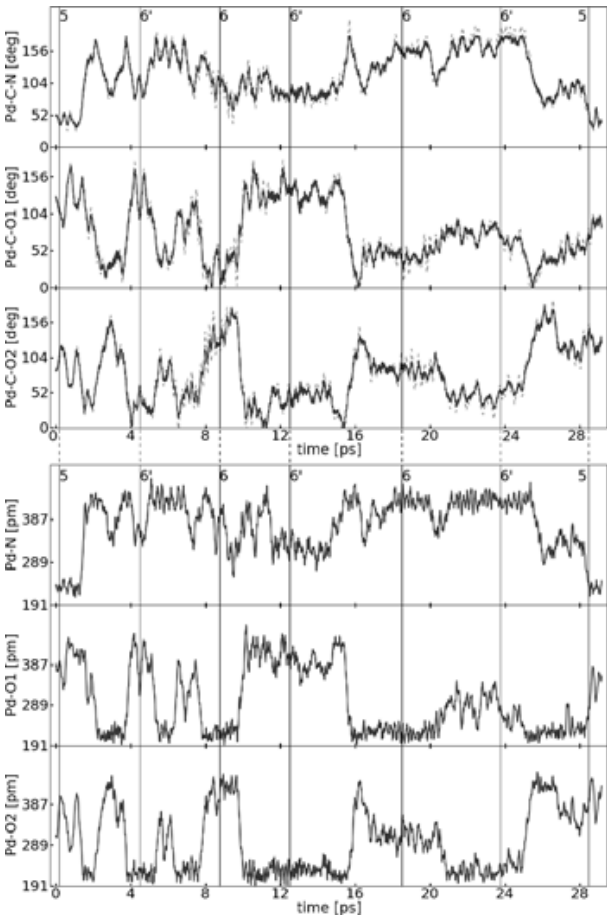

Figure 4. Dynamic of the three CCs/CVs and distances. The verticle lines highlight points which corresponds to conformers of **5**, **6**. *Top*: Dynamic of the three CCs (solid) and the corresponding CVs (dashed); *bottom*: Dynamic of the three distances (solid) in the metadynamics simulation.

It is noteworthy, that there is no physical difference between the ligands coordinated via O1 or O2 to the Pd center. The two isomers are referred to **6** and **6'** in the following discussion. The close resemblance between the selected CVs and the three distances can be observed in Figure 4, although no restrictions to the distances were applied during the simulation. The vertical lines in Figure 4 denote some conformers of **5** and **6** to illustrate some of the reaction/rearrangement events which occurred within the metadynamics simulation. Multiple events for the

rearrangement between **6** and **6'** were observed as seen from the numerous occurrences of **6** and **6'**. For step **E** only two reaction events were observed, one from **5** to **6** and one from **6** to **5** event. From the angle development (Figure 4) we find that the two Pd-C-O angles change inversely. While ∠(Pd-C-O1) shows a decrease from ≈ 1 ps to ≈ 3 ps, the ∠(Pd-C-O2) increases. This inverse behavior is found over the whole simulation time and is a consequence of the fact, that both angles are connected through the planar geometry of the carboxyl group formed by the addition of CO_2. Furthermore, at approximately 10 ps we find that ∠(Pd-C-O1) increases once more, while ∠(Pd-C-O2) drops by more than 100 degree, and at approximately 16 ps this process reverses. ∠(Pd-C-O1) decreases dramatically while ∠(Pd-C-O2) increases again. This change can be identified as a Pd-O1 to Pd-O2 bounded complex rearrangement. At approximately 10 ps the sudden angle flip is accompanied by a drastic change in the Pd-O1 and Pd-O2 distances. The Pd-O1 increases at 10 ps by more than 200 pm while the Pd-O2 distance decreases by the same amount. The Pd-O1 and Pd-O2 distances provide the same inverse relation as the corresponding angles. This shows that a doubly bounded carboxyl group to the Pd center is not stable. Despite the short simulation time, this instability is supported by the reconstructed FES and sudden change in the simulations show a more frequent rearrangement than the Pd-N to Pd-O rearrangement, the Pd-O1 to Pd-O2 with a lower barrier than the first rearrangement.

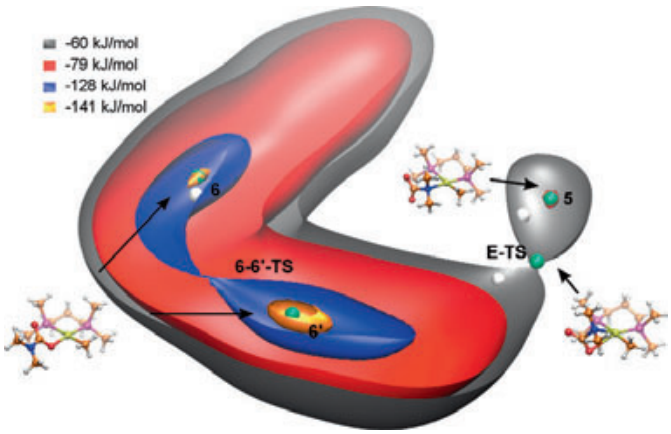

Figure 5. Reconstructed FES of the metadynamic run. The green points denote the minima and the transition state according to the FES. The white points stand for the same structures obtained with QM calculations. The isosurfaces are drawn at the following values: orange (-141 kJ mol^{-1}), blue (-129 kJ mol^{-1}), red (-79 kJ mol^{-1}) and gray (-60 kJ mol^{-1}).

In Figure 5 the reconstructed FES from the simulation is presented, i.e., its isovalue surface at four different energies. The coordinates of **6**, **5,** and of two transition states are mapped on the FES. The green points indicate the characteristic points obtained from the AIMD simulation and the white points correspond to the static quantum chemical calculations. The transition state of step **E** is labeled **E-TS**. The second transition state (**6-6'-TS**) corresponds to the Pd-O1/Pd-O2 rearrangement between **6** and **6'**. Complex **5** lies approximately on the red isovalue surface (F = -79 kJ mol^{-1}) while the transition state to **6**/**6'** lies on the gray surface with F = -60 kJ mol^{-1}. Therefore, the height of the transition state for step **E** amounts to $\Delta F^{\#}$ = 19 kJ mol^{-1}. The transition state is characterized by the constriction in the dark gray surface indicating a saddle point. Both parts of the surface, i.e., the first part surrounding **5** and the second part surrounding **6** and **6'**, meet at the saddle point, i.e., the transition state. The activation barrier of approximately 19 kJ mol^{-1} from the metadynamics AIMD simulation is therefore in close agreement with the static barrier of approximately 22 kJ mol^{-1}. Dynamic and solvent effects have therefore only little or no influence on the transition state barrier. The similar behaviour is also observed on geometries. In Table 2 the angles for both, dynamic and static, transition states are compared.

Table 2. Comparison of the structures obtained from the static quantum chemical (QM) calculations and the AIMD simulation

Angle[a]	AIMD				QM		
	6'	**6**	**5**	**E-TS**	**6**	**5**	**E-TS**
Pd-C-N	135	152	41	54	150	45	64
Pd-C-O1	110	39	123	145	36	110	135
Pd-C-O2	35	96	106	75	90	100	66

[a] In degree.

Additionally, the reagent (**5**) and the product (**6** and **6'**) angles are listed. For the transition state **E-TS**, the difference in angles is about 10 degree. These small differences can be explained by dynamic effects, steric obstruction from the solvent, and the method for locating the dynamic transition state. In comparison to the static quantum chemical calculations where the transition state is perfectly defined and refined by the geometry optimization procedure, the dynamic transition state is determined from the time development of the angles (Figure 4). The largest slopes of the angle time development were used to define approximately the transition state. Despite these difficulties in characterizing a transition state using molecular dynamics, the characteristics of the static and the dynamic transition state are very similar, energetically as well as geometrically. From isovalue surfaces, the reaction energy for step **E** is evaluated to be approximately -62 kJ mol^{-1}. Determination from static quantum chemical calculations is around 20 kJ mol^{-1} higher. This could be due to the different methodology used in both the cases.

The second transition state for the Pd-O1/Pd-O2 rearrangement is obtained on the blue surface (F = -128 kJ mol^{-1}). The products **6**/**6'** lie approximately on the orange surface (F = -141 kJ mol^{-1}). Therefore, for the second transition state a similar activation barrier of $\Delta F^{\#}$ = 13 kJ mol^{-1} is found, in comparison to $\Delta G^{\#}$ = 30 kJ mol^{-1} from static calculations. Both transition state barriers are approximately 19 and 13 kJ mol^{-1} high and are therefore easily accessible at ambient conditions.

Summary

We simulated the Pd-N to Pd-O rearrangement of reaction **E** *with the metadynamics approach (Scheme 1). For the simulation we used angles as collective variables instead of distances. The static quantum chemical calculations and the metadynamics barriers for this reaction are* $\Delta G^{\#}$ = 22 *and* $\Delta F^{\#}$ = 19 kJ mol^{-1}, *respectively. Therefore, finite temperature as well as solvent effects from the surrounding* CO_2 *have almost no influence on the energy. However, the structural parameters of the transition states, like distances and angles, change slightly due to the motion in the simulation. Static and dynamic calculations show that the energy barrier for the Pd-N to Pd-O rearrangement is* $\Delta G^{\#}/\Delta F^{\#} \approx$ 20 kJ mol^{-1} *and therefore accessible at ambient reaction conditions.*

Zusammenfassung

Wir simulierten die PdN-zu-PdO-Umlagerung von Reaktion **E** *mittels Metadynamik (Schema 1). Für die Simulationen nutzten wir Winkel anstelle von Abständen als kollektive Variable. Die statischer Quantenchemie und Metadynamikbarrieren für diese Reaktion sind* $\Delta G^{\#}$ = 22 *bzw.* $\Delta F^{\#}$ = 19 kJ mol^{-1}. *Dies zeigt, dass Temperatur- sowie Lösungsmitteleffekte der* CO_2*-Lösungsmittelmoleküle kaum Einfluss auf die Energiebarriere haben. Abstände wie Winkel in den Übergangszuständen verändern sich wenig aufgrund der Bewegung der Moleküle in der Simulation. Die statischen und dynamischen Rechnungen ergaben Energiebarrieren für die PdN-zu-PdO-Umlagerung von* $\Delta G^{\#}/\Delta F^{\#} \approx$ 20 kJ mol^{-1} *und damit eine auch unter milden Reaktionsbedingungen überwindbare Barriere.*

Acknowledgement

This work was supported by the DFG, in particular by the project KI 768/6-1, the ERA-Chemistry, and the ESF. Computer time from the RZ Leipzig was gratefully acknowledged.

Philipp di Dio[1] *is currently studying mathematics at the University of Leipzig and works as a research assistant in the group of Barbara Kirchner.*

Email: didio@uni-leipzig.de

Barbara Kirchner[1] *has a current position in Leipzig as chair of theoretical chemistry.*

Email: bkirchner@uni-leipzig.de

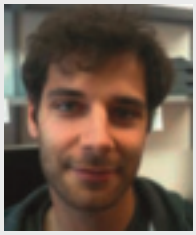

Marc Brüssel[1] *joined the group of Barbara Kirchner at the University of Leipzig, Germany, for his PhD studies.*

Email: marc.bruessel@uni-leipzig.de

Rupashree Shyama Ray[2] *is presently continuing as a Lecturer in the Department of Chemistry, School of Physical Sciences, Ravenshaw University, Odisha.*
Email: rsray@ravenshawuniversity.ac.in

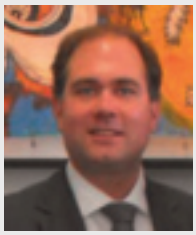

Kilian Muñiz[3] *joined the Institute of Chemical Research of Catalonia (ICIQ) as Group Leader, where he is currently ICREA Research Professor for Chemistry.*

Email: kmuniz@iciq.es

Stefan Zahn[4] *started recently his postdoctoral research in the groups of Ekaterina Izgorodina and of Douglas MacFarlane at Monash University.*

Email: stefan.zahn@monash.edu

Addresses:

[1] *Wilhelm-Ostwald-Institut für Physikalische und Theoretische Chemie, Universität Leipzig, Linnéstr. 2, D-04103 Leipzig (Germany)*

[2] *Department of Chemistry, School of Physical Sciences, Ravenshaw University, Cuttack, 753003, Odisha (India)*

[3] *Institute of Chemical Research of Catalonia (ICIQ), Av. Pañïsos Catalans 16, E-43007 Tarragona (Spain)*

[4] *School of Chemistry, Monash University, Clayton, Vic 3800 (Australia)*

[1] M. Aresta, C. F. Nobile, V. G. Albano, E. Forni, M. J. Manassero, *Chem. Soc., Chem. Commun.* **1975**, 636–637.

[2] a) P. G. Jessop, T. Ikariya, R. Noyori, *Chem. Rev.* **1995**, *95*, 259–272; b) W. Leitner, *Coord. Chem. Rev.* **1996**, *153*, 257–284; c) D. H. Gibson, *Chem. Rev.* **1996**, *96*, 2063–2095; d) P. G. Jessop, F. Joó, C.-C. Tai, *Coord. Chem. Rev.* **2004**, *248*, 2425–2442; e) M. Aresta, A. J. Dibenedetto, *Chem. Soc., Dalton Trans.* **2007**, 2975–2992; f) A. Urakawa, M. Iannuzzi, J. Hutter, A. Baiker, *Chem. Eur. J.* **2007**, *13*, 6828–6840; g) M. Mikkelsen, M. Jørgensen, F. C. Krebs, *Energy Environ. Sci.* **2010**, *3*, 43–81.

[3] A. Behr, *Angew. Chem.* **1988**, *100*, 681–698, *Angew. Chem. Int. Ed. Engl.* **1988**, *27*, 661–678.

[4] a) M. Sakamoto, I. Shimizu, A. Yamamoto, *Organometallics* **1994**, *13*, 407–409; b) E. Dinjus, W. Leitner, *Appl. Organomet. Chem.*

1995, *9*, 43–50; c) F. Bergamini, F. Panella, R. Santi, E. J. Antonelli, *Chem. Soc., Chem. Commun.* **1995**, 931–932; d) C. S. Yi, N. Liu, *Organometallics* **1995**, *14*, 2616–2617; e) V. V. Grushin, C. Bensimon, H. Alper, *Organometallics* **1995**, *14*, 3259–3263; f) A. Fukuoka, N. Gotoh, N. Kobayashi, M. Hirano, S. Komiya, *Chem. Lett.* **1995**, 567–568; g) C.-C. Chang,; B. Srinivas, M.-L. Wu, W.-H. Chiang, M. Y. Chiang, C.S. Hsiung, *Organometallics* **1995**, *14*, 5150–5159; h) W. Leitner, *Angew. Chem.* **1995**, *107*, 2391–2405, *Angew. Chem. Int. Ed.* **1995**, *34*, 2207–2221; i) A. Vigalok, Y. Ben-David, D. Milstein, *Organometallics* **1996**, *15*, 1839–1844; j) M. Shi, K. M. Nicholas, *J. Am. Chem. Soc.* **1997**, *119*, 5057–5058; k) M. Hirano, M. Akita, K. Tani, K. Kumagai, N. C. Kasuga, A. Fukuoka, S. Komiya, *Organometallics* **1997**, *16*, 4206–4213; l) C.-C. Chang, C.-S. Hsiung, H.-L. Su, B. Srinivas, M. Y. Chiang, G.-H. Lee, Y. Wang, *Organometallics* **1998**, *17*, 1595–1601; m) Y. Musashi, S. J. Sakaki, *J. Am. Chem. Soc.* **2002**, *124*, 7588–7603; n) G. P. Chiusoli, M. Costa, L. Cucchia, B. Gabriele, G. Salerno, L. J. Veltri, *Mol. Cat. A* **2003**, *204–205*, 133–142; o) B. Gabriele, G. Salerno, R. Mancuso, M. Costa, *J. Org. Chem.* **2004**, *69*, 4741–4750; p) C. S. Yeung, V. M. Dong, *J. Am. Chem. Soc.* **2008**, *130*, 7826–7827; q) J. Langer, W. Imhof, M. J. Fabra, P. García-Oduña, H. Görls, F. J. Lahoz, L. A. Oro, M. Westerhausen, *Organometallics* **2010**, *29*, 1642–1651.

[5] A. Correa, R. Martin, *Angew. Chem.* **2009**, *121*, 6317–6320, *Angew. Chem. Int. Ed.* **2009**, *48*, 6201–6204.

[6] D. J. Darensbourg, M. W. Holtcamp, *Coord. Chem. Rev.* **1996**, *153*, 155–174.

[7] a) D. Aguilar, R. Navarro, T. Soler, E. P. Urriolabeitia, *J. Chem. Soc., Dalton Trans.* **2010**, *39*, 10422–10431; b) A. Iglesias, E. G. Pérez, K. Muñiz, *Angew. Chem.* **2010**, *122*, 8286–8288, *Angew. Chem. Ind. Ed.* **2010**, *49*, 8109–8111; c) G.-W. Wang, T.-T. Yuan, D.-D. Li, *Angew. Chem.* **2011**, *123*, 1416–1419, *Angew. Chem. Int. Ed.* **2011**, *50*, 1380–1383; d) W. Li, Z. Xu, P. Sun, X. Jiang, M. Fang, *Org. Lett.* **2011**, *13*, 1286–1289; e) C. Pierre, O. Baudoin, *Org. Lett.* **2011**, *13*, 1816–1819.

[8] a) D. C. Powers, D. Y. Xiao, M. A. L. Geibel, T. Ritter, *J. Am. Chem. Soc.* **2010**, *132*, 14530–14536; b) A. Ariafard, C. J. T. Hyland, A. J. Canty, M. Sharma, N. J. Brookes, B. F. Yates, *Inorg. Chem.* **2010**, *49*, 11249–11253; c) B. Butschke, H. Schwarz, *Organometallics* **2011**, *30*, 1588–1598; d) H. Liu, Z. Geng, Y. Wang, X. Wang, J. Wu, J. Zhou, *Comput. Theor. Chem.* **2011**, *963*, 470–474.

[9] a) G. Dyker, *Angew. Chem.* **1999**, *111*, 1808–1822, *Angew. Chem. Int. Ed.* **1999**, *39*, 1698–1712; b) A. Dedieu, *Chem. Rev.* **2000**, *100*, 543–600; c) R. H. Crabtree, *J. Chem. Soc., Dalton Trans.* **2001**, *17*, 2437–2450; d) J. A. Labinger, J. E. Bercaw, *Nature* **2002**, *417*, 507–514; e) M. Lersch, M. Tilset, *Chem. Rev.* **2005**, *105*, 2471–2526; f) K. Muñiz, *Angew. Chem.* **2009**, *121*, 9576–9588, *Angew. Chem. Int. Ed.* **2009**, *48*, 9412–9423; g) D. Balcells, E. Clot, O. Eisenstein, *Chem. Rev.* **2010**, *110*, 749–823; h) *C-H Activation* (Eds.: J.-Q. Yu, Z. Shi) in *Top. Curr. Chem.*, Vol. 292, Springer, **2010**; i) T. W. Lyons, M. S. Sanford, *Chem. Rev.* **2010**, *110*, 1147–1169; j) G. B. Shul'pin, *Org. Biomol. Chem.* **2010**, *8*, 4217–4228; k) E. M. Beccalli, G. Broggini, A. Fasana, M. Rigamonti, *J. Organomet. Chem.* **2011**, *696*, 277–295; l) C. E. Engelin, P. Fristrup, *Molecules* **2011**, *16*, 951–969; m) F. Collet, C. Lescot, P. Dauban, *Chem. Soc. Rev.* **2011**, *40*, 1926–1936; n) L. Ackermann, *Angew. Chem.* **2011**, *123*, 3926–3928, *Angew. Chem. Int. Ed.* **2011**, *50*, 3842–3844.

[10] M. Brüssel, P. J. di Dio, K. Muñiz, B. Kirchner, *Mol. Sci.* **2011**, *12*, 1389–1409.

[11] R. Ahlrichs, M. Bär, M. Häser, H. Horn, C. Kölmel, *Chem. Phys. Lett.* **1989**, *162*, 165–169.

[12] a) A. D. Becke, *Phys. Rev. A* **1988**, *38*, 3098–3100; b) C. Lee, W. Yang, R. G. Parr, *Phys. Rev. B* **1988**, *37*, 785–789.

[13] A. D. Becke, *J. Chem. Phys.* **1993**, *98*, 5648–5652.

[14] F. Weigend, R. Ahlrichs, *Phys. Chem. Chem. Phys.* **2005**, *7*, 3297–3305.

[15] D. Andrae, U. Häußermann, M. Dolg, H. Stoll, H. Preuß, *Theor. Chim. Acta* **1990**, *77*, 123–141.

[16] J. Neugebauer, M. Reiher, C. Kind, B. A. Hess, *J. Comput. Chem.* **2002**, *23*, 895–910.

[17] a) G. Lippert, J. Hutter, M. Parrinello, *Theor. Chem. Acc.* **1999**, *103*, 124–140; b) CP2k developers group under the terms of the GNU General Public Licence; see http://cp2k.berlios.de/index.html.

[18] a) S. Nosé, *J. Chem. Phys.* **1984**, *81*, 511–519; b) W. G. Hoover, *Phys. Rev. A* **1985**, *31*, 1695–1697; c) G. J. Martyna, M. L. Klein, M. E. Tuckerman, *J. Chem. Phys.* **1992**, *97*, 2635–2643.

[19] J. VandeVondele, R. Ayala, M. Sulpizi, M. Sprik, *J. Electroanal. Chem.* **2007**, *607*, 113–120.

[20] a) S. Goedecker, M. Teter, J. Hutter, *Phys. Rev. B* **1996**, *54*, 1703–1710; b) C. Hartwigsen, S. Goedecker, J. Hutter, *Phys. Rev. B* **1998**, *58*, 3641–3662.

[21] a) S. Grimme, *J. Comput. Chem.* **2004**, *25*, 1463–1473; (b) S. Grimme, *J. Comput. Chem.* **2006**, *27*, 1787–1799.

[22] J. D. Hunter, *Comput. Sci. Eng.* **2007**, *9*, 90–95.

[23] W. Humphrey, A. Dalke, K. Schulten, *J. Molec. Graphics* **1996**, *14*, 33–38.

[24] a) A. Laio, M. Parrinello, *Proc. Natl. Acad. Sci. U.S.A.* **2002**, *99*, 12562–12566; b) M. Iannuzzi, A. Laio, M. Parrinello, *Phys. Rev. Lett.* **2003**, *90*, 238302; c) B. Ensing, A. Laio, M. Parrinello, M.; M. Klein, *J. Phys. Chem. B* **2005**, *109*, 6676–6687; d) A. Laio, A. Rodriguez-Fortea, F. Gervasio, M. Ceccarelli, M. Parrinello, *J. Phys. Chem. B* **2005**, *109*, 6714–6721.

Glycan Cantilever Array Sensors

Sensing Carbohydrate–Protein Interactions at Picomolar Concentrations Using Cantilever Arrays

Kathrin Gruber, Bianca A. Hermann, Peter H. Seeberger

Carbohydrates are important mediators of many biological processes that underlie cellular communication and disease mechanisms. Therapeutic agents include carbohydrate-based vaccines and the potent anti-viral protein Cyanovirin-N (CV-N). CV-N acts by specifically binding the carbohydrate structures decorating the cell surface of deadly viruses including human immunodeficiency virus (HI-V) or Ebola. In search for new carbohydrate – binding proteins and the development of sensors that exploit carbohydrate – protein interactions the label-free cantilever array technique can provides a fast, parallel and low-cost approach.

1. Glycans. Structure and Interaction

Diverse glycans decorate the cell surface of many organisms, typically in the form of glycoconjugates such as glycoproteins, proteoglycans and glycolipids.[1] Carbohydrate – protein interactions regulate cellular interactions with the extracellular environment, mediate cell adhesion, signal transduction and help to organize protein interactions.[2] Specific carbohydrate structures are expressed on the surfaces of bacteria, viruses, parasites and cancer cells.[3] The function of many glycans remains unknown and cell surface carbohydrates possess underexplored potential as both diagnostic and therapeutic targets.[4] These glycans show promise as a safe, fast and reliable means to screen for the presence of cancer cells and pathogens.[3]

The glycome is structurally more diverse than both the genome and proteome, as was revealed by recent advances in sequencing technologies.[5] Carbohydrate structure and glycan function have to be analyzed in detail both biochemically and microbiologically. In recent years, technologies such as glycan microarrays have been developed to rapidly measure carbohydrate – protein interactions.[6] However, additional low cost technologies with fast response times are necessary to complement these approaches and identify specific carbohydrate binding partners to fuel progress in the emerging field of functional glycomics. Glycan cantilever array sensors offer label-free detection and short measurement times for the detection of clinically relevant proteins and pathogens that interact with carbohydrates.

2. Cantilever Array Sensors

The cantilever sensor technique is based on micrometer silicon levers that are employed in atomic force microscopy (AFM). Cantilever sensors use the lever surface itself for (bio)chemical reactions.[7] The resulting nanometer sized cantilever deflection is read out via beam deflection or piezoresistive elements. In principle cantilever sensor setups can be operated in vacuum, air or liquid. Two typical modes of operation are employed. In the dynamic mode, very small changes in mass due to material adsorption are detected by the corresponding change in resonant frequency.[8] In the static mode the adsorption of the sample induces surface stress, which the cantilever relieves by bending up- or downwards. This deflection is tracked in real-time as a function of the amount of material adsorbed.[9] The technique is highly mass sensitive and constitutes a powerful, label-free transducer of biomolecular interactions.[9,10] The glycome and specific carbohydrate – ligand interactions are still largely neglected since most studies have focused on DNA and protein interactions.

3. Sensitive and Specific Protein Recognition with Glycan Cantilever Array Sensors

We describe the development of a carbohydrate based cantilever array sensor for the sensitive and specific detection of carbohydrate binding proteins.[11] To create the sensing layers, trimannose (**1**), galactose (**2**) and nonamannose (**3**) equipped with a thiol linker (see Figure 1a), were self-assembled on gold coated cantilever arrays by inserting them in glass capillaries filled with carbohydrate solutions. Figure 1b schematically depicts cantilever arrays functionalized with trimannose (red) and galactose (blue). Protein detection on this glycan cantilever array sensor was tested with Cyanovirin-N (CV-N), an 11 kDa protein isolated from cyanobacteria. CV-N has potent anti-vial activity as it has been demonstrated to bind and inhibit the human immunodeficiency virus (HIV).[12] Due to the clinical relevance of the protein, CV-N was chosen as an ideal candidate to test the functionality of the glycan cantilever array sensor.

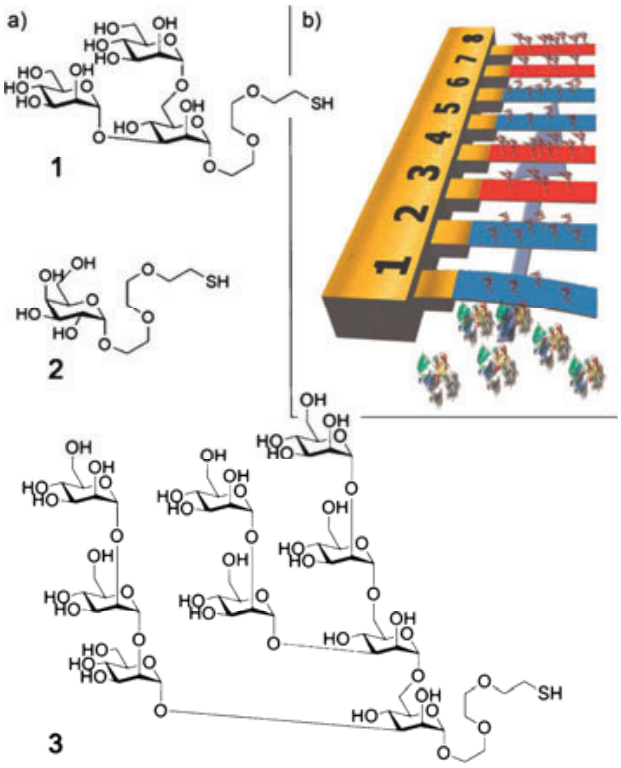

Figure 1: Sugar Structures and Sensor Coating: a) Trimannose (1), galactose (2) and nonamannose (3) were used to functionalize the sensor surface. b) Schematic of a cantilever sensor array containing eight individual cantilevers coated with mannose structures for protein recognition (red) and galactose as reference channels (blue).

3.1. Detecting Cyanovirin-N

A typical experiment with a CV-N sample results in negative deflections for all cantilevers. The *averaged* signals for the trimannose and galactose cantilevers of an array as shown in Figure 1b were calculated and are plotted in the upper panel in Figure 2. The trimannose signal is considerably larger than the galactose signal and is attributed to both *specific* protein – sugar binding due to the high affinity of CV-N for mannose sugars as well as to *nonspecific* protein attachment (total signal). The smaller galactose signal is attributed to nonspecific binding effects of CV-N to the carbohydrate structure, the thiol linker or the cantilever surface (nonspecific signal). In both cases the signal is generated by the protein attachment on the carbohydrate covered cantilevers inducing a difference in surface stress between the top and bottom side, which is relieved by the cantilever bending.[13] The lower panel in Figure 2 depicts the *differential* signal that is derived by subtracting the nonspecific galactose signal form the trimannose total signal. The *differential* deflection represents the amount of *specific* CV-N binding to the cantilever sensor (specific signal).

As different mannose structures vary in their respective binding strength to certain proteins, an array was functionalized with trimannose and additionally with nonamannose layers (see Figure 1a), to determine the capability of the sensor setup to resolve these fine differences. Indeed, a distinctively larger averaged as well as differential signal can be observed for nonamannose **3** when compared to the trimannose **1** cantilevers. The larger nonamannose molecule probably binds to more than one protein. In some cases it is possible that CV-N attaches via both binding pockets to the mannose layer. These so-called multivalent and multisite binding effects, are more likely for nonamannose than for trimannose, and accordingly are presumed to cause the larger sensor signal. Thus, the glycan cantilever array sensor is able to discriminate different sugar structures *via* smaller and larger sensor signals.

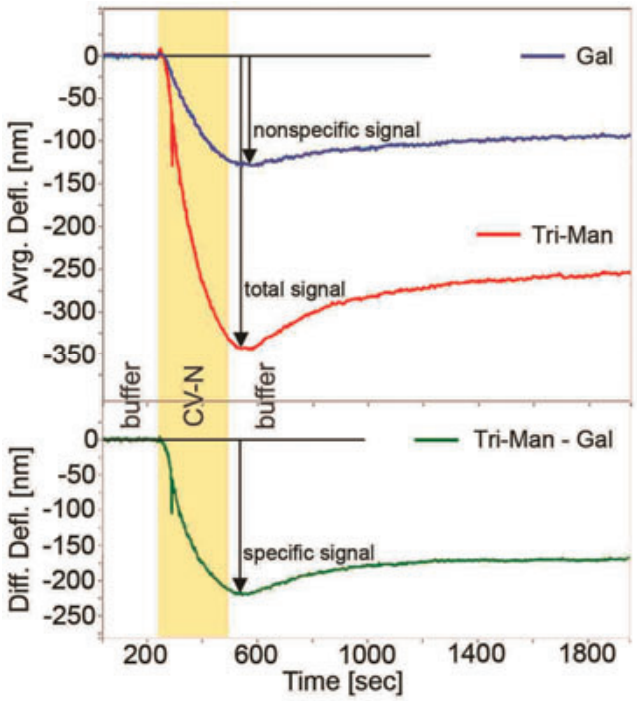

Figure 2: Detection of the Anti-Viral Protein Cyanovirin-N (0.1 mg/mL; 9.1 µM) with the Glycan Cantilever Array Sensor: Upper panel: *Averaged* deflections of the trimannose cantilevers (red) and galactose cantilevers (blue) of an array as shown in Figure 1b. As CV-N specifically binds to the mannose sugars, the trimannose signal is significantly larger. The smaller galactose signal represents only the nonspecific part of the binding. Lower panel: *Differential* signals were calculated by subtracting the galactose reference signal from the trimannose signal. Thus the resulting curve represents the specific recognition of CV-N proteins by mannose sugars.

3.2. Sensitivity

The utility of any sensor critically depends on the detection limit. Consequently the sensitivity of the glycan array sensor was tested with very low CV-N concentrations. Even after a high sample concentration of 10^{-2} mg/mL (0.9 µM) was injected into the measurements chamber, and immediately following experiment with only 10^{-6} mg/mL (90.9 pM) resulted in a significant differential deflection. Both measurement curves (dark

and light green, respectively) are depicted overlaid for better comparability in figure 3. The inset emphasizes the picomolar sensitivity that is attributed to the high affinity of the protein to the trimannose-coated sensors by enlarging the corresponding section of the graph. Since the relevant CV-N concentrations for biological applications lie in the nanomolar regime,[14] the picomolar detection limit demonstrated here more than qualifies this sensor setup as a valuable tool. The picomolar sensitivity of the glycan cantilever array sensor exceeds the capabilities of other cantilever assays that detect protein – protein binding[15] and matches an immunosorbent competition assay that was developed specifically for CV-N detection in plasma.[14b]

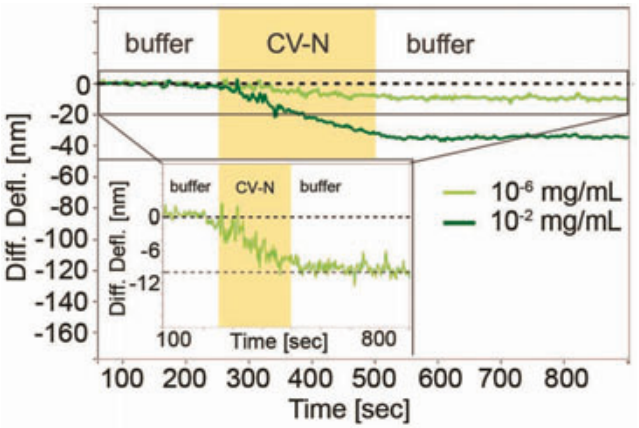

Figure 3: Sensitivity of the CV-N Detection: Two consecutive CV-N measurements were overlaid for better comparability. First a sample of high concentration with 10^{-2} mg/mL (0.9 µM) shows a distinctive differential deflection (dark green curve). The immediately following measurement with a very low concentration of only 10^{-6} mg/mL (90.9 pM) still caused a significant differential signal (light green curve). The inset depicts an enlargement of the relevant section that demonstrates the picomolar sensitivity of the sensor setup. Reprinted with permission from the American Chemical Society.

3.3. Concentration Dependence and Dissociation Constant

To test the applicability of the glycan cantilever array sensor over a wide range of analyte concentrations, a series of increasing amount of CV-N sample was conducted. The resulting differential deflection increases with the corresponding protein concentration (Figure 4). Concentrations over a range of five orders of magnitude can be detected down to picomolar amounts (Figure 3).

For a quantitative evaluation, a Langmuir isotherm was fitted to the deflections of the concentration series (inset Figure 4). Thereby, the dissociation constant was determined as a measure to describe the affinity of protein – carbohydrate binding. The Langmuir isotherm states:

maximum differential deflection = a x c / (K_d + c),

where *c* is the sample concentration and *a* is a proportionality constant. This model contains the assumption that individual protein – sugar complexes on the cantilever surface are independent and unaffected by neighboring binding events (1:1 binding model). With this analysis for the CV-N – trimannose interaction an average K_d value of (1.06 ± 0.69) µM was determined. The value for *tri*mannose **1** compares well to a K_d value for a CV-N - *di*-mannoside binding published as 1.5 µM.[16] The sensor accurately measures the binding affinity of the CV-N protein to mannose carbohydrates.

To assess the reproducibility of the individual detection experiments, measurements on six independent cantilever arrays were examined. Initial results showed that five out of six signal sizes agreed within a standard deviation of 30% - an acceptable range for new sensor methods. Over time more experience was gained in sensor handling and sample preparation to improve the performance to values below 20%.

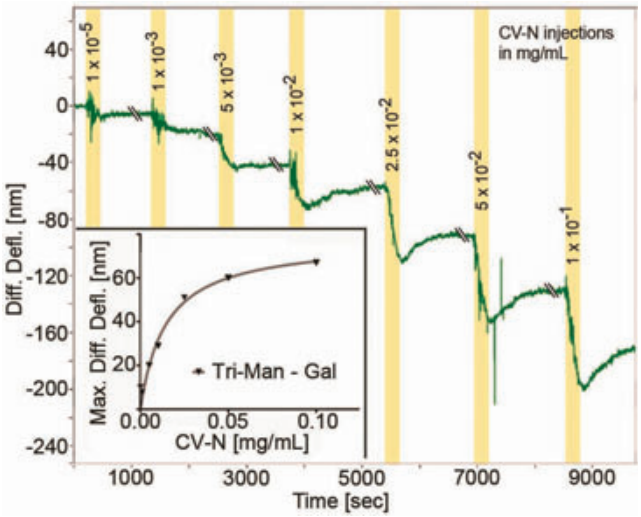

Figure 4: Concentration Dependence and Dissociation Constant: A series of seven consecutive measurements with increasing CV-N concentrations shows increasing sensor signals. Together with the picomolar sensitivity of the sensor these results demonstrate a detectable concentration range for CV-N over five orders of magnitude. When plotted against the respective sample concentration, the maximum differential deflections of the concentration series can be fitted against a Langmuir isotherm, see the inset. The Langmuir analysis results in a value for the dissociation constant that characterizes the protein – sugar binding and is comparable to other literature reports. Reprinted with permission from the American Chemical Society.

3.4. Specificity

Analyte specificity is a valuable measure indicating how well a sensor differentiates the intended analyte from other agents possibly present in the sample that might lead to false positive results. To demonstrate the specificity of the CV-N – mannose recognition, the binding was challenged by a competitive inhibition assay. After an initial reference experiment, free

mannose (100 mM) was added to the running buffer. For the following injection of a CV-N sample with free mannose present in the buffer, only about one third of the original deflection size was observed. As the free mannose competes with mannose sugars attached to the cantilever surface for binding with CV-N, fewer proteins bind to the sensor and the resulting deflection is reduced. The reduced signal size in mannose buffer confirms the specificity of the CV-N – mannose interaction.

3.5. Versatility of the Sensor for Protein Recognition

For general utility, the sensor needs to be able to detect more than only one protein. Thus, a second carbohydrate binding protein was analyzed. The generic 104 kDa lectin Concanavalin A (ConA) consists of four identical monomers with one high affinity mannose binding site each and is well recognized as standard protein to probe carbohydrate interactions.[17]

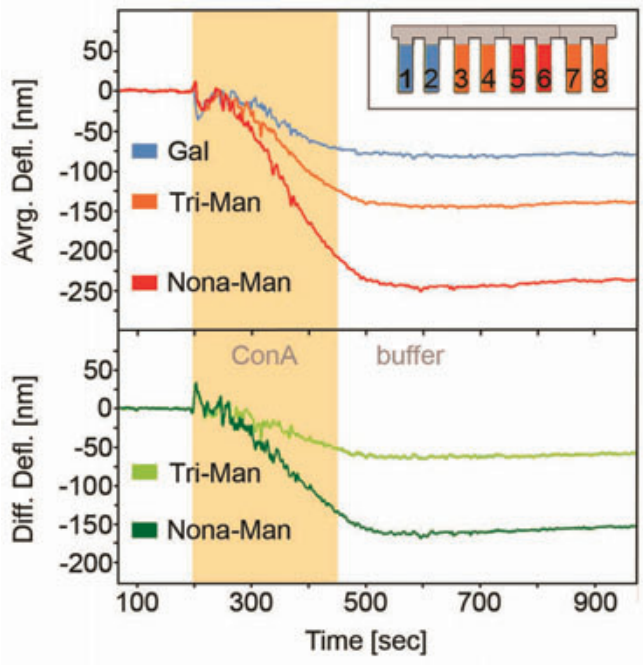

Figure 5: Versatility of the Glycan Cantilever Array Sensor for Protein Detection: A sensor coated with nonamannose, trimannose and galactose (see inset) was tested for recognition of the lectin ConA. Upper panel: The *averaged* deflections of the nonamannose and trimannose cantilevers are significantly larger and indicate the specific recognition of the protein. The larger nonamannose signal is attributed to increased multivalent and multisite binding. In contrast, the smaller signal of the galactose reference cantilevers represents the nonspecific part of the binding. Lower panel: The *differential* signal represents the specific protein binding and again is larger for the nonamannose compared to the trimannose sensor. Reprinted with permission from the American Chemical Society.

For the ConA measurements, a cantilever array was functionalized with trimannose, nonamannose and galactose layers. In analogy to the CV-N detection, negative deflections for all carbohydrate-coated cantilevers were recorded. The respective averaged and differential deflections for a typical ConA experiment (2 mg/mL; 19.2 µM) are plotted in Figure 5. Both the averaged and differential responses of the tri- and nonamannose functionalized cantilevers are significantly stronger than the galactose reference cantilevers. As was observed for CV-N recognition, the averaged and differential signals of the nonamannose sensors were significantly larger than that of the trimannose cantilevers.

As the proteins attach to the cantilever surface, interactions on the cantilever surface induce surface stress that leads to the observed cantilever bending. ConA is more likely to bind to the multivalent nonamannose so that the differences in signal size can be attributed to these effects. Again, the signals of the galactose reference are assigned to nonspecific binding to galactose, the thiol linker or the cantilever surface.

As for CV-N, the parameters validating the quality of the sensor setup were examined. The sensitivity, concentration dependence and specificity of the glycan cantilever array sensor for ConA binding were verified. For ConA detection, concentrations down to the nanomolar level (1 µg/mL (9.6 nM)) were detected even in direct succession of a highly concentrated ConA measurement (10 mg/mL (96.2 µM)). This detection limit compares well to standard surface bound techniques such as surface plasmon resonance (SPR), quartz crystal microbalance (QCM) and glycan microarrays.[18] The sensor signal increases with increasing protein concentrations. Here the Langmuir isotherm analysis resulted in a K_d value of 15.3 µM in good agreement with published values.[19] Also, a competitive inhibition assay verifyed the specificity of ConA – mannose binding. Finally, an experimental setup aiming at a more realistic scenario involving complex solutions was examined. For measurements in the presence of background BSA (0.007 mg/mL; 0.1 µM) in the running buffer, ConA sample concentrations of 2 mg/mL (19.2 µM) resulted in signal sizes that compare well to the signals observed without BSA. These results independently demonstrate the selectivity of protein binding to the carbohydrates active layers on the glycan cantilever array sensor.

4. Extending the Sensor to Detect Bacteria

Accurate detection of pathogens and other microorganisms is crucial for clinical applications and environmental control.[20] As traditional methods rely on time consuming culturing of bacterial samples that require from several hours to days,[21] the short detection times of the cantilever sensor technique provide a significant advantage. Certain *Escherichia coli* (*E.coli*) strains recognize mannose sugars *via* the mannose binding protein FimH at their pilii. Such bacteria can potentially be recognized against a galactose reference by the glycan cantilever array sensor setup, as is schematically illustrated in Figure 6. The capability of the cantilever sensor to detect different *E.coli* strains is currently investigated and first measurements show promising results.

5. Conclusions

We describe the development and use of a glycan cantilever array sensor to sensitively and specifically detect clinically relevant carbohydrate – protein interactions. This sensor detects concentrations down to picomolar amounts of CV-N, an oligomannoside binding protein with potent anti-viral activity. This detection limit matches the best reported results for CV-N detection with other methods. The glycan cantilever array sensor is reliable, readily prepared and reusable. This cantilever sensor setup represents the first carbohydrate - protein detection setup based on the label-free, parallel and fast cantilever technique devised for the growing field of glycomics that using the interaction of the anti-viral protein Cyanovirin-N (CV-N) and oligomannosides as example. Further development of this assay and expansion to bacterial detection may lead to quick, sensitive methods to study and detect medically relevant carbohydrate – protein and pathogen interactions.

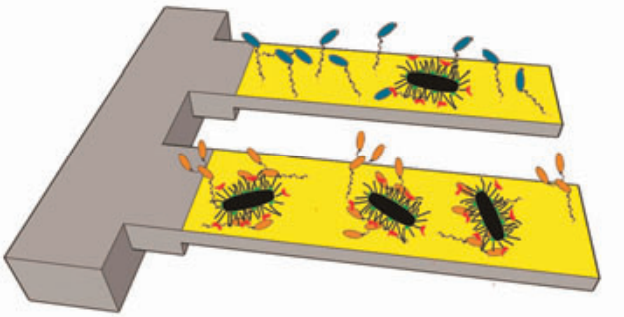

Figure 6: Detection of Bacteria with Glycan Cantilever Array Sensors: Microorganisms specifically recognizing mannose sugars (orange) could be detected against a galactose reference (blue). First testing with *E.coli* strains that carry a mannose specific protein shows promising results.

Summary

Glycans on cell membranes play crucial roles in many cell – cell communication processes and the transmission of dangerous diseases like AIDS or malaria. The protein Cyanovirin-N (CV-N) is able to bind and block nonamannose structures found on the surface of the human immunodeficiency virus (HIV) and prevents cell infection. To accurately determine the prophylactic or therapeutic potency of such proteins, specifically designed sensors are required. The cantilever array technique provides advantages like label free detection, short measurement times and up to eight parallel reference channels. A novel cantilever array sensor for the detection of carbohydrate – protein interactions is introduced. Parameters that describe sensor quality such as sensitivity, concentration dependence of signal size and specificity of the recognition, are discussed. To this end, a cantilever array was coated with trimannose and nonamannose sugars to create specific sensing channels. Additional galactose layers were applied on cantilevers of the same array to act as reference and determine the amount of nonspecific binding. With this setup CV-N concentrations could be detected over five orders of magnitude down to picomolar levels. The sensor differentiates trimannose from nonamannose coatings via *smaller and larger sensor signals. Finally, the specificity of CV-N – mannose binding was verified by a competitive inhibition assay. Additional tests with the generic protein Concanavalin A (ConA) demonstrate the versatility of this glycan cantilever array sensor for protein detection. Sensitivity in the nanomolar regime and the dissociation constant are in accordance with literature reports. The specificity of ConA recognition was independently demonstrated by competitive inhibition. As certain medically relevant bacteria also specifically recognize mannose structures, the detection of Escherichia coli (E.coli) is currently investigated. First results indicate that this sensor setup can be expanded successfully from protein to bacteria recognition. The described glycan cantilever array sensor poses a potent and versatile tool to analyze and detect carbohydrate interactions that may advance drug design and diagnostic applications.*

Zusammenfassung

Kohlenhydrate auf der Außenseite der Zellmembranen spielen eine entscheidende Rolle bei der Zellkommunikation und der Übertragung von gefährlichen Krankheiten wie AIDS oder Malaria. Das Protein Cyanovirin-N (CV-N) ist in der Lage, die Nonamannosen an der Oberfläche des Humanimmunodefizienz-virus (HIV) zu erkennen, zu blockieren und dadurch Infektionen zu verhindern. Um die prophylaktische und therapeutische Wirksamkeit solcher Proteine zu untersuchen, sind speziell dafür entwickelte Sensoren nötig. Die Cantilever-Array-Technik zeichnet sich dabei durch Detektion ohne Markierung und kurze Messzeiten mit bis zu acht parallelen, internen Referenzkanälen aus. Dieser Artikel stellt einen neuartigen Cantilever-Array-Sensor zur Detektion von Kohlenhydrat-Protein-Interaktionen vor und beleuchtet die für die Qualität eines Sensors kritischen Parameter wie Sensitivität, konzentrationsabhängige Signal-größen und Erkennungsspezifität. Zu diesem Zweck wurden einzelne Cantilever eines Array mit Trimannose- oder Nonammanose-Zuckern beschichtet, um daraus die spezifischen Sensorkanäle zu erzeugen. Zusätzliche Galactose-beschichtete Cantilever desselben Arrays dienen als Referenz und zur Bestimmung der Größe von nichtspezifischen Bindungen. Mit diesem Setup konnten CV-N-Konzentrationen über fünf Größenordnungen bis zu pikomolaren Mengen detektiert werden. Die Sensitivität und die Dissoziationskonstanten der Bindung stimmen gut mit Literaturberichten überein. Der Sensor unterscheidet Trimannose- von Nonamannosebeschichtungen durch unterschiedliche Sensorsignale. Schließlich konnte die Spezifität der (CV-N)-Mannose-Bindung durch kompetitive Hemmung verifiziert werden. Zusätzliche Tests mit dem Protein Concanavalin A (ConA) zeigen die vielseitige Anwendbarkeit dieses Glykan-Cantilever-Array-Sensors zur Proteindetektion. Sowohl die für dieses Lektin gezeigte Sensitivität im nanomolaren Bereich als auch die Dissoziationskonstante entsprechen Litera-turwerten. Die Spezifität der ConA-Erkennung konnte unabhängig durch kompetitive Hemmung und durch Messungen im Hintergrund von Rinderserumalbuminen (BSA) gezeigt werden. Da auch bestimmte, medizinisch relevante Bakterien-stämme spezifisch Mannosestrukturen erkennen können, wird gegenwärtig die Detektion von Escherichia coli (E. coli) untersucht. Erste Resultate weisen darauf hin, dass dieser Aufbau

erfolgreich von Protein- auf Bakterienerkennung übertragen werden kann. Folglich stellt der hier beschriebene Glykan-Cantilever-Array-Sensor ein leistungsfähiges und vielseitiges Werkzeug dar, um Kohlehydratinteraktionen zu untersuchen und die Entwicklung von Medikamenten und diagnostische Anwendungen weiter voranzutreiben.

Kathrin Gruber [1] *is a Ph.D. student at the Ludwig-Maximilians-Universität München. Address:*

Email: kathrin.gruber@wmi.badw.de

Bianca A. Hermann [1] *is group leader at the Ludwig-Maximilians-Universität München.*

Email: b.hermann@cens.de

Peter H. Seeberger [2] *is director at the Max Planck Institute of Colloids and Interfaces and professor at the Freie Universität Berlin.*

E-mail: peter.seeberger@mpikg.mpg.de

Adresses:

[1] *Walther-Meissner-Institute, Ludwig-Maximilians University München, Walther-Meissner-Str. 8, 85748 Garching, Germany*

[2] *MPI Colloids and Interfaces, Department of Biomolecular Systems, Arnimallee 22, 14195 Berlin, Germany*

Project description & Acknowledgment

This projects aims to probe hierarchical self-assemblies that are relevant for drug and vaccine design based on the example of carbohydrate – Cyanovirin-N interactions. Combining different areas of expertise in a transnational collaboration, new insights and methods regarding carbohydrate chemistry and novel sensing techniques were targeted.

We acknowledge the generous support provided by the ERA-Chemistry program, the Nanosystems Initiative Munich (NIM), the Center for Nano Science (CeNS), the elite network of Bavaria, the Walther-Meissner-Institute of the Bavarian Academy of Science and Humanities, the Swiss National Fonds (SNF) and the Max-Planck Society.

[1] A. Varki, R. D. Cummings, J. D. Esko, H. H. Freeze, P. Stanley, C. R. Bertozzi, G. W. Hart, M. E. Etzler, 2nd ed., Cold Spring Harbor Laboratory Press, USA, **2009**.

[2] a) J. B. Lowe, *Cell* **2001**, *104*, 809-812; b) G. S. Kansas, *Blood* **1996**, *88*, 3259-3287; c) S. J. Danishefsky, J. R. Allen, *Angew. Chem. Int. Ed.* **2000**, *39*, 836-863.

[3] M. Tamborrini, D. B. Werz, J. Frey, G. Pluschke, P. H. Seeberger, *Angew. Chem. Int. Ed.* **2006**, *45*, 6581-6582.

[4] a) P. H. Seeberger, D. B. Werz, *Nat. Rev. Drug. Discov.* **2005**, *4*, 751-763; b) P. H. Seeberger, D. B. Werz, *Nature* **2007**, *446*, 1046-1051.

[5] a) C. R. Bertozzi, L. L. Kiessling, *Science* **2001**, *291*, 2357-2364; b) O. J. Plante, E. R. Palmacci, P. H. Seeberger, *Science* **2001**, *291*, 1523-1527.

[6] a) O. Blixt, S. Head, T. Mondala, C. Scanlan, M. E. Huflejt, R. Alvarez, M. C. Bryan, F. Fazio, D. Calarese, J. Stevens, N. Razi, D. J. Stevens, J. J. Skehel, I. van Die, D. R. Burton, I. A. Wilson, R. Cummings, N. Bovin, C.-H. Wong, J. C. Paulson, *Proc. Natl. Acad. Sci. U. S. A.* **2004**, *101*, 17033-17038; b) S. Fukui, T. Feizi, C. Galustian, A. M. Lawson, W. Chai, *Nat Biotech* **2002**, *20*, 1011-1017; c) D. M. Ratner, E. W. Adams, M. D. Disney, P. H. Seeberger, *ChemBioChem* **2004**, *5*, 1375-1383; d) J. C. Paulson, O. Blixt, B. E. Collins, *Nat. Chem. Biol.* **2006**, *2*, 238-248; e) T. Horlacher, P. H. Seeberger, *Chem. Soc. Rev.* **2008**, *37*, 1414-1422.

[7] J. K. Gimzewski, C. Gerber, E. Meyer, R. R. Schlittler, *Chem. Phys. Lett.* **1994**, *217*, 589-594.

[8] K. M. Goeders, J. S. Colton, L. A. Bottomley, *Chem. Rev.* **2008**, *108*, 522-542.

[9] H. P. Lang, M. Hegner, C. Gerber, *Mater. Today* **2005**, *8*, 30-36.

[10] P. S. Waggoner, H. G. Craighead, *Lab Chip* **2007**, *7*, 1238-1255.

[11] K. Gruber, T. Horlacher, R. Castelli, A. Mader, P. H. Seeberger, B. A. Hermann, *ACS Nano* **2011**, *5*, 3670-3678.

[12] a) M. Boyd, K. Gustafson, J. McMahon, R. Shoemaker, B. O'Keefe, T. Mori, R. Gulakowski, L. Wu, M. Rivera, C. Laurencot, M. Currens, J. Cardellina, 2nd, R. Buckheit, Jr, P. Nara, L. Pannell, R. Sowder, 2nd, L. Henderson, *Antimicrob. Agents Chemother.* **1997**, *41*, 1521-1530; b) A. J. Bolmstedt, B. R. O'Keefe, S. R. Shenoy, J. B. McMahon, M. R. Boyd, *Mol. Pharmacol.* **2001**, *59*, 949-954.

[13] a) W. Haiss, *Rep. Prog. Phys.* **2001**, *64*, 591; b) A. M. Moulin, S. J. O'Shea, R. A. Badley, P. Doyle, M. E. Welland, *Langmuir* **1999**, *15*, 8776-8779; c) P. Dutta, C. A. Tipple, N. V. Lavrik, P. G. Datskos, H. Hofstetter, O. Hofstetter, M. J. Sepaniak, *Anal. Chem.* **2003**, *75*, 2342-2348; d) J. Koeser, et al., *Journal of Physics: Conference Series* **2007**, *61*, 612.

[14] a) C. A. Bewley, S. Otero-Quintero, *J. Am. Chem. Soc.* **2001**, *123*, 3892-3902; b) S. D. Bringans, B. R. O'Keefe, M. Bray, C. A. Whitehouse, M. R. Boyd, *Anal. Bioanal. Chem.* **2004**, *380*, 269-274.

[15] a) M. Yue, J. C. Stachowiak, H. Lin, R. Datar, R. Cote, A. Majumdar, *Nano Lett.* **2008**, *8*, 520-524; b) N. Backmann, C. Zahnd, F. Huber, A. Bietsch, A. Plückthun, H.-P. Lang, H.-J. Güntherodt, M. Hegner, C. Gerber, *Proc. Natl. Acad. Sci. U. S. A.* **2005**, *102*, 14587-14592.

[16] P.-H. Liang, S.-K. Wang, C.-H. Wong, *J. Am. Chem. Soc.* **2007**, *129*, 11177-11184.

[17] J. L. Wang, B. A. Cunningham, G. M. Edelman, *Proceedings of the National Academy of Sciences* **1971**, *68*, 1130-1134.

[18] S. Park, M.-r. Lee, S.-J. Pyo, I. Shin, *J. Am. Chem. Soc.* **2004**, *126*, 4812-4819.

[19] Y. Zhang, S. Luo, Y. Tang, L. Yu, K.-Y. Hou, J.-P. Cheng, X. Zeng, P. G. Wang, *Anal. Chem.* **2006**, *78*, 2001-2008.

[20] a) K. R. Buchapudi, X. Huang, X. Yang, H.-F. Ji, T. Thundat, *Analyst* **2011**, *136*, 1539-1556; b) M. Zourob, S. Elwary, A. P. F. Turner, *Vol. XXXII*, **2008**, p. 970.

[21] M. D. Disney, P. H. Seeberger, *Chem. Biol.* **2004**, *11*, 1701-1707.

Advanced Analytics

Electrochemistry/Liquid Chromatography/Mass Spectrometry as a Tool in Metabolism Studies

Helene Faber, Sandra Jahn, Jens Künnemeyer, Hannah Simon, Daniel Melles, Martin Vogel, Uwe Karst

***E**lectrochemistry/liquid chromatography/mass spectrometry is a powerful complementary tool for the simulation of the oxidative metabolism of drugs and other xenobiotics.*

Drug Development and Oxidative Metabolism

Although the combination of the two groups of analytical techniques electrochemistry (EC) and mass spectrometry (MS) has not gathered massive scientific or commercial interest yet, it has a surprisingly long history. However, while it was initially only used to investigate the gases formed in an electrochemical reactor using MS with a membrane inlet, the number and kind of its applications has expanded significantly in recent years. Currently, EC/MS is on the brink of becoming a widespread tool for metabolism studies. The reasons for this as well as the potential and the limitations of the respective approaches are presented within this paper.

In pharmaceutical industries, the fate of an active substance in the body has to be investigated at an early state during drug development to gather information on its distribution, metabolism and excretion. Metabolites have to be identified and quantified in human body fluids, as some metabolites may be the cause for adverse reactions of the drug.[1] The oxidative metabolism of drugs, which mainly takes place in the liver due to oxidation reactions catalyzed by enzymes of the cytochrome P450 group, is generally considered as a detoxification mechanism of the organism. As the formed functionalized (phase I) metabolites typically are more polar than the parent drug, their water solubility is increased and they are easily excreted via the kidneys and the urine. However, some metabolites, e.g., dehydrogenation products as quinoid compounds, which may be formed from catechols, are less polar than the parent drugs and may react by covalent linkage to functional groups in the body. Quinoids, for example, are susceptible to attach thiol groups of small molecules as the amino acid cysteine or the tripeptide glutathione.[2] These reactions are used to detoxify reactive metabolites, because the highly polar products are again prone to rapid excretion from the body. Most frequently, glutathione adducts of reactive metabolites are formed as phase II metabolites. If the concentration of reactive metabolites exceeds the available concentration of thiols in the liver, covalent attachment of the reactive metabolites to free thiol groups of liver proteins may take place.[3] This may cause a limitation in protein functionality and thus liver toxicity may be observed.

Conventional Methods

For this reason and related toxicological aspects, pharmaceutical industries as well as pesticide manufacturers or producers of food additives and consumer products have great interest to investigate new chemical entities with respect to their metabolism in the body. A large number of testing systems has been developed for this purpose, including in vitro assays based on isolated enzymes of the cytochrome P450 group, perfused liver, liver slices or liver cell microsomes.[4] All of these methods are laborious and time consuming and/or depend on the availability of biological materials in reproducible quality. In all of these cases, the formed products are extracted from the biological matrices and are subsequently analyzed by liquid chromatography/mass spectrometry (LC/MS). However, reactive metabolites formed in these experiments frequently experience covalent binding to biological macromolecules and are therefore not detected in LC/MS[5] in most cases. Additionally, EU regulations prohibit the use of animal testing to assess the toxicity of constituents of particular groups of products, e.g., cosmetics.[6] Therefore, there is a strong demand for alternative methods, which are less prone to differ in their biological variability and which are easy to use and well reproducible. For these reasons, these methods should ideally be based on purely instrumental approaches, although the comparability of the results with the biological reality has to be investigated carefully.

Electrochemical Set-up

The combination of EC and MS, sometimes assisted by a LC separation prior to MS analysis, has proven strong potential for the simulation of the oxidative metabolism of xenobiotics in recent years.[7-10] The set-up of a respective instrument is presented in figure 1. A solution of the compound of interest,

typically as a 1-100 µM solution in a suitable aqueous/organic solvent, is transported through the electrochemical cell by a syringe pump. The potential of the cell is controlled by a potentiostat. The formed products are either directly infused into the mass spectrometer to record mass voltammograms (see below) or are loaded into the sample loop of an injection valve. In this case, the valve is switched subsequently to start the chromatographic run with mass spectrometric detection.

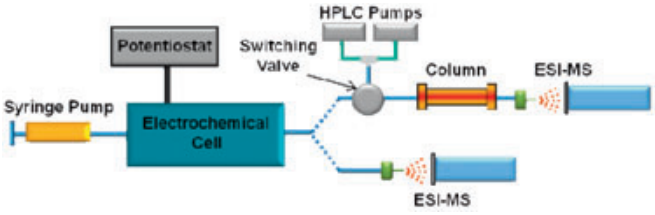

Figure 1. Schematic set-up of the EC/LC/MS system for simulation of phase I metabolism. In case of EC/LC/MS (upper pathway), the effluent of the electrochemical cell is collected in a sample loop mounted on an injection valve. By switching the valve, the reactions products are flushed onto the LC column, separated and analyzed by ESI-MS. In case of EC/MS (lower pathway), the effluent from the electrochemical cell is directly transferred to the ESI-MS.

Two different types of electrochemical cells are currently used for EC/MS experiments. While both consist of a three electrode arrangement with working, counter and reference electrode, they are distinguished by different working electrode materials, sizes and geometries. Large volume porous flow-through electrodes are suitable for comparably large flow rates of up to several hundred µL/min with high conversion rates ("coulometric" cells). The large surface area also accounts for the limited influence of electrode fouling and limited requirement for maintenance. Traditionally, they are available with glassy carbon (GC) as surface material. Thin layer cells, on the other hand, are more flexible with respect to the exchange of working electrode materials, as not only GC, but also boron doped diamond (BDD) as well as metals (Pt, Au, Ag, Cu) are available. Furthermore, maintenance is easy, as the electrode surfaces can be accessed, polished and exchanged rapidly. While earlier EC/MS measurements were mainly performed on GC electrodes, BDD is gaining interest due to the higher potential range, which may allow to purposely generate radicals in the cell. While the applied counter electrodes in these electrochemical cells consist of stainless steel or Teflon doped with graphite, the reference electrodes typically are Pd/H_2 systems, which are depending on the pH of the solution of the xenobiotic compound. Therefore, to assure reproducibility of the method, EC/MS data should always be accompanied with information about the composition and the pH of the solution investigated.

Mass Spectrometric Detection in EC/MS

Requirements for mass spectrometers suitable for EC/MS include excellent full scan sensitivity and the possibility for structure elucidation based on fragmentation, as unknown compounds have to be identified. For this reason, ion trap instruments typically are more useful in EC/MS than quadrupole mass spectrometers. Another important aspect is rapid switching between the positive and the negative ion modes, as there may be some metabolites, which are favourably or even exclusively detectable in the positive ion mode, while others formed at the same time are preferably analyzed in the negative ion mode. Time of flight instruments or orbitrap mass analyzers add high resolution and high mass accuracy, adding the possibility to assign molecular formulae only from mass spectrometric experiments. Hybrid quadrupole-time of flight, ion trap-orbitrap or the new quadrupole-orbitrap instruments combine excellent full scan sensitivity, recording of accurate masses and structure elucidation by fragmentation and are therefore ideally suited for EC/MS. Regarding ionization techniques, electrospray ionization-mass spectrometry (ESI-MS) has been used most frequently due to the comparably high polarity of most compounds of interest. Typically, $[M+H]^+$ or $[M-H]^-$ are the most abundant ions in the positive and the negative ion mode, respectively, while adduct ions with ammonium, sodium or potassium (positive ion mode) or formate, acetate or chloride (negative ion mode) are frequently observed as well. However, atmospheric pressure chemical ionization (APCI) and atmospheric pressure photoionization (APPI) are attractive alternatives in case of less polar analytes.

If liquid chromatography is integrated between EC and MS, the reversed-phase separation mode is mostly used. For more polar drugs or metabolites, hydrophilic interaction liquid chromatography (HILIC) on zwitterionic phases is one suitable alternative. Carbon-based stationary phases are also showing promising retention properties for highly polar drugs and their metabolites. In general, the LC separation should be carried out with the fastest possible separation times to minimize the use of the expensive MS detection system per analysis and to increase sample throughput.

Optimizing the Electrochemical Oxidation

The basic approach in EC/MS consists of recording a mass voltammogram, a plot of the mass spectrum depending on varying working potentials. Over a time period of between five and 30 minutes, the electrochemical potential is constantly increased and the mass spectrum is recorded continuously. The signal-to-noise ratio may be improved by longer recording times, although at the expense of analysis time. A typical mass voltammogram for paracetamol (acetaminophen, APAP) over a small mass range from m/z 148 to m/z 155 is presented in figure 2. While the $[M+H]^+$ signal of the parent drug is decreasing, the reaction product N-acetyl-p-benzoquinoneimine (NAPQI) is formed with increasing potential at its respective m/z ratio.

The mass voltammogram may vary depending on solvent composition, pH value and electrode material. Therefore, it should either be recorded at varying conditions or under carefully selected conditions. The mass voltammogram allows to find the

most suitable cell potential for further EC/LC/MS or adduct formation experiments.

In literature, many pharmaceuticals and other xenobiotics have already been investigated using this approach in comparison to established techniques based on liver cell microsomes, animal

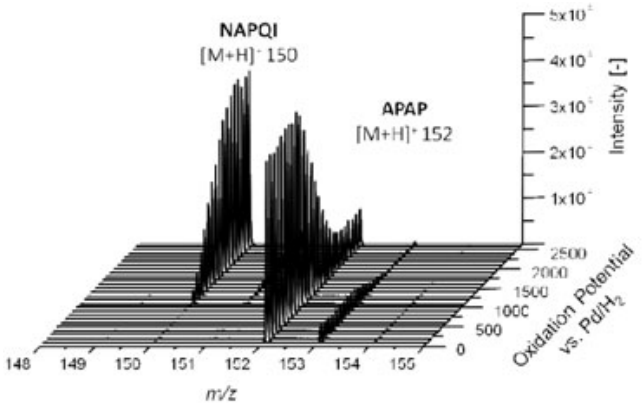

Figure 2. Electrochemical oxidation of paracetamol ($1 \cdot 10^{-5}$M in NH_4formate $1 \cdot 10^{-2}$M, pH 7.4/ACN 70/30 v/v). The mass voltammogram was recorded as described above, using a thin-layer cell equipped with a boron doped diamond working electrode.

experiments or studies with patients. Despite the different mechanisms associated with the instrumental and the enzymatic approaches, a surprisingly good agreement has been found in many cases, thus proving the usefulness of the approach for metabolism screening purposes.

Glutathione Adduct Formation of Reactive Metabolites

The EC/MS approach can also be expanded to phase II (conjugation) experiments by adding a solution of a trapping agent (cysteine, glutathione or a protein) after the electrochemical cell. Reactive metabolites are converted into products, which can be detected mass spectrometrically. The experiment using small thiols as trapping agents can be performed in a simple approach, where a solution of the thiol is continuously added to the effluent from the electrochemical cell and is then directly transferred to the mass spectrometer. An extract of the respective mass voltammogram of the addition of the reactive metabolite of paracetamol (NAPQI) with glutathione (GSH) in the m/z range from 440 to 500 is presented in figure 3. It is obvious that the signal intensity of the $[M+H]^+$ and the $[M+Na]^+$ signals of the NAPQI-GSH adduct as well as the respective ^{13}C isotope patterns are increasing above a potential of 1000mV vs. Pd/H_2 reference. A comparison with the data from figure 2, where the signal of APAP decreases at the same potential due to formation of the reactive metabolite NAPQI shows that these data correlate well.

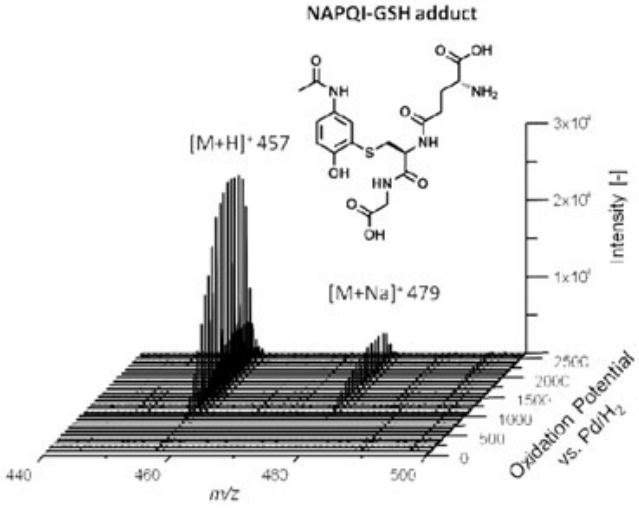

Figure 3. Electrochemical oxidation of paracetamol ($2 \cdot 10^{-5}$M) and trapping with glutathione ($1 \cdot 10^{-4}$M). The potential was ramped from 0-2500mV in 250s and glutathione was added to the effluent from the EC cell via a mixing T-piece and a second syringe pump. Conjugation products were monitored with an ESI-ToF-MS in the positive ion mode.

Formation of Protein Adducts from Electrogenerated Reactive Metabolites

For trapping experiments with proteins additional measures have to be taken: Due to the comparably high salt content of many proteins and the resulting signal suppression in ESI-MS, a LC separation has to be inserted after protein adduct formation with the goal to obtain some retention of the protein adducts, while inorganic and small organic salts, which are prone to cause ion suppression, will elute within the void volume of the system. This approach drastically minimizes suppression effects and increases the signal to noise ratio for the protein adducts. Protein adduct formation of reactive metabolites can best be tested with the 18kDa milk protein β-lactoglobulin A. Although this protein is of little relevance for toxicological studies, it is an excellent model protein due to a reasonable size and structural homogeneity. It can therefore be detected very well in ESI-MS, contains only one free and well accessible thiol group and has shown excellent reactivity with reactive metabolites, particularly quinoid compounds.[11] While the proteins hemoglobin (from rat or human origin) or human serum albumin (HSA) are more relevant with respect to toxicological studies, they are more difficult to analyze due to different subunits as the α- and β-chains of hemoglobin or the significantly larger size (approximately 66kDa) and structural heterogeneity of HSA. Therefore, it is recommended to always start studies on protein adduct formation with β-lactoglobulin A and to subsequently use more relevant proteins in case the initial studies prove a reactivity of the electrochemically generated metabolites. Figure 4 shows the adduct formation of electrogenerated NAPQI with β-lactoglobulin A. While the upper data show the ESI-MS of the

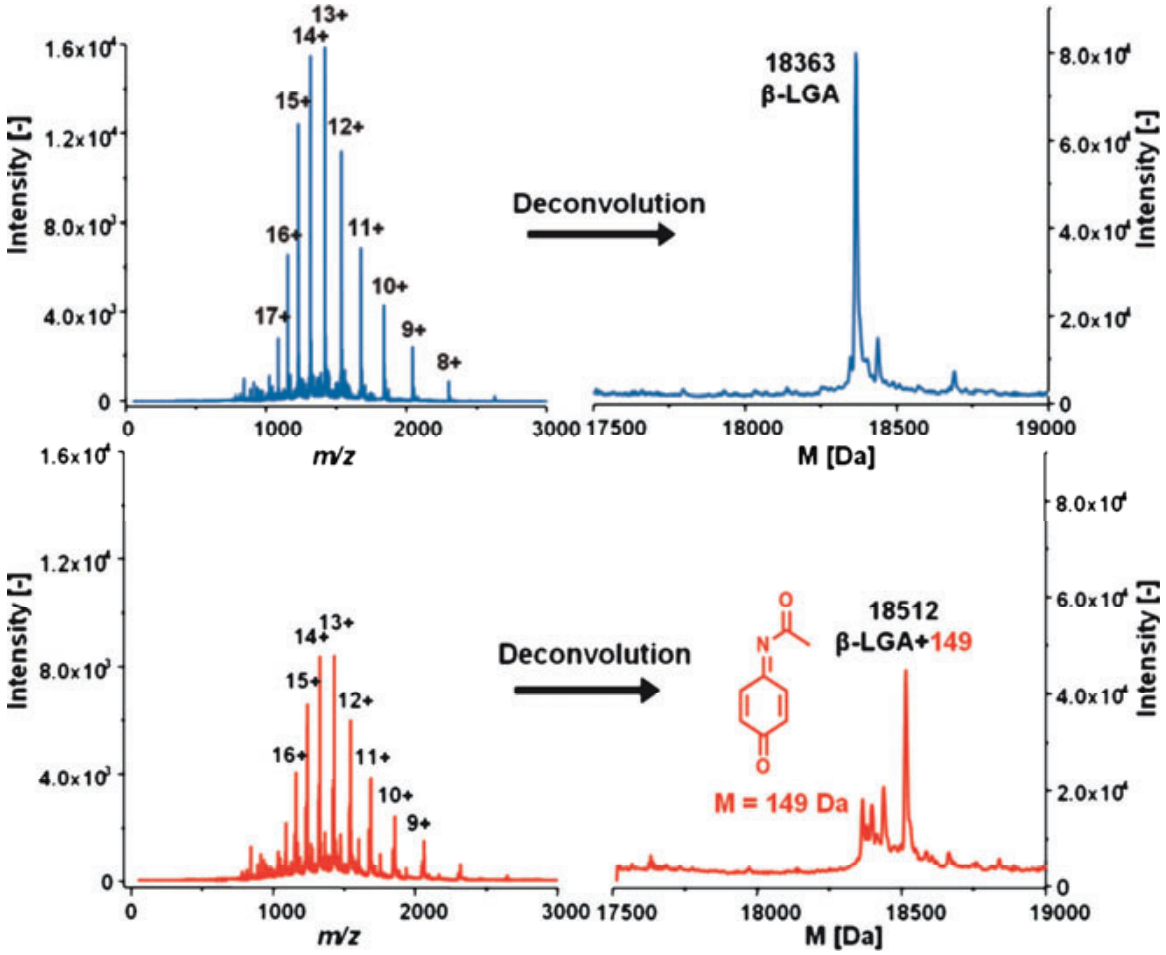

Figure 4. Adduct formation of electrochemical generated NAPQI with β-LGA. A solution of APAP ($1 \cdot 10^{-4}$M) was oxidized at a constant potential (1500mV) and the effluent of the EC cell was collected in a vial containing β-LGA ($1 \cdot 10^{-5}$M). The mixture was injected onto the LC/MS system and analyzed by ToF-MS. Blue: unmodified β-LGA, red: β-LGA after reaction with NAPQI.

native protein with the raw spectrum with multiply charged ions on the left and the deconvoluted spectrum on the right, the lower data show the respective situation after addition of electrogenerated NAPQI. The deconvoluted data clearly show that there is a high conversion yield of the protein with one molecule of the reactive metabolite. With the high resolution/high mass accuracy MS used in this work, the observed mass difference can unambiguously be assigned to one molecule of the reactive metabolite.

Protein adduct formation with HSA or hemoglobin will lead to more complex mass spectra, but also to more relevant information with respect to possible protein binding in the plasma or the red blood cells. Future work should concentrate on the attachment to other physiologically relevant proteins, e.g., those most frequently found in liver cells, to use this system for the prediction of liver toxicity.

Comparison to Established Methods

Comparison of the data obtained by EC/MS with established approaches is very important: As liver cell microsome experiments are established tools for the simulation of the oxidative metabolism of xenobiotics, they should always be carried out in parallel with the EC/MS studies. Most literature studies confirm a significant degree of agreement between both methods despite the different oxidation mechanisms.[12] However, there are aspects, where EC/MS provides important additional information as in case of reactive metabolites, which are typically not detected at all in liver cell microsome experiments due to covalent protein binding, which prevents them from being extracted from the biological matrix and thus from the subsequent LC/MS analysis. The structures of the products formed upon oxidation of amodiaquine (AQ) in electrochemical or microsomal incubation are shown in figure 5, while a comparison of the formed products is presented in table 1. An excellent correlation

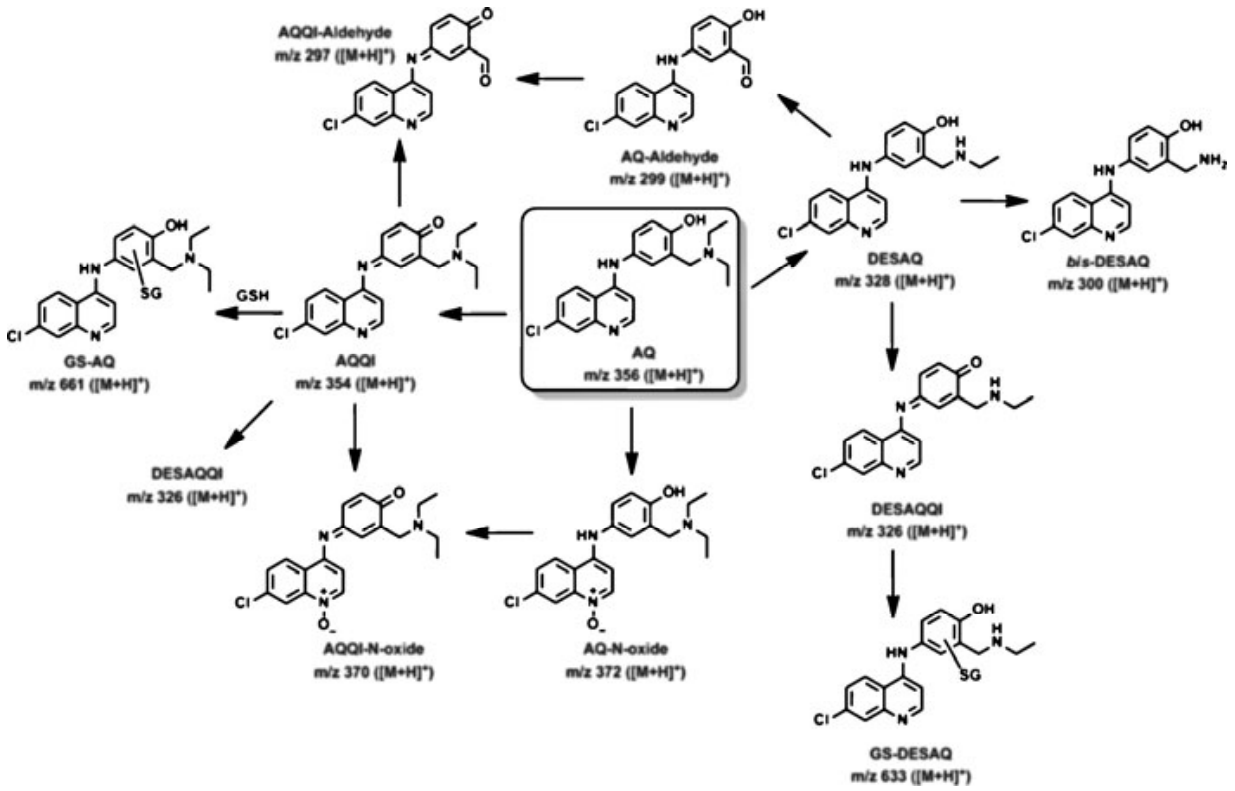

Figure 5. Overview of possible oxidation products and metabolites derived from electrochemical oxidation and microsomal incubations. For detailed information regarding their occurrence see Table 1.

at the qualitative scale is typically observed for N-dealkylation reactions (see figure 5 and table 1), while the reactive metabolites formed in the liver cell microsomes can only be detected indirectly via their glutathione adducts, when glutathione is added in excess concentrations as trapping agent.

Table 1. Comparison of Oxidation Products/Metabolites derived from Electrochemical Oxidation and *In vitro* Incubations with Rat Liver Microsomes

m/z	Metabolite	Electrochemical Oxidation	Microsomal Incubation
356	AQ	+	+
354	AQQI	+	+[a]
328	DESAQ	+	+
326	DESAQQI	+	+[a]
300	*bis*-DESAQ	-	+
299	AQ-Aldehyde	+	+
297	AQQI-Aldehyde	+	-
372	AQ-N-oxide	-	+
370	AQQI-N-oxide	+	-

[a] only detectable after trapping with glutathione

Preparative Scale Electrogeneration of Metabolites

An important issue in drug metabolism is the unambiguous identification of the formed metabolites. Nuclear magnetic resonance (NMR) studies provide the most valuable information for this purpose but do, unfortunately, require significant amounts of the generated metabolites. Due to this reason, the electrochemical synthesis of the metabolites using larger synthesis cells with similar functions as described above for analytical use has been introduced. The metabolites are collected after flow-through synthesis and are subsequently purified by (semi)preparative LC using stationary phases of the same kind, but with larger dimensions than for analytical use.[9]

Quantification of (Reactive) Metabolites

Quantification of the electrogenerated metabolites can be performed with external or internal calibration in case that the respective pure compounds (external calibration) or isotope-labelled analogues (internal calibration) are available. While external calibration is well possible for the solutions used for electrochemical metabolite generation due to their low matrix load, quantification in body fluids will require internal standards, which are very difficult to obtain. Therefore, an alternative approach based on inductively coupled plasma-mass

spectrometry (ICP-MS) is needed. Base of this method is the fact that in the ICP, all compounds are atomized and then ionized and detected, so that the signal intensity of a detectable ion is only dependent on its concentration, but not on its chemical nature or ionization properties as in case of ESI-MS. However, the approach is best suited for the electropositive elements, which can most easily be ionized. While the analysis of metals leads to excellent limits of detection down to the subnanomolar concentration range even after separation, elements as phosphorous, sulfur, chlorine, bromine or iodine can still be detected with reasonable limits of detection.[13-15] Quantification can be carried out with any standard of known concentration and a retention time in LC, which differs from that of the metabolites. The electrochemically generated metabolites are separated therefore by LC and subsequently detected by ICP-MS, and the signal intensity of any peak at an element trace is directly proportional to the concentration of the respective analyte. It should be noted, however, that the signal is only independent on the nature of the analyte, when identical plasma conditions are applied. Therefore, isocratic elution in LC is preferable over gradient elution, as the change in mobile phase composition, particularly a varying aqueous/organic content, will lead to varying plasma conditions. For this reason, complex separations that have to be carried out under gradient elution conditions should be accompanied by a post-column countergradient approach to adjust the solvent composition to a constant value.

Future Trends

Due to the strong development of this field within the last few years, it is expected that there will be important method and application development in the upcoming years. This should also include technical solutions for an improved possibility for screening of larger numbers of compounds in less time. It can be expected that these methods will not only find more widespread use in pharmaceutical analysis, but also in the food/beverages and chemical industries.

One major challenge associated with the rapid and efficient use of the EC/MS technology is the removal of the starting materials and the oxidation products from the electrode surfaces. This is particularly valid in those cases where substances are electropolymerized at the surfaces, thus leading to products, which are only sparingly soluble in the solution of the xenobiotic compound. Different approaches have been selected to overcome this problem: Rinsing with solvents, which are known to dissolve the products well, is an obvious solution, although it is not always efficient. The use of a strong oxidizer as 0.5M nitric acid is more efficient, but the electrochemical cells and all parts of the instrumentation, which are contacted with the acid, have to be checked previously with respect to their stability under these conditions. A promising future approach is the application of microfluidic chip-based electrochemical cells, as the respective electrode surfaces and geometrical dimensions can be prepared in a very flexible way and as these cells are suited for single use provided they can be produced at low prices in mass production. In this case, the cells can simply be discarded after single use, and memory effects from the cells will therefore not be an issue anymore. Odijk et al. have recently described the design and the applications[16,17] of such a microfluidic chip in detail.

Summary

The on-line combination of the three analytical techniques electrochemistry (EC), liquid chromatography (LC) and mass spectrometry (MS) has been introduced in recent years as a new tool for the simulation of the oxidative metabolism of drugs and other xenobiotics. The purely instrumental approach is useful for the prediction of many phase I and phase II metabolic reactions, including the adduct formation with small biogenic thiols as glutathione or even thiol-containing proteins. While the different mechanisms taking place in electrochemical and enzyme-catalyzed metabolic reactions do not allow a complete simulation of the biological situation by the instrumental approach, many reactions observed in vivo are observed by EC/LC/MS as well. Particular advantages are found for the instrumental system in case of reactive metabolites, which can be observed directly when using this approach. Other advantages are the possibility to synthesize small quantities of the metabolites in an electrochemical cell with the goal to allow their further characterization by NMR spectroscopy and to generate calibration standards of the metabolites. For selected heteroatom-containing metabolites, quantification may be carried out without a substance-specific internal standard by inductively coupled plasma-mass spectrometry (ICP-MS) after LC separation.

Zusammenfassung

Die on-line-Kombination der drei analytischen Techniken Elektrochemie (EC), Flüssigchromatographie (LC) und Massenspektrometrie (MS) wurde in den letzten Jahren als neues Verfahren zur Simulation des oxidativen Metabolismus von Pharmazeutika und anderen Xenobiotika eingeführt. Die rein instrumentelle Methode ermöglicht die Vorhersage vieler Phase I- und Phase II-Metaboliten. Hierunter fällt auch die Bildung von Addukten aus elektrochemisch generierten Metaboliten mit kleinen biogenen Thiolen und Proteinen mit freien Thiolgruppen. Obwohl eine vollständige Simulation der im Organismus entstehenden Metaboliten bereits aufgrund der verschiedenen Oxidationsmechanismen nicht möglich sein kann, werden experimentell überraschend viele Übereinstimmungen zwischen den mit der EC/LC/MS erhaltenen Daten und solchen aus biologischen Systemen gefunden. Besondere Vorteile weist das instrumentell-analytische Verfahren für reaktive Metabolite auf, da diese direkt nachgewiesen werden können. Ein weiterer Vorteil ist die Möglichkeit zur elektrochemischen Herstellung kleiner Substanzmengen der Metabolite für die weitergehende Charakterisierung mittels der NMR-Spektroskopie und als Kalibrationsstandards. Für heteroatomhaltige Metaboliten kann eine Quantifizierung ohne substanzspezifische Standards mit der induktiv gekoppelten Plasma-Massenspektrometrie (ICP-MS) nach flüssigchromatographischer Trennung durchgeführt werden.

Prof. Dr. Uwe Karst [1)]
is professor at the Westfälische Wilhelms-Universität Münster at the Institute of Inorganic and Analytical Chemistry

E-mail: uk@uni-muenster.de

Helene Faber, Sandra Jahn, Hannah Simon and Daniel Melles are Ph.D. students in the research group of Prof. Karst at the University of Münster (pictures in the name order).

Dr. Jens Künnemeyer (left) is postdoctoral research associate and Dr.Martin Vogel (right) is staff scientist in the research group of Prof. Karst.

[1)] Address: *Correnssstr. 30, 48149 Münster*

Project description & Acknowledgment

The project LC/Electrochemistry/Mass Spectrometry in (Bio)Analytical Chemistry, Drug Metabolism and Proteomics was funded by the DFG (Bonn, Germany) under registration number KA 1093/7-1. A parallel project with the principal investigators Dr. Wouter Olthuis/Prof. Dr. Albert van den Berg (University of Twente, The Netherlands) and Dr. Andries Bruins/Prof. Dr. Rainer Bischoff (University of Groningen, The Netherlands) was funded by the Dutch Technology Foundation STW. The present article highlights one major aspect of the project. The authors of this article would like to thank the DFG for financial support.

[1] D. C. Liebler, F. P. Guengerich, *Nat. Rev. Drug. Discovery* **2005**, *4*, 410.

[2] J. L. Bolton, M. A. Trush, T. M. Penning, G. Dryhurst, T. J. Monks, *Chem. Res. Toxicol.* **2000**, *13*, 135.

[3] R. Rinaldi, E. Eliasson, S. Swedmark, R. Morgenstern, *Drug Metab. Dispos.* **2002**, *30*, 1053.

[4] E. F. Brandon, C. D. Raap, I. Meijerman, J. H. Beijnen, J. H. Schellens, *Toxicol. Appl. Pharmacol.* **2003**, *189*, 233.

[5] A. Baumann, W. Lohmann, T. Rose, K. C. Ahn, B. D. Hammock, U. Karst, N. H. Schebb, *Drug Metab. Dispos.* **2010**, *38*, 2130.

[6] Regulation (EC) No 1223/2009 of the European Parliament and of the Council of 30 November 2009 on cosmetic products.

[7] W. Lohmann, U. Karst, *Anal. Bioanal. Chem.* **2006**, *386*, 1701.

[8] U. Jurva, H. V. Wikstrom, L. Weidolf, A. P. Bruins, *Rapid Commun. Mass Spectrom.* **2003**, *17*, 800.

[9] K. G. Madsen, G. Grönberg, C. Skonberg, U. Jurva, S. H. Hansen, J. Olsen, *Chem. Res. Toxicol.* **2008**, *21*, 2035.

[10] K. G. Madsen, C. Skonberg, U. Jurva, C. Cornett, S. H. Hansen, T. N. Johansen, J. Olsen, *Chem. Res. Toxicol.* **2008**, *21*, 1107.

[11] W. Lohmann, H. Hayen, U. Karst, *Anal. Chem.* **2008**, *80*, 9714.

[12] K. G. Madsen, J. Olsen, C. Skonberg, S. H. Hansen, U. Jurva, *Chem. Res. Toxicol.* **2007**, *20*, 821.

[13] K. De Wolf, L. Balcaen, E. Van De Walle, F. Cuyckens, F. Vanhaecke, *J. Anal. Atom Spectrom.* **2010**, *25*, 419.

[14] O. Corcoran, J. K. Nicholson, E. M. Lenz, F. Abou-Shakra, J. Castro-Perez, A. B. Sage, I. D. Wilson, *Rapid Commun. Mass Spectrom.* **2000**, *14*, 2377.

[15] W. Lohmann, B. Meermann, I. Möller, A. Scheffer, U.Karst, *Anal. Chem.* **2008**, *80*, 9769.

[16] M. Odijk, A. Baumann, W. Lohmann, F. T. G. van den Brink, W. Olthuis, U. Karst, A. van den Berg, *Lab Chip* **2009**, *9*, 1687.

[17] M. Odijk, A. Baumann, W. Olthuis, A. van den Berg, U. Karst, *Biosens. Bioelectron.* **2010**, *26*, 1521.

Magnetic Nanosensor Particles with Luminescence Upconversion Capability

Stefan Wilhelm, Thomas Hirsch, Elisabeth Scheucher, Torsten Mayr, Otto S. Wolfbeis

Nanoparticles (NPs) exhibit interesting size-dependent electrical, optical, magnetic, and chemical properties that cannot be observed in their bulk counterparts. The synthesis of NPs (i.e., crystalline particles ranging in size from 1 to 100 nm) has been intensely studied in the past decades.[1] Magnetic nanoparticles (MNPs) form a particularly attractive class of NPs and have found numerous applications such as in magnetic resonance imaging to visualize cancer, cardiovascular, neurological and other diseases. Other uses include drug targeting,[2] tissue imaging,[3] magnetic immobilization,[4] hyperthermia,[5] and magnetic resonance imaging.[6] MNPs, due to their magnetic properties, can be easily separated from (often complex) matrices and manipulated by applying an external magnetic field.[7] Near-infrared to visible upconversion luminescent nanoparticles (UCLNPs) form another type of unusual nanoparticles. They are capable of emitting visible light upon NIR light excitation. Lanthanide-doped (Yb, Er) hexagonal $NaYF_4$ UCLNPs are the most efficient upconversion phosphors known up to now.[8] The use of UCLNPs for in vitro imaging of cancer cells and in vivo imaging in tissues has been demonstrated.[9,10] UCLNPs show great potential as a new class of luminophores for biological, biomedical, and sensor applications.[11-14] We are reporting here on our first results on the combination of MNP and UCLNP technology within an ongoing project supported by the DFG and the FWF (Austria).

1. Magnetic Nanoparticles (MPNs)

Magnetic nanoparticles (MNPs) made from magnetite (Fe_3O_4) have been studied for biomedical applications. Magnetite-based MNPs are virtually nontoxic and biocompatible. They can act as magnetic single domain crystals below a critical size d_c (i.e., a diameter of 25 nm) and exhibit super-paramagnetic behavior at room temperature.[15] Super-paramagnetic NPs can be magnetized under an external magnetic field (H), reaching a maximum moment (*saturation magnetization,* M_S) when the field is strong enough. Their net magnetic moment is randomized to zero without an external magnetic field and therefore no remanent magnetic moment exists. We have synthesized monodisperse (average size is 10 nm) magnetite MNPs capped with oleic acid according to literature.[16] A typical transmission electron microscopy (TEM) image of such MNPs is shown in Fig. 1.

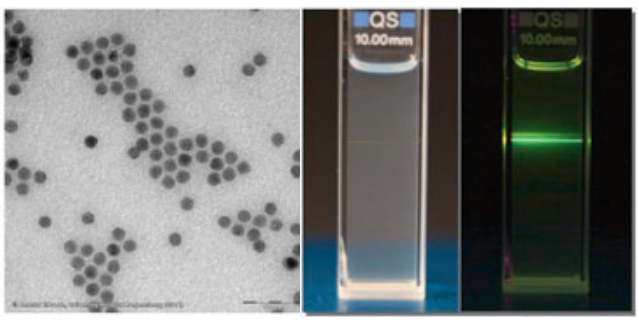

Figure 1. *Left:* TEM image of oleic acid capped Fe_3O_4 magnetic nanoparticles. Scale bar: 50 nm. *Right:* Colloidal solution of β-$NaYF_4$ (20% Yb, 2% Er) upconversion luminescent nanoparticles under daylight (*left*) and under 980 nm laser excitation (*right*).

2. Upconversion Luminescent Nanoparticles (UCLNPs)

Near-infrared (NIR)-to-visible upconversion luminescent nanoparticles (UCLNPs) display the unique property of converting NIR light (with wavelengths of typically 800 to 1,000 nm) into visible luminescence.[17] It mainly occurs with rare-earth doped solids and relies on the sequential absorption of two or more NIR photons by the dopants. Three main mechanisms are discussed, viz. excited state absorption, energy transfer upconversion, and photon avalanche processes.[18] Hexagonal $NaYF_4$ nanocrystals doped with lanthanide ions are particularly efficient in terms of upconversion. The upconverted luminescence can be varied in terms of color and intensity by proper doping. For example, UCLNPs doped with Yb^{3+}/Er^{3+} emit mainly green light (510 to 570 nm) and red light (630 to 680 nm). The green emission is dominant in fluoride-based lattices (e.g. $NaYF_4$), while oxide-based lattices (such as Y_2O_3) display predominantly red emission. Dopants such as Tm^{3+} result in blue upconversion luminescence (450 to 500 nm) that is accompanied by a weak red luminescence in certain host materials. The transitions and energy transfers between Yb^{3+} acting as the sensitizer, and the ions Er^{3+} and Tm^{3+} acting as the activators is illustrated in Fig. 2.

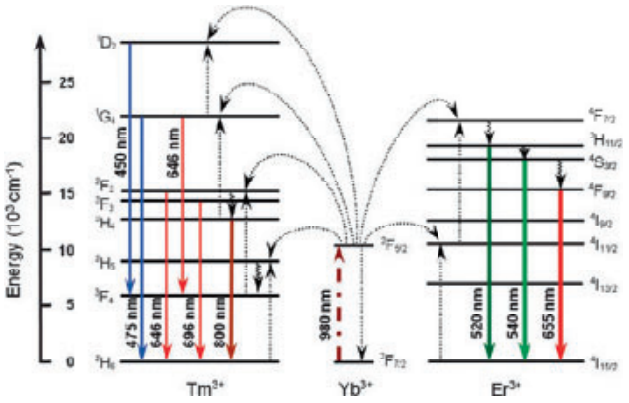

Figure 2. Energy transfer and upconversion emission mechanisms in a $NaYF_4$ nanocrystal doped with Yb^{3+}, Er^{3+}, and Tm^{3+} under 980-nm excitation. The dashed-dotted, dotted, curly, and full arrows refer to photon excitation, energy transfer, multi-photon relaxation, and upconversion emission, respectively. Reproduced from ref. [17], Fig 2, with kind permission from Springer Science+Business Media.

Compared to organic fluorophores and semiconductor nanocrystals, UCLNPs offer high photochemical stability, sharp emission bandwidths, and large anti-Stokes shifts (of up to 500 nm) that separate discrete emission peaks from the infrared excitation. The absence of visible autofluorescence in biological specimens under NIR light excitation also is notable. These benefits make UCLNPs ideal tools for use as luminescent labels and probes. We are using lanthanide-doped hexagonal $NaYF_4$ nanoparticles that can be prepared, - in essence - according to a known method where oleic acid is used as a kind of surfactant solvent.[19] A TEM image of $NaYF_4$ (20% Yb, 2% Er) nanoparticles and the respective XRD pattern are shown in Fig. 3.

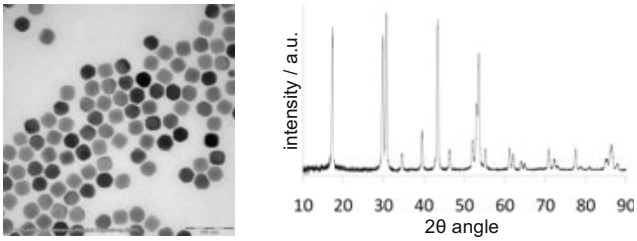

Figure 3. *Left:* TEM image of oleic acid-capped $NaYF_4$ (20% Yb, 2% Er) nanoparticles. Scale bar: 100 nm. The average size of the UCLNPs is 30 nm. *Right:* XRD pattern of hexagonal $NaYF_4$ (20% Yb, 2% Er).

3. Magnetic Nanoparticles with Luminescence Upconversion Capability

Based on the experience with the magnetic and the upconverting nanoparticles described before, we have synthesized a new type of nano-scaled hybrid core/shell particles. These offer magnetic response and upconversion luminescence at the same time. Super-paramagnetic magnetite nanocrystals with an average size of 10 nm and capped with oleic acid were used as seed crystals. A layer of hexagonal $NaYF_4$ doped with Yb^{3+} and Er^{3+} was deposited on their surface as shown in Fig. 4.

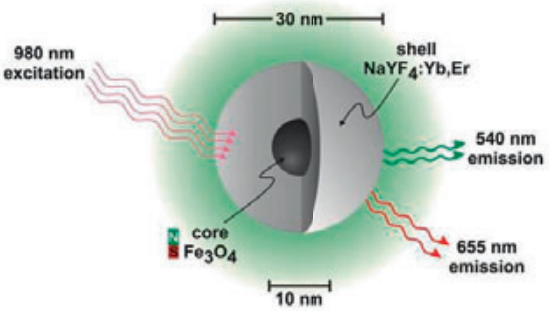

Figure 4. Schematic representation of magnetic UCLNPs, consisting of a magnetite core and a shell of hexagonal $NaYF_4$ doped with 20% of Yb^{3+} and 2% of Er^{3+} ions.

Such a core/shell architecture represents an elegant way to combine the magnetic properties of the MNPs with the upconversion capability of the UCLNPs. Figure 5 shows two pictures that illustrate the properties of such core/shell nanoparticles. The particles were collected at a distinct spot by applying an external magnetic field, as can be seen in Fig. 5A. The visible luminescence on excitation with a 980 nm (30 mW cw) laser is displayed in Fig. 5B. The emission spectra of upconversion luminescent nanoparticles with and without magnetic core do not show any significant differences.

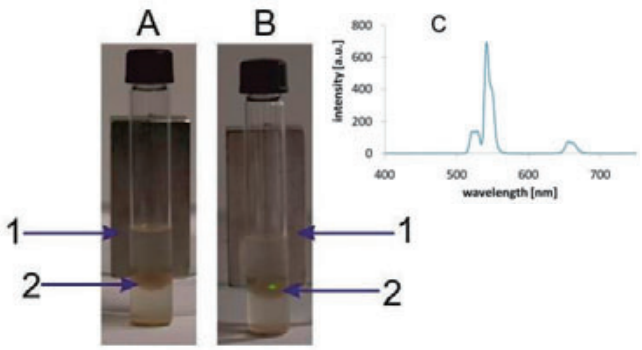

Figure 5. Pictures of upconverting nanoparticles with a magnetic core (UCLMNPs) in hexane. (**A**) Under daylight; (**B**) Under 980 nm laser excitation. Also shown is the permanent magnet in the back (**1**) and the spot of the UCLMNPs collected (**2**). (**C**) Emission spectrum of the UCLMNPs under photoexcitation at 980 nm using a 30 mW laser.

We are currently investigating on how magnetic upconverting luminescent nanoparticles can be modified at their surface, for example by click chemistries,[20] with the final goal to immobilize molecular probes and biorecognition elements thereon. We also note that the luminescence of such particles strongly depends on temperature in the physiological range which suggests their use in the determination of temperature, for example in hyperthermal treatment of cancer. We expect the resulting magnetic UCLNPs to offer a potential that is comparable to that of magnetic quantum dots, for example as imaging probes for microRNA,[21] and for stem cell labeling,[22] or of magnetic nanoparticles covered with fluorescent conjugated polymers.[23]

Summary

Nanoparticles made of magnetite and with an average size of 10 nm have been used as seed crystals to further grow, on their surface, a layer of upconverting material consisting of Yb,Er-doped hexagonal $NaYF_4$. The resulting multifunctional upconverting and magnetic nanoparticles represent a novel material for potential use in magnetic resonance imaging, as "nanolamps", and in bioimaging. Such particles may also form the basis for a new generation of optical immunosensors or gene sensors that can be separated from complex biomatter by magnetic force and where fluorescent signals can be generated using a 980 nm diode laser whose light easily penetrates most tissue.

Zusammenfassung

Nanopartikel aus Magnetit (Fe_3O_4) und mit einer Durchschnittsgröße von 10 nm wurden als Kristallisationskeime eingesetzt, um darauf eine Hülle aus Yb,Er-dotiertem $NaYF_4$ aufzubringen. Diese Hülle ermöglicht eine Aufkonvertierung von infrarotem in sichtbares Licht. Derartige Kern/Schale-Nanopartikel stellen ein neuartiges Material dar, das für einen Einsatz in bildgebenden Verfahren (wie z. B. der Kernspintomographie) geeignet ist. Es ist außerdem für den Einsatz in einer neuen Klasse optischer Immunosensoren und Gen-Sensoren vorgesehen. Aufgrund der magnetischen Eigenschaften des Partikelkerns wird es möglich, die Sensoren auch aus komplexen biologischen Matrices durch Anlegen eines äußeren Magnetfeldes abzutrennen und aufzukonzentrieren. Die Anregung mit dem nah-infraroten Licht eines 980-nm-Diodenlasers, für welches Gewebe sehr gut permeabel ist, liefert anschließend das Lumineszenzsignal der aufkonvertierenden Schale.

Otto S. Wolfbeis[1)*] *is a Professor of Analytical and Interface Chemistry at the University of Regensburg.*

*Email: otto.wolfbeis@chemie.uni-r.de**

** corresponding author*

Working departments of coauthors: Stefan Wilhelm [1)], Thomas Hirsch [1)], Elisabeth Scheucher [2)], Thorsten Mayr [2)].

Addresses:

[1)] University of Regensburg, Institute of Analytical Chemistry, Chemo- and Biosensors, 93040 Regensburg, Germany

[2)] Graz University of Technology, Institute of Amalytical Chemistry and Food Chemistry, 8010 Graz, Austria

Project description:

The respective DFG project (Wo-669/12-1) is entitled Magnetic Nanosensor Particles with Luminescence Upconversion Capability and performed in cooperation with partners at the Graz University of Technology. We will develop methods for the preparation of particles with magnetic and luminescent upconversion capability as outlined in this article and with the aim to design new nanosized chemical sensors and biosensors with unique properties.

[1] J. Park, J. Joo, S.G. Kwon, Y. Jang, T. Hyeon, *Angew. Chem.* **2007**, *119*, 4714-4754; *Angew. Chem. Int. Ed.* **2007**, *46*, 4630-4660.

[2] T. Tanaka, T. Matsunaga, *Anal. Chem.* **2000**, *72*, 3518-3522.

[3] W. S. Seo, J. H. Lee, X. Sun, Y. Suzuki, D. Mann, Z. Liu, M. Terashima, P. C. Yang, M. V. McConnell, D. G. Nishimura, H. Dai, *Nature Materials* **2006**, *5*, 971-976.

[4] X. Hong, X. Gao, L. Jiang, *J. Am. Chem. Soc.* **2007**, *129*, 1478-1479.

[5] M. Kettering, J. Winter, M. Zeisberger, S. Bremer-Streck, H. Oehring, C. Bergemann, C. Alexiou, R. Hergt, K. J. Halbhuber, W. A. Kaiser, I. Hilger, *Nanotechnology* **2007**, *18*, 175101.

[6] M. Zhang, S. Shi, J. Meng, X. Wang, H. Fan, Y. Zhu, X. Wang, Y. Qian, *J. Phys. Chem. C* **2008**, *112*, 2825-2830.

[7] W. W. Yu, E. Chang, C. M. Sayes, R. Drezek, V. L. Colvin, *Nanotechnology* **2006**, *17*, 4483-4487.

[8] H. S. Mader, P. Kele, S. M. Saleh, O. S. Wolfbeis, *Curr. Opin.Chem. Biol.* **2010**, *14*, 582-596.

[9] C. Liu, H. Wang, X. Li, D. Chen, *J. Mater. Chem.* **2009**, *19*, 3546-3556.

[10] F. Wang. Y. Han, C. S. Lim, Y. Lu, J. Wang, J. Xu, H. Chen, C. Zhang, M. Hong, X. Liu, *Nature* **2010**, *463*, 1061-1065.

[11] D. E. Achatz, R. J. Meier, L. H. Fischer, O. S. Wolfbeis, *Angew. Chem.* **2011**, *123*, 274-277; *Angew. Chem. Int. Ed.* **2011**, *50*, 260-263.

[12] R. Ali, T. Lang, S. M. Saleh, R. J. Meier, O. S. Wolfbeis, *Anal. Chem.* **2011**, *82*, 2846-2851.

[13] H. H. Gorris, R. Ali, S. M. Saleh, O. S. Wolfbeis, *Adv. Mater.* **2011**, *23*, 1652-1655.

[14] L. H. Fischer, G. S. Harms, O. S. Wolfbeis, *Angew. Chem.* **2011**, *123*, 4640-4645; *Angew. Chem. Int. Ed.* **2011**, 50, 20, 4546–4551.

[15] K. M. Krishnan, A. B. Pakhomov, Y. Bao, P. Blomqvist, Y. Chun, M. Gonzales, K. Griffin, X. Ji, B. K. Roberts, *J. Mater. Sci.* **2006**, *41*, 793-815.

[16] W. W. Yu, J. C. Falkner, C. T. Yavuz, V. L. Colvin, *Chem. Commun.* **2004**, 2306-2307.

[17] D. E. Achatz, A. Reham, O. S. Wolfbeis, *Topics Curr. Chem.* **2011**, *300*, 29-50.

[18] F. Auzel, *Chem. Rev.* **2004**, *104*, 139-173.

[19] Z. Li, Y. Zhang, S. Jiang, *Adv. Mater.* **2008**, *20*, 4765-4769.

[20] H. S. Mader, M. Link, D. E. Achatz, K. Uhlmann, X. Li, O. S. Wolfbeis, *Chem.-Eur. J.* **2010**, *16*, 5416-5424.

[21] D. W. Hwang, I. C. Song, D. S. Lee, S. Kim, *Small* **2010**, *6*, 81–88.

[22] L. Wang, K. G. Neoh, E. T. Kang, B. Shuter, S. C. Wang, *Biomaterials* **2010**, *31*, 3502-3511.

[23] P. Howes, M. Green, A. Bowers, D. Parker, G. Varma, M. Kallumadil, M. Hughes, A. Warley, A. Brain, R. Botnar, *J. Am. Chem. Soc.* **2010**, *132*, 9833–9839

Constrained Dynamics in Interphases of Model Filled Elastomers: Role of Interface Chemistry on Crosslinking, Local Stress Distribution and Mechanics

François Lequeux, Didier Long, Paul Sotta, Kay Saalwächter

The Franco-German consortium "DINaFil" (Dynamics at the Interface of Nanoscopic Fillers), located at Paris, Lyon and Halle, and co-funded by the ANR and the DFG, is a multidisciplinary endeavour concerned with a quantitative understanding of the complex behaviour of filled elastomers, a class of daily-life materials with as many uses as fundamentally open questions.

1. Introduction: Filler Effects in Elastomers

Almost any rubber that is used for real-life applications is a highly complex, heterogeneous material consisting of a cross-linked polymer matrix (an elastomer) and significant amounts of inorganic, often nanometer-sized particles such as carbon black or silica.[1-3] Without such fillers, rubber materials would not exhibit the favourable and fascinating combination of properties such as elasticity, large deformability, high toughness, durability (abrasion resistance) and, in particular when tire applications are in the focus, traction on wet or icy roads and low viscous losses (low rolling resistence). In particular the optimization of the latter while not compromising the other relevant properties, related to the development of "green" tires for lower fuel consumption, is a field of active industrial development that is characterized by a lack of rational design principles and an in-depth theoretical understanding.

Some aspects of the complex mechanical behaviour of filled elastomers are highlighted in Fig. 1, where in the sketch in Fig. 1a it is emphasized that the spatial distribution of the nanoparticles plays a key role. In most application-relevant cases, the particles themselves form a network with a complex structural hierarchy over many decades in length scale,[1,3] starting at primary particles on the few-nm range, via aggregates and agglomerates, finally forming a macroscopically percolated structure that can transmit mechanical load. To illustrate its effect, Fig. 1b shows the storage modulus G'(100 Hz) from frequency-dependent shear experiments of the industrially relevant tire material SBR (styrene-butadiene rubber) as a function of temperature.[4] The large drop in G' over 3 decades marks the glass transition of the matrix at around -15°C. While in the ensuing rubber plateau region, unfilled SBR exhibits the expected positive temperature dependence as expected from the entropic models of rubber elasticity, filled SBR has a much higher modulus which usually *decreases* significantly on heating. This is emphasized by plotting the reinforcement factor $R(\Delta T) = G'_{\text{filled}}/G'_{\text{unfilled}}$[5] at constant temperature difference to the glass transition shown in the inset, which is seen to be highest at temperatures around and above the glass-rubber transition. While below, the low reinforcement can be explained on the basis of simply considering the additive effect of a certain volume of high-moduls material, values exceeding $R = 10$ indicate the important synergistic effect of a filler network. Importantly, the decrease of R at even higher temperatures indicates non-trivial interfacial effects of the polymer-filler system that are in the focus of our research initiative.

Based on such observations, some of us[5] have previously developed a model based on the existence of a "glassy layer" of immobilized polymer material on the particle surface that constitutes a "sticker" between the particles and simply softens at higher temperature.[6,7] Other important features of filled rubbers that must ultimately be captured by a quantitative model are the well-known dramatic decrease of R in the range of higher deformations, the so-called Payne effect that can be attributed to a mechanical breakdown of the filler network, and history and hysteresis effects under conditions of cyclic mechanical load, so-called Mullins effects, related to the evolution of structural complexity.[2,3]

Preliminary NMR experiments on a well-dispersed model system have indeed provided direct evidence of an interphase consisting of immobilized polymer.[8] These studies provided the starting point for the present work, where we seek to systematically study such interphase fractions and their impact on the macroscopic properties. Notably, in systems that are closer to actual applications, having much more inhomogeneous particle dispersions, interphases have as yet not been observed directly. Rather, the existence of "glassy layers" was for the case of carbon black indirectly inferred from so-called bound-rubber extraction or dielectric experiments,[1-3,9] or from fits of mechanical models to rheological data.[3] Direct studies by advanced NMR methods have as yet neither revealed significant amounts of

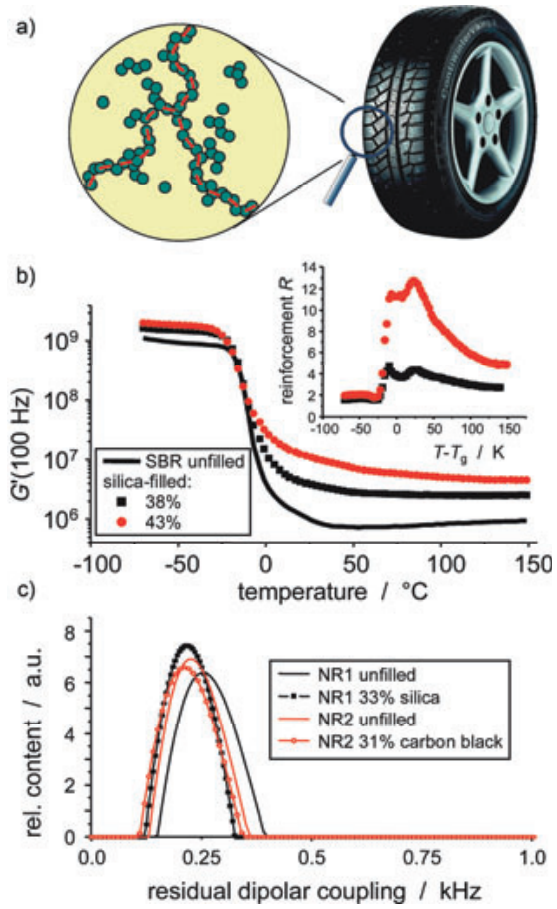

Figure 1. (a) Inhomogeneous nanoparticle distribution in a filled rubber for, e.g., tire applications. Tire image by courtesy of Continental AG. (b) Storage moduls G' at a shear frequency of 100 Hz of unfilled vs. silica-filled SBR as a function of temperature. The inset shows the reinforcement $R = G'_{filled}/G'_{unfilled}$ as a function of temperature difference to the glass transition. Data from ref. [4]. (c) Distributions of cross-link density, as measured in terms of the RDC taken from NMR experiments, for pure NR and NR filled with silica or carbon black.[10]

glassy layer, nor did they give any indication of substantial changes in the network matrix. Corresponding results from the Halle lab in collaboration with the ICTP-CSIC in Madrid are shown in Fig. 1c.

In a broad study comprising a wide range of traditional and modern nano-fillers in commercially relevant rubber materials, NR (natural rubber) and SBR, revealed *no* substantial effect of any filler on the actual rubber matrix.[10] One of the NMR methods used, namely ^{1}H multiple-quantum (MQ) NMR,[11] is able to provide information on the cross-link density ν_c of the materials based on network chain mobility. Its result is the so-called residual dipolar coupling (RDC) constant associated with the protons in each monomer. Generally, the RDC is directly proportional to the crosslink density, or to the number of elastically active network chains of weight M_c in the sample, which in turn determines the modulus. Thus, RDC $\propto G' \propto \nu_c \propto 1/M_c$. The feature that ^{1}H NMR detects all monomers at once means that structural inhomogeneity, i.e., the coexistence of lowly and highly cross-linked regions, is directly reflected in the data. For the given method, it is possible to extract the *distribution* of the RDC, which directly reflects the distribution in local cross-link densities. The data in Fig. 1c is typical in that, first, vulcanized elastomers were commonly found to be very homogeneous, and second, that fillers of any type hardly affect this homogeneity. The only significant filler effect turned out to be the observation that the cross-link density in a filled system is always somewhat lower that that of the unfilled counterpart, which is straightforwardly attributed to a partial de-activation of the vulcanization system by the high-surface filler.

The conclusion is clear: if effects of glassy layers or locally modified cross-link density should be responsible for the mechanical properties (Fig. 1b), their volume fraction must be very low, i.e. below the limit of NMR detectability on the percent level. If can of course be imagined that in aggregated/agglomerated systems, the internal surface is much lower as compared to isolated nanofillers, such that even small amounts of interphase material close to the particles can affect large changes of the total system. The important question to be resolved in our work is now to establish a link between tunable model systems, which as shown below do exhibit the mentioned features of glassy layers and inhomogeneous rubber matrix, and the systems of application relevance.

2. Interdisciplinary Approach to Unravel Detailed Structure-Property Relations

2.1. Model nano-composites based on PEA, NR and SBR

Industrial samples are simply made by strong mechanical mixing of all the constituents: solid particles, grafting agent and surfactant, polymer, crosslinker, and various catalysts. The spatial arrangement of the nanoparticles is far from equilibrium and depends crucially on the energy and time of mixing. Indeed, during the mixing, it is known that the molecular weights of the chains decrease, probably in a different manner for the polymer adsorbed at the particle surface and in the bulk. Thus the mechanical properties are relatively sensitive to mixing conditions. In addition, it is also known that the time elapsed between mixing and crosslinking (curing by, e.g. vulcanisation) has an influence on the mechanical properties because of slow rearrangements of the nanoparticles. Lastly, the surface agents – grafters and surfactants – are also known to modify the arrangement of the nano-particles in the samples. This complexity has unfortunately hindered the understanding of the physics of these systems. Thus, it is crucial – in order to get quantitative and comprehensive experimental results – both to synthesize model nano-composites with extremely well-controlled arrangement and to be able to characterize their nanoparticles arrangements. The characterization is rather simple if we are able to use spherical nearly polydisperse nanoparticles. The most versatile particles for that are silica particles that are easy to prepare, and to modify

chemically. Moreover, they exhibit a natural contrast against the polymer for neutron scattering experiments.[12]

The trick we have been using in recent years was to prepare solutions of colloidal silica particles in a solvent consisting of the monomers with crosslinker and eventually additional solvent – and to polymerize and crosslink the monomer controlling the colloidal stability during the whole process. This was quite simple in the case of polyacrylates – specifically poly(ethyl acrylate), PEA – and has allowed us to get systems with nearly crystalline arrangement of nanoparticles.[12] Thanks to these samples, we were thus the first to put into evidence the effect of gradient of glass transition temperature in nanocomposites[6] as well as the role of particles arrangement on mechanical properties.[13] The next challenge is to use polymers relevant in the industrial word – poly(styrene-co-butadiene), SBR, or natural rubber, NR, for instance – which are more convenient for large strain tests than polyacrylates. The latter are in fact quite fragile mechanically. In the case of SBR and NR, however, it is rather difficult to polymerize the monomer in the presence of particles. The project will thus consist in mimicking the industrial mixing process grafting and/or adsorbing polymer chains and dispersing them afterwards in the polymer matrix

2.2. NMR detection and characterization of dynamic interphases and network inhomogeneities

In previous NMR work, we have developed quantitative approaches to the determination of the phase composition in dynamically heterogeneous materials, based on simple ^{1}H low-field spectrometers.[14] Generally, the distinction is based upon the orientation dependence of inter-proton dipolar couplings and their potential averaging due to fast rotational motions of the molecules. Thus, immobile regions associated with strong dipolar couplings are characterized by quickly decaying time domain signals (broad lines in the frequency domain spectra), while more mobile components are only subject to weak or almost negligible RDC, leading to slower signal decay. Using a set of spin-echo based magnetization filters, signals belonging to differently mobile components can be measured separately, allowing for a determination of fitting parameters for simple free-induction decay (FID) data. With such an approach, we have performed an in-depth study of the phases that can be identified in the PEA-based model systems described above. Parts of these results have been published recently,[15] and we here summarize these and some more current findings.

Fig. 2a shows a typical FID from a highly filled PEA network, where three components can be identified: glassy (fully rigid), strongly immobilized ("intermediate": only local, highly anisotropic small-amplitude mobility) and mobile (network chains and free chains. The total amount of interphase material (glassy + intermediate) is seen to reach up to 20% of the overall polymer signal. Detailed temperature-dependent studies (Fig. 2b) provided a direct proof the hypothesis on the softening of potential glassy bridges between fillers that, according to our model,[5] may explain the temperature-dependent decrease of

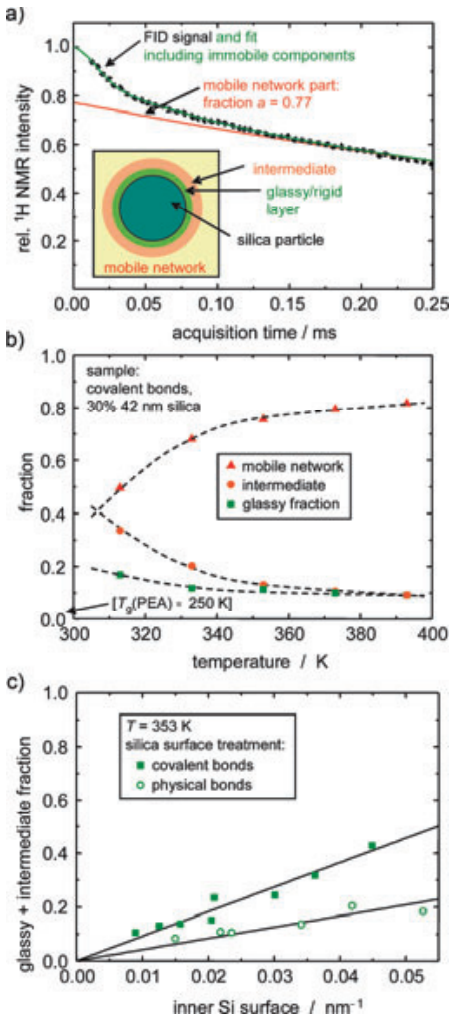

Figure 2. (a) Low-field ^{1}H NMR free-induction decay data reflecting quantitatively interphases of reduced mobility in PEA-based nanocomposites. (b) Temperature dependence of the three distinguishable fit components, demonstrating an apparently increased glass transition temperature of the interphase material. (c) Relation of the amount of interphase material with the known inner surface (total surface area per volume) of different samples for two cases of different surface interaction. See ref. [15].

the reinforcement. A notable difference was found between the materials that are just characterized by silica particle surface that provide physical adsorption sites for the polymer, and those that have a high density of chemical surface grafting sites (Fig. 2c). We stress that even in the former systems, significant amounts of immobilized polymer could be evidenced.

Currently, we are analyzing data from NMR spin diffusion experiments,[14] which are able to provide estimates of the thickness of the different domains and their spatial arrangement. First results are consistent with estimates based on the data in Fig. 2 that indicate a total interphase thickness of 5–6 nm at the lowest temperatures, as simply estimated from the determined volume fractions and the known internal surfaces. This corrects our previous lower, less quantitative results.[8] Analyzing in-depth the spin diffusion across the three distinguishable phases, we

have indications that the region of intermediate mobility does not simply form a homogenous layer around the glassy shell, but is inhomogeneously distributed.

Finally, we used the ^{1}H MQ NMR method to probe the homogeneity of the mobile network phase in these systems. The results are summarized in terms of RDC (~cross-link density) distributions in Fig. 3, and they differ significantly in some aspects from previous findings on commercially relevant systems, refs. [4,10] and Fig. 1c. First, the PEA networks appear much more inhomogeneous (note the log scale), which is attributed to the more complex spin system (side chain with lower RDC) and inhomogeneities intrinsic to the cross-linking process in this system. So even though the systems nicely exhibit average NMR-detected cross-link densities that follow the trend expected for increasing cross-linker concentrations (Fig. 3a), the intrinsic width of the distributions poses limitations to a fully detailed analysis. This point will be improved upon by way of the up-coming model composites based on NR, with their high intrinsic homogeneity. However, the findings for the filled PEA systems are also rather clear already: while the fillers with only physical bonds to the polymer phase (Fig. 3b) lead to no detectable changes of the rubber matrix, in analogy to our previous work (Fig. 1c), the fillers with dense grafts (Fig. 3c) significantly affect the matrix in that its cross-link density is generally increased and appears more inhomogeneous. The latter effect is seen in terms of broader peaks and shoulders on the high-cross-link side of the distribution functions, with even a trend to bimodality for the samples with the highest internal surface.

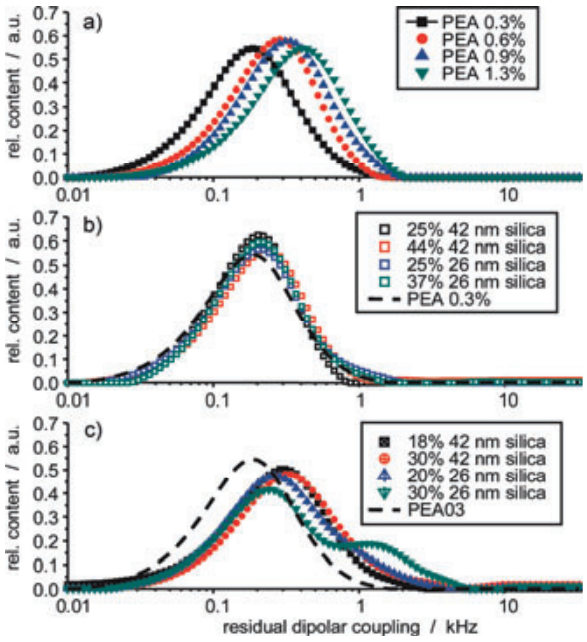

Figure 3. RDC distributions reflecting local cross-link density distributions as derived from ^{1}H low-field MQ NMR experiments, based on data from ref. [15]. (a) PEA networks with varying amount of cross-linker given in wt-%. (b,c) PEA networks with 0.3% cross-linker and varying amounts of well-dispersed silica spheres that are modified so as to provide (b) just favourable adsorptive interactions or (c) a high density of chemical bonds (grafts) between the particles and the elastomer.

These results give a convincing demonstration of the changes of the polymer matrix as arising from well-dispersed high-surface nanofillers. Ongoing mechanical studies on these and the new model systems, and in particular on systems with controlled nanoparticle aggregation states, in combination with more refined computer simulations, will help in elucidating the relevance of polymer interphases with modified properties in general.

2.3. NMR experiments on strained samples

A second, important aspect of the NMR part of the project is concerned with MQ NMR on deformed (stretched or compressed) samples, giving access to the orientation distribution and stretching states of the network chains. In this way, we seek to address the question whether in filled systems there is an inhomogeneous local strain distribution that may play a role in determining the unusual mechanical properties (high reinforcement, Payne and Mullins effects). In unfilled elastomers quite far above T_g, the effect of uniaxial strain on the distribution of residual NMR interactions (related to local strain at the scale of network chains) has been analyzed within the confines of standard rubber elasticity theories and the assumption of affine deformation.[16] In this case, the degree of anisotropy induced upon stretching is related directly to the average residual interaction measured in the relaxed state. In filled elastomers, a first evidence for a local strain distribution was obtained.[17] The distribution of local strain (at a given macroscopic strain) was shown to be related to the filler morphology and dispersion state.

MQ NMR will give quantitative access to the distribution of local chain stretching (or equivalently local strain) at a given macroscopic strain, as regards both the magnitude and the orientation (local 3D effects). To discriminate magnitude and orientation effects on the distribution of residual couplings, the orientation of the stretching axis with respect to B_0 is varied. The angular variation gives access to orientation effect. Then, by combining experiments done at many different orientations, an effective powder spectrum can be reconstructed. Preliminary work has shown that the proposed analysis is indeed feasible. This analysis of the residual NMR interactions (MQ signal) can then be done as a function of the macroscopic strain imposed to the sample. We will then correlate the obtained distributions of residual NMR interactions in stretched samples to the tuned surface interactions and to the related heterogeneities of elastic modulus and the local (gradient of) mobility within the matrix.

2.4. Simulations of reinforced rubber systems

As described above, elastomers filled with carbon black or silica particles have a shear modulus much (up to a few 100 times) higher than that of the pure elastomer and exhibit a high dissipative efficiency. Another important feature is their non-linear behaviour. When submitted to deformations with ampli-

tudes γ of the order of a few percent or more, the elastic modulus $G'(\omega)$ decreases down to values much smaller than the value in the linear regime: this is the so-called Payne effect. During subsequent deformations, the elastic modulus in the linear regime is smaller than that of the initial system, but recovers progressively (at least partially) to the initial value: this is the so-called Mullins effect. Recently, some of us have proposed a mesoscale model that explains these basic features.[18] The model is based on the presence of a glassy layer around the fillers when the interaction between the matrix and the fillers is sufficiently strong,[7,8,13] see Fig. 2 for our experimental quantification of this effect. We have proposed that the mechanical properties of nano-filled elastomers are governed by the kinetics of rupture and re-birth of glassy bridges which link neighbouring nanoparticles and from large rigid clusters of finite lifetimes. These lifetimes depend on various parameters such as temperature, nanoparticle-matrix interactions, and distance between neighbouring fillers. Most importantly, these lifetimes depend on the deformation history of the samples. We have shown that the unusual non-linear and plastic behaviour of these systems can be predicted by this death and re-birth process.

A major challenge of the physics of filled elastomers is that the relevant space and time scales are very large compared to molecular scales. Thus, they are totally inaccessible to numerical simulations at the molecular scale, by many orders of magnitude. One must thus devise mesoscale models. Since numerical simulations cannot cover more than 6-7 decades in time, it is nevertheless an impossible task to address all the issues mentioned above in a single picture. Depending on the issues of interest, one must primarily focus on some particular aspect of the physical behaviour and use a coarse-grained description of the system. Two different scales are of particular interest. (i) A scale of about ten nanometers, corresponding to confined polymers layers, e.g. between two fillers, or two thin films deposited on a substrate, and (ii) the scale of a few hundreds of nanometers, corresponding to the size of filler aggregates. The latter bridges the gap between the former and the macroscopic continuous scale.

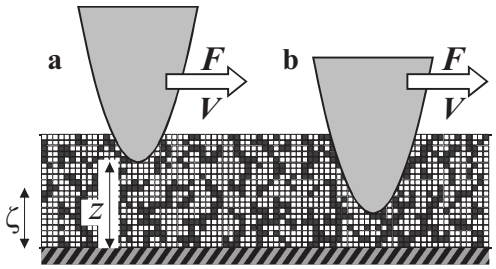

Figure 4. Schematics of a film at a temperature $T > T_g$. In (a), the mechanical probe is at a distance z from the substrate larger than the size ξ of the slow aggregates. The slow aggregates can move freely around it, and the viscosity is smaller than the viscosity at T_g. In (b), the mechanical probe is closer to the substrate. Moving parallel to the film requires deforming slow aggregates: the viscosity is larger than that at the bulk T_g.

An essential feature of polymers dynamics close to the glass transition is that it is strongly heterogeneous on a scale of a few nanometers, typically 3 nm.[19] Some of us have proposed that these dynamical heterogeneities correspond to density fluctuations and that the macroscopic dynamics is controlled by the slowest percolating subunits.[20,21] This so-called "Percolation of Free Volume Distribution" (PFVD) model [22] allows to explain: (a) the heterogeneous nature of the dynamics, (b) the violation of the Stokes law observed for small probes, (c) essential features of ageing and rejuvenation, and (d) the shift of glass transition at interfaces. Fig. 4 illustrates the implications on the local mechanical properties of this films.

The predicted glass transition temperature at a distance z from an interface is described by

$$T_g(z) \approx T_g\left(1+\left(\frac{\beta}{z}\right)^{1/\nu}\right), \qquad (1)$$

where T_g is the bulk glass transition temperature of the pure rubber. The exponent $\nu \cong 0.88$ is the critical exponent for the correlation length in 3D percolation. The value of the length β depends on the polymer-substrate interactions. For strong interactions, it is of the order 1 nm. In its current development the model does not incorporate the description of the mechanical behaviour explicitly, for instance for calculating a storage and a dissipative modulus. It also does not include the effect of imposed deformation on the dynamical state (e.g. plastic deformation of polymers). One aim of this project will be to extend the PFVD model in order to describe and calculate the (linear and non-linear) mechanical properties of confined polymers. We will thus be able to describe the evolution of a confined polymer layer under imposed deformations with a 2-3 nm scale resolution and on time scales spanning from 10 ns to 10^4 s typically. For this purpose, we will develop a 3D model, which we will solve by numerical simulations. In this 3D model, the basic units will be the subunits (3 nm) of dynamical heterogeneities. Their dynamical evolution (aging/rejuvenating) will be coupled to the stress field which results from the imposed deformations. We will thus describe the stress field at the nanometer scale (2-3 nm), as well as the strain field, and the dynamical state of each of the subunits.

The PFVD model was used by Berriot et al.[5–8] for explaining the microscopic origin of the reinforcement in filled elastomers, as a consequence of the presence of a gradient of glass transition temperature around the fillers, as described by Eq. (1) and illustrated in Fig. 5. This provided the link between thin films dynamics (a few tens of nanometers) and the physical behaviour of filled elastomers. This equivalence between thin film dynamics and filled elastomer properties was subsequently stressed by experimental[23] and simulation[24] studies. In the presence of a local stress σ, we assume that the glass transition temperature in between two fillers is given by

$$T_g(z,\sigma) \approx T_g\left(1+\left(\frac{\beta}{z}\right)^{1/\nu}\right) - \frac{\sigma}{K} \qquad (2)$$

The first term in the right hand side of Eq. (2) represents the effect of the filler-matrix interactions. The second term is the decrease of T_g due to the local stress, which is the plasticizing

effect of an applied stress. K depends on the polymer. This parameter is known from macroscopic experiments. It relates the yield stress σ_y to the temperature T and the polymer glass transition temperature T_g by $\sigma_y = K(T_g - T)$, and is typically of the order 10^6 Pa/K.

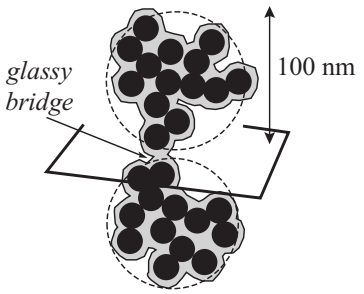

Figure 5. The macroscopic stress in a filled elastomer is supported by the glassy polymer fraction which bridges two neighboring filler aggregates. Aggregates of about 100 nm made of primary particles of 10 nm are schematized. They are surrounded by a glassy layer which is sketched. The fraction of glassy polymer in a section normal to the applied stress is $\Sigma \sim 1\%$. The macroscopic deformation is amplified between the fillers by a factor typically $l \sim 10$, which results in a macroscopic modulus G´ of the order 10^7 to 10^8 Pa.

When glassy layers overlap, the macroscopic shear modulus G' is related to the shear modulus of the glassy polymer G'_g through geometrical effects. Indeed, a macroscopic deformation ε is amplified locally in between the fillers by an amplification factor λ, which is the ratio between the diameter of the fillers and the distance between two neighboring fillers. In a plane normal to the direction of elongation, the stress is supported by glassy bridges which represent an area fraction $\Sigma < 1$. Both parameters λ and Σ depend on the considered systems. The macroscopic modulus is thus given by

$$G' \approx G'_g \lambda \Sigma \,. \qquad (3)$$

Assuming that the fillers are spherical particles of 10 nm diameter with typical interparticle distance of a few nanometers, we deduce that λ is of order a few units and Σ is of order a few 10^{-2}, depending on the ratio between the glassy layer thickness and the nearest neighbor distance. Since $G'_g \sim 10^9$ Pa, we obtain a macroscopic shear modulus of about 10^8 Pa, which corresponds to very strong reinforcement. Consider a macroscopic deformation ε of a few percent. The local stress σ is then of order $\sigma \sim \lambda\varepsilon G'_g \sim 10^8$ Pa. With $K \sim 10^6$ Pa.K^{-1}, a local T_g reduction of 100 K is obtained. Therefore, glassy bridges yield, which results in a lowering of the shear modulus, for macroscopic deformations of order a few percent.

The glassy bridges are not permanent, rather, they break under applied strain. Within a glassy bridge in between two neighbouring particles, at equilibrium, we assume that the polymer has locally the dominant relaxation time τ_α given by the William-Landel-Ferry (WLF) law of the corresponding polymer, modified by the T_g shift due to interfacial effects and the local stress σ. We assume that the breaking times of glassy bridges are comparable to the local dominant relaxation times τ_α of the glassy bridges. The breaking time is thus given by

$$\log\left(\frac{\tau_\alpha(z,\sigma)}{\tau_g}\right) = \log\left(\frac{\tau_{WLF}\left(T - T_g(z,\sigma)\right)}{\tau_g}\right) = -\frac{C_1\left(T - T_g(z,\sigma)\right)}{C_2 + \left(T - T_g(z,\sigma)\right)} \qquad (4)$$

Here, $\tau_g = 100$ s (the relaxation time at T_g) and T is the temperature. C_1 and C_2 are the WLF parameters of the considered polymer.

Eq. (4) gives the equilibrium value of the breaking time, which is obtained when the distance z, the local stress σ and the temperature T have been maintained fixed for a long time. In general, the breaking time depends on the history of the glassy bridge and is denoted by $\tau_\alpha(t)$. We assume that, at any time, a glassy bridge has a probability for breaking per unit time, dP/dt, given by

$$dP = \alpha \frac{dt}{\tau_\alpha(t)} \qquad (5)$$

where α is a number of order 1, but smaller than 1. When a glassy bridge breaks, the local stress σ is relaxed and drops to a much smaller value, which is the rubbery contribution. Immediately after breaking, we assume that τ_α relaxes to a value $\tau_{\min} \sim \dot{\gamma}^{-1}$, where $\dot{\gamma}$ denotes the local deformation rate. In practice, typical deformation rates in our simulations are of order $\dot{\gamma} \approx 0.1$ s^{-1}. The local breaking time $\tau_\alpha(t)$ undergoes a subsequent evolution, analogous to an ageing process. Thus the evolution of the breaking time of a glassy bridge, $\tau_\alpha(t)$, is given by

$$\frac{\partial \tau_\alpha(t)}{\partial t} = 1 \qquad (6)$$

if

$$\tau_\alpha(t) \le \tau_{WLF}\left(T - T_g(z,\sigma)\right). \qquad (7)$$

By definition, we set the time τ_α to be bounded by the time $\tau_{WLF}(T - T_g(z,\sigma))$ given by Eq. (4). Eqs. (5), (6) and (7) describe the evolution of the local breaking times and lead to very complex behavior. When simulated in the presence of a few thousand beads, the evolution of these relaxation times determines the mechanical behavior of filled elastomers, enabling to explain or predict very specific non-linear behaviours of filled elastomers.[7]

3. Conclusions

The research project of the DINaFil consortium aims at an in-depth understanding of the physical properties of filled elastomers. As highlighted in the artcile, it combines (i) the synthesis of well-controlled model systems, employing concepts from surface chemistry and colloid science, (ii) the application of advanced NMR techniques for the quantitative study of immobilized polymer phases and filler-induced inhomogeneities in the rubber matrix, and (iii) the molecular characterization of local deformations in samples studied under strain. These studies are supplemented by dielectric and mechanical spectroscopy. A major goal consists in feeding the experimental insights into multi-scale computer simulations in order to test and improve predictive theoretical models of filled-elastomer behavior.

So far, we have been able to quantify exactly the temperature-dependent content of polymer involved in "glassy layers" between the filler and the changes in the elastomer matrix in previously established model systems based upon poly(ethyl acrylate), and the studies are currently extended to other polymers. Our NMR techniques proved applicable to the study of strained samples, from which we are currently deducing the distribution of local strain. With the recent improvements in our theoretical model that is based on the temperature and yielding behavior of "glassy bridges" between the filler particles, we are confident that the project will contribute significantly to the development of rational-design approaches of filled elastomer materials.

Summary

In this contribution, we summarize first results and future perspectives of the DFG-ANR joint project "DINaFil" that is concerned with elucidating the synergistic effects of inorganic nanoparticle filler structures in cross-linked polymer networks. NMR investigations on a first model system based on poly(ethyl acrylate) have revealed quantitative relationships between the amount of immobilized polymer at the particle surface, i.e. an interphase, and the total internal surface, depending on temperature, the dispersion state and further on the specific surface modification of the particles. Notably, only systems with dense chemical surface grafts show an additional pronounced inhomogeneity of the surrounding rubber matrix. Current efforts are devoted to the extension of the model approach to polymers of actual application relevance, such as polyisoprene (natural rubber), further developing the NMR approaches to the study of stretched samples, the correlation of the NMR results with structural details and the thermo-mechanical properties of the systems, as well as the modelling of the results by computer simulations.

Zusammenfassung

Dieser Beitrag gibt einen Überblick über erste Resultate and Perspektiven im DFG-ANR Gemeinschaftsprojekt „DINaFil", welches sich mit der Aufklärung synergistischer Effekte von anorganischen Füllstoffstrukturen in vernetzten Polymernetzwerken beschäftigt. NMR-Untersuchungen eines ersten Modellsystems auf Basis von Polyethylacrylat ergaben einen quantitativen Zusammenhang zwischen dem Gehalt an auf der Partikeloberfläche immobilisiertem Polymer (Interphase) und der inneren Oberfläche in Abhängigkeit von Temperatur, Dispersionszustand und der spezifischen chemischen Modifikation der Oberfläche. Erwähnenswert sind insbesondere Inhomogenitäten in der Vernetzungsdichte, welche nur bei chemischer Anbindung des Polymers an die Oberfläche auftreten. Aktuelle Arbeiten befassen sich mit der Erweiterung der Modellsysteme auf Polymere mit direkter Anwendungsrelevanz wie z.B. Polyisopren (Naturgummi), die Weiterentwicklung von NMR-Methoden zum Studium verstreckter Proben, die Korrelation der NMR-Resultate mit der Struktur bzw. der Morphologie sowie der thermisch-mechanischen Eigenschaften der Proben, sowie der Modellierung dieser Eigenschaften mit Computersimulationen.

François Lequeux [1] *is research director at CNRS and Dean for Research at Ecole Supérieure de Physique et Chimie Industrielle.*

E-mail: francois.lequeux@espci.fr

Didier Long [2] *is research director at CNRS at the CNRS/Rhodia joint research unit Laboratory for Advanced Materials*

E-mail: didier.long-exterieur@eu.rhodia.com

Paul Sotta [2] *is research director at CNRS at the CNRS/Rhodia joint research unit Laboratory for Advanced Materials*

E-mail:paul.sotta-exterieur@eu.rhodia.com

Kay Saalwächter [3] *is professor of Experimental Physics at Martin-Luther-Univ. Halle-Wittenberg*

E-mail: kay.saalwaechter@physik.uni-halle.de

Addresses:

[1] *ESPCI, 10 rue Vauquelin 75231 Paris France*

[2] *LPMA, CRTL, 85 rue des frères Perret 69192 Saint-Fons, France*

[3] *Institut für Physik – NMR, Martin-Luther-Universität Halle-Wittenberg, Betty-Heimann-Str. 7, 06120 Halle (Saale), Germany*

Project description & Acknowledgment

The relations between internal structure, inhomogeneous molecular dynamics, and the mechanical properties of filled elastomers are investigated by way of preparing and studying model (nano-) composites of different crosslinked polymers filled with silica particles of known and controlled particle size, surface properties and distribution. The project combines results from advanced NMR spectroscopy, scattering techniques, dielectric and mechanical spectroscopy, and computer simulations, in order to finally establish quantitative structure-property relationships.

The authors thank all doctoral students, post-doctoral researchers and scientists that are contributing to this project: Hélène Montes, Aurélie Papon, Dongmei Yang, Kerstin Schäler, Henriette Meyer, Martin Schiewek, Horst Schneider, Roberto Pérez-Aparicio, Ludovic Odoni, Loïc Vanel, and Alain Dequidt.

[1] J. E. Mark, B. Erman, F. R. Eirich, *The Science and Technology of Rubber*, Elsevier, Amsterdam **2005**.

[2] M.-J. Wang, *Rubber Chem. Technol.* **1998**, *71*, 520-589.

[3] M. Klüppel, *Adv. Polym. Sci*. **2003**, *164*, 1-86.

[4] A. Mujtaba, M. Keller, S. Ilisch, H.-J Radusch, T. Thurn-Albrecht, K. Saalwächter, M. Beiner, *in preparation.*

[5] H. Montes, F. Lequeux, J. Berriot, *Macromolecules* **2003**, *36*, 8107-8118.

[6] J. Berriot, H. Montès, F. Lequeux, D. Long, P. Sotta, L. Monnerie, *Europhys. Lett*. **2003**, *64*, 50.

[7] J. Berriot, H. Montès, F. Lequeux, D. Long, P. Sotta, *Macromolecules* **2002**, *35*, 9756.

[8] J. Berriot, F. Lequeux, H. Montes, L. Monnerie, D. Long, P. Sotta, *J. Non-Cryst. Solids* **2002**, *307*, 719–724.

[9] J. G. Meier, J. W. Mani, M. Klüppel, *Phys. Rev. B* **2007**, *75*, 054202.

[10] J. L. Valentín, I. Mora-Barrantes, J. Carretero-González, M. A. López-Manchado, P. Sotta, D. R. Long, K. Saalwächter, *Macromolecules* **2010**, *43*, 334-346.

[11] K. Saalwächter, *Progr. NMR Spectrosc*. **2007**, *51*, 1-35.

[12] J. Berriot, H. Montes, F. Martin, M. Mauger, W. Pyckhout-Hintzen, G. Meier, H. Frielinghaus, *Polymer* **2003**, *44*, 4909-4919.

[13] H. Montes, A. Papon, L. Guy, T. Chaussée F. Lequeux, *Eur. Phys. J. E* **2010**, *3*, 263-268.

[14] M. Mauri, Y. Thomann, H. Schneider, K. Saalwächter, *Solid State Nucl. Magn. Reson.***2008**, *34*, 125-141.

[15] A. Papon, K. Saalwächter, K. Schäler, L. Guy, F. Lequeux, H. Montes, *Macromolecules* **2011**, *44*, 913-922.

[16] P. Sotta, *Macromolecules* **1998,** *31,* 3872-3879.

[17] S. Dupres, D. Long, P.-A. Albouy, P. Sotta, *Macromolecules*, **2009**, 42, 2634–2644.

[18] S. Merabia, P. Sotta, D. R. Long, *Macromolecules* **2008**, *41*, 8252-8266.

[19] M. D. Ediger, *Annu. Rev. Chem*. **2000**, *51*, 99.

[20] D. Long, F. Lequeux, *Eur. Phys. J. E* **2001**, *4*, 371.

[21] S. Merabia, P. Sotta, D. Long, *Eur. Phys. J. E* **2004**, *15*, 189.

[22] K. Chen, E. J. Saltzman, K. S. Schweizer, *J. Phys. Cond. Mat.* **2009**, *21*, 503101.

[23] P. Rittigstein, R. D. Priestley, L. J. Broadbelt, J. M. Torkelson, *Nat. Mater.* **2007**, *6*, 278-282.

[24] V. Pryamitsyn, V. Ganesan, *Macromolecules* **2006**, *39*, 844-856.

Fachkollegienwahl 2011

DFG

Wählen Sie
Ihre Vertreterinnen und Vertreter
in die fachlichen Bewertungsgremien
der Deutschen Forschungsgemeinschaft

vom
7. November 2011 (14 Uhr)

bis zum
5. Dezember 2011 (14 Uhr)

über das
Online-Wahlsystem

Ihre Stimme für die Wissenschaft

▸ Wer darf wählen?

Alle promovierten Wissenschaftlerinnen und Wissenschaftler, die bei Wahlbeginn an einer Einrichtung forschen, die Wahlstelle der Fachkollegienwahl 2011 ist, oder als Einzelwählende erfasst sind.

Ihre Wahlstelle

RWTH Aachen
Universität Augsburg
Universität Bamberg
Universität Bayreuth
Freie Universität Berlin
Technische Universität Berlin
Humboldt-Universität Berlin
Charité - Universitätsmedizin Berlin
Universität Bielefeld
Ruhr-Universität Bochum
Universität Bonn
Technische Universität Braunschweig
Universität Bremen
Hochschule Bremen
Technische Universität Chemnitz
Technische Universität Clausthal
Brandenburg. Techn. Univ. Cottbus
Technische Universität Darmstadt
Technische Universität Dortmund
Technische Universität Dresden
Universität Düsseldorf
Universität Duisburg-Essen
Kath. Universität Eichstätt-Ingolstadt
Universität Erfurt
Universität Erlangen-Nürnberg
Universität Frankfurt/Main
Europa-Univ. Viadrina Frankfurt/Oder
Techn. Univ. Bergakademie Freiberg
Universität Freiburg
Pädagogische Hochschule Freiburg
Universität Gießen
Universität Göttingen
Universität Greifswald
FernUniversität Hagen
Universität Halle-Wittenberg
Universität Hamburg
Techn. Univ. Hamburg-Harburg
Univ. d. Bundeswehr Hamburg
Universität Hannover
Med. Hochschule Hannover
Stiftung Tierärztl. HS Hannover
Universität Heidelberg
Stiftung Universität Hildesheim
HS f. angew. Wissenschaft u. Kunst Hildesheim/Holzminden/Göttingen
Universität Hohenheim
Techn. Universität Ilmenau
Universität Jena
Techn. Universität Kaiserslautern
Universität Kassel
Universität Kiel
Universität Koblenz-Landau
Universität Köln
Deutsche Sporthochschule Köln
Universität Konstanz
Universität Leipzig
Universität Lübeck
Universität Lüneburg
Universität Magdeburg
Universität Mainz
Universität Mannheim
Universität Marburg
Universität München
Technische Universität München
Universität der Bundeswehr München
Universität Münster
Universität Oldenburg
Universität Osnabrück
Universität Paderborn
Universität Passau
Universität Potsdam
Universität Regensburg
Universität Rostock
Universität des Saarlandes
Universität Siegen
Dt. HS f. Verwaltungswiss. Speyer
Universität Stuttgart
Universität Trier
Universität Tübingen
Universität Ulm
Wiss. HS f. Unternehmensführung, Vallendar
Universität Vechta
Universität Weimar
Private Universität Witten/Herdecke
Universität Würzburg
Universität Wuppertal
Deutsches Archäologisches Institut (DAI), Berlin
Helmholtz-Zentrum für Materialien und Energie (HZB), Berlin
Bundesanstalt für Materialforschung und -prüfung Berlin (BAM)
Max-Delbrück-Centrum für Molekulare Medizin (MDC), Berlin-Buch
Stiftung Preußischer Kulturbesitz (SPK)
Wissenschaftsgemeinschaft Gottfried Wilhelm Leibniz (WGL), Bonn
Physikalisch-Technische Bundesanstalt (PTB), Braunschweig und Berlin
Alfred-Wegener-Institut für Polar- und Meeresforschung (AWI), Bremerhaven
GSI Helmholtzzentrum für Schwerionenforschung, Darmstadt
Helmholtz-Zentrum Dresden-Rossendorf e.V. (HZDR)
Deutsches Elektronen-Synchrotron (DESY), Hamburg
Bundesanstalt für Geowissenschaften und Rohstoffe (BGR), Hannover
Deutsches Krebsforschungszentrum (DKFZ), Heidelberg
Forschungszentrum Jülich
KIT Karlsruher Institut für Technologie
Deutsches Zentrum für Luft- und Raumfahrt (DLR), Köln
Museen der Stadt Köln
Helmholtz-Zentrum für Umweltforschung (UFZ), Leipzig
Zentralinstitut für Seelische Gesundheit, Mannheim
Max-Planck-Gesellschaft (MPG), München
Fraunhofer-Gesellschaft, München
Bayerische Staatsgemäldesammlungen Kunstareal München
Helmholtz Zentrum München, Dt. Forschungszentrum für Gesundheit und Umwelt
Helmholtz-Zentrum Potsdam, Deutsches GeoForschungsZentrum (GFZ)
Julius Kühn-Institut, Bundesforschungsinstitut für Kulturpflanzen
Friedrich-Loeffler-Institut, Bundesforschungsinstitut für Tiergesundheit
Max Rubner-Institut, Bundesforschungsinstitut für Ernährung und Lebensmittel
Berlin-Brandenburgische Akademie der Wissenschaften (BBAW), Berlin
Akademie der Wissenschaften zu Göttingen
Heidelberger Akademie der Wissenschaften
Sächsische Akademie der Wissenschaften zu Leipzig
Akademie der Wissenschaften und der Literatur, Mainz
Bayerische Akademie der Wissenschaften, München
Deutsche Akademie der Naturforscher Leopoldina, Halle

▸ Wie kann ich wählen?

Ihre Wahlstelle vor Ort

Erfassung der Wahlberechtigten

Ausgabe der Wahlunterlagen

Stimmabgabe von Ihrem Computer aus über das Online-Wahlsystem

Alle Informationen zur Fachkollegienwahl im DFG-Wahlportal:
www.dfg.de/fk-wahl2011

DFG

The Deutsche Forschungsgemeinschaft

The Deutsche Forschungsgemeinschaft (DFG, German Research Foundation) is the central self-governing organisation responsible for promoting research in Germany. According to its statutes, the DFG serves all branches of science and the humanities. The DFG supports and coordinates research projects in all scientific disciplines, in particular in the areas of basic research. Particular attention is paid to promoting young researchers. DFG's total annual funding budget is approximately 2,5 billion €. Researchers who work at a university or research institution in Germany are eligible to apply for DFG funding. Proposals will be peer reviewed. The final assessment will be carried out by review boards, the members of which are elected by researchers in Germany in their individual subject areas every four years.

Further Information on the DFG

For detailed information on the DFG, please visit our website at: www.dfg.de/en

Annual Report
Vol. 1: *Activities and Results* (in German only)
Vol. 2: *Programmes and Projects* (bilingual, available on DVD-ROM or at: www.dfg.de/jahresbericht)

forschung – Magazin der DFG, Wiley-VCH Verlag, Weinheim (published four times a year)

german research – Magazine of the DFG, WILEY-VCH Verlag, Weinheim (published three times a year)

GEPRIS – German Project Information System: www.dfg.de/gepris

Research Explorer - The Research Directory of the DFG and DAAD: www.dfg.de/en/rex

DFG Funding Ranking 2009, Institutions – Regions – Networks. Thematic Profiles of Higher Education Institutions and Non-University Research Institutions in Light of Publicly Funded Research, WILEY-VCH Verlag, Weinheim 2010: www.dfg.de/en/ranking

Publications my be obtained directly through the DFG by contacting: Michael.Hoenscheid@dfg.de

Impressum

Illustrations: Front figure from Englert et al. this issue, background picture copyright from Nature 2010 publishing group (Cover); DFG/Frenz (Foreword)

Edited by: Deutsche Forschungsgemeinschaft, Chemistry and Process Engineering Division

Contact: Dr. Sibylle Grandel, Kennedyallee 40, 53175 Bonn, sibylle.grandel@dfg.de

Publisher: WILEY-VCH Verlag GmbH & Co. KGaA, P.O. Box 10 11 61, D-69541 Weinheim